The Thesis committee for Yuta Nakamura
Certifies that this is the approved version of the following thesis:

Impact of Height Control on Constant Volume Simple Shear Testing on Sand

APPROVED BY

SUPERVISING COMMITTEE:

Chadi El Mohtar, Supervisor

Ellen M. Rathje

Impact of Height Control on Constant Volume Simple Shear Testing on Sand

by

Yuta Nakamura, B.S.E.

THESIS

Presented to the Faculty of the Graduate School of

The University of Texas at Austin

in Partial Fulfillment

of the Requirements

for the Degree of

Master of Science in Engineering

THE UNIVERSITY OF TEXAS AT AUSTIN

August 2017

To my family, who believed in me and gave every opportunity for me to be where I am today.

Acknowledgments

First and foremost, I would like to thank my advisor, Dr. Chadi El Mohtar, for his guidance throughout my time at Texas. He has been there for me when I needed his advice, and helped me find a different topic of research when the first topic seemed to be stuck. I would also like to thank my second reader, Dr. Ellen Rathje, as well as all the professors at UT I had the pleasure of learning from. I would also like to thank (now Doctor) Wing Shun Kwan and (soon to be Doctor) Hamza Jaffal for teaching me how to use the different equipments as well as helping me whenever I had issues in the lab. I would also like to show my special appreciation to Dr. Youssef Hashash at the University of Illinois at Urbana-Champaign for allowing me to get started with undergraduate research with him and first learn about the field of geotechnical engineering.

I would like to acknowledge Mrs. Reta Mae Moore and Dr. Walter L. Moore for their generous gift to the Walter L. and Reta Mae Moore Graduate Fellowship which provided me with great financial support.

My 2 years in Austin have definitely been enriched by all the friends and colleagues I've met here. Naming everyone who I met here who had a positive impact on my life would end up longer than the actual thesis, but I would like to give a special thank you to Kaleigh McLaughlin, Patricia Bennett, Udit

Dasgupta, Brandon Smith, Andrew Keene, Jillian Montalvo, Anna Casady, Andrew Stolte, Dave Teague, and Aaron Potkay for making my time in Austin especially memorable. I would like to thank all of my friends back home in Illinois for giving me the support I needed during some harder times. It was nice to know that there are people I could talk or message to easy my stress and have a great laugh.

Last, but certainly not least, I would like to thank my family for believing in me. I could not have done all I have done without their unwavering support, and for that there are no amount of appreciation I could show to do it justice.

Impact of Height Control on Constant Volume Simple Shear Testing on Sand

Yuta Nakamura, M.S.E.

The University of Texas at Austin, 2017

Supervisor: Chadi El Mohtar

Liquefaction is a failure behavior of saturated sand under undrained condition experiencing transient, usually seismic, loading. Current laboratory procedures for evaluating liquefaction behaviors and potentials include using simple shear tests to simulate a vertical propagating seismic wave or a monotonic load. To better simulate field conditions, the sand specimens are tested at saturation under undrained conditions. However, undrained condition can be simulated by keeping the volume of the specimen constant during the test. When performing simple shear tests under constant volume condition, ASTM Standard D6528 allows up to 0.05% volume change of the specimen to be considered a valid equivalent undrained test. Volumetric change of the specimen during constant volume shear impacts the changes in the normal stresses caused by the contractive or dilative behaviors of sand under constant volume condition. This impact on the change in the normal stress, even while the vertical deformations are within the allowed range, can be significant and is a function of the specimen properties.

For this research, simple shear tests were run on different sand specimens using the modified UT Cyclic Simple Shear device. The previous version of the device tested saturated sand specimens under truly undrained conditions, while the modifications allowed dry sand specimens to be tested under constant volume conditions to simulate undrained condition. The modifications to the device were to increase the rigidity of the system and overall quality of the results. Monotonic and cyclic loading test results were obtained from the modified testing device. Analyzing the monotonic test results found that even small height changes to the specimen will affect the contractive and dilative behaviors of the specimen. Contractive height change of loose specimens decreased the amount of generated positive change in the axial stress during contraction, while the dilative height change to the dense specimens increased the dilative stress changes at high shear strains. Cyclic test results were compared to the results from corresponding tests obtained from the previous version of the testing device to verify the effect of the modification, as well as comparing the results of constant volume and undrained conditions. The results show that specimens tested under constant volume condition displayed lower strength than the specimen under undrained condition. The dense specimens showed a more significant reduced strength with the difference increasing with the amplitude of vertical movement of the top platen during cyclic loading. Finally, methods of remediating the stress change were proposed. These methods, while experimental, could be modified and used to improve the quality of the simple shear test results under constant volume

condition.

Table of Contents

List of Tables

List of Figures

Chapter 1

Introduction

1.1 Background

In geotechnical engineering, obtaining accurate soil properties are crucial for characterizing the site and for designing. Undisturbed samples or reconstituted soil specimens are tested under different laboratory tests to see how they react under different field conditions, and by using simulated seismic loading, the soils liquefaction potential and resistance can be obtained as well. The test data provides information on the soil strength and resistivity to shear, as well as time of liquefaction triggering and the strength behavior for a seismic event. From a cyclic loading test, the dynamic soil properties can be obtained and used to estimate the damage from transient seismic waves. Shear modulus, G, is how the soil reacts to shear, and damping ratio, D, is the ratio between the dissipated energy and maximum strain energy at a given strain amplitude. Geology of a site can be simplified as horizontal layers of soil or rock, and shear modulus and damping ratio are assigned to each layer. Seismic-induced shear waves are amplified at certain frequencies depending on the properties of the layer which it passes through, and the resulting wave at the surface are taken into account when designing building against seismic damage.

Laboratory tests can be used to find soil strength properties. For example, simple shear test can be used to simulate the soil condition at a failure surface. The stress-strain plots can be used to determine the behavior of the soil, and the strength can be found by using the shear stress applied on the soil at the strain of interest. Simple shear tests can be run in drained or undrained conditions, and the data obtained in each condition are used in different scenarios. Strength obtained from drained conditions are predominantly for sandy sites and for long-term stability conditions, while undrained conditions are more relevant for clayey sites for short-term conditions, as well as sandy sites for liquefaction potential analysis when loading the specimen with seismic ground motions.

For analyzing soils behavior during a seismic event, a cyclic simple shear test is suitable, as it is best able to simulate vertically propagating shear waves and in-situ stress conditions generated during an earthquake. Shear modulus is obtained as the slope of the shear stress vs shear strain graph. Because the soil is a nonlinear material, the shear modulus changes depending on the strain range. Soil acts linearly elastic at very small strains (shear strain, $\gamma \leq 10^{-3}$ %), nonlinearly elastic at small strains (10^{-3} % $\leq \gamma \leq 10^{-2}$ %), and nonlinearly inelastic at higher strain ($\gamma > 10^{-2}$ %). Shear modulus of soil reduces as strain increases (strain softening behavior), and is generally normalized by the maximum shear modulus and presented as a normalized modulus reduction curve. The maximum shear modulus, G_{max}, is the shear modulus obtained at the linear elastic range.

Material damping ratio can be found from the stress-strain plot from a cyclic test, as shown in figure 1.1; the stress path is called a hysteresis loop. Using the Masing behavior, the damping ratio is estimated as the ratio of the area inside the loop and the area of the triangle beneath the loop.

Shear Stress, τ

G

1

A_T

A_L

Shearing Strain, γ

$G = \tau / \gamma$

$D = A_L / (4 \pi A_T)$
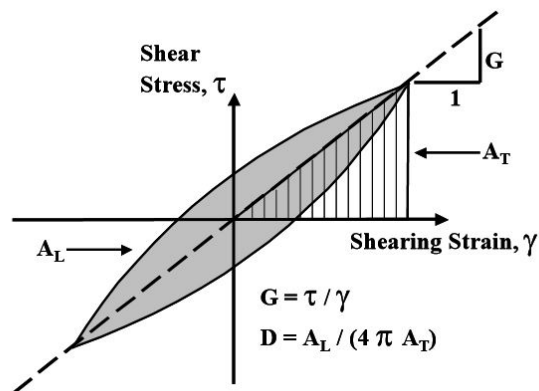
Figure 1.1: Estimation of shear modulus and material damping ratio during cyclic loading (Darendeli, 2001)

Traditionally, drained and undrained behaviors of sand under shear stress are studied using fully saturated specimens. Drained condition is achieved by opening the drainage and allowing water to flow in or out of the specimen, and undrained condition is achieved by closing the drainage and preventing flow from the specimen, thus generating excess pore pressure. While this method may simulate the field condition under the water table closely, it is a hassle to prepare the specimen to full-saturation. This process may involve carefully applying the membrane to prevent any leakage, slowly flushing the specimen with carbon dioxide and then water, and applying backpressure to

3

dissolve any air that may still be in the specimen.

Dyvik et al. (1987) has published a study where they ran undrained direct simple shear tests with pore pressure measurements on normally consolidated Drammen clay, and then compared the results with constant volume direct simple shear test. They have concluded that stress-strain plots obtained from the two tests were practically identical, and change in vertical stress required to maintain constant volume throughout the direct simple shear test was equal to the pore pressure generated in saturated undrained direct simple shear test. This study has been cited to justify using constant volume conditions instead of saturating the specimen and running it under undrained conditions. Current ASTM standard for constant volume simple shear test allows the height of the specimen to change up to 0.05% of its original height from contraction or dilation.

The goal of this research project was to study the shear-stress curve and dynamic soil properties in the nonlinear inelastic range obtained from simple shear tests on dry specimen under constant volume condition. Reconstituted specimens of granular soil were tested to obtain the stress-strain curves. The specimen was one-dimensionally consolidated (K_0 consolidation) and sheared. Vertical movement of the piston was controlled using screw and nut restraining device. The stress deviation caused by the small volume change of the specimen was investigated by comparing the stress behavior with change in specimen height. Obtaining the correct strength is important when designing geotechnical structures, and not obtaining the correct maximum or minimum

strength due to volume change could have a large impact when considering liquefaction potential.

1.2 Objective

The primary objective of this research is to test the validity of the data obtained using simple shear test under constant volume conditions on dry specimen. Geotechnical Consulting and Testing Service (GCTS) manufactured Simple Shear testing equipment at the University of Texas at Austin was used to test the soil under monotonic and cyclic shear loading conditions. Previous study of the topic (Kwan, 2015) used a cyclic simple shear equipment with a pressure chamber, which allows for back-pressure saturation of the specimen. The tests for this research were conducted using a modified version of GCTS Simple Shear equipment which allowed testing on dry specimen under conditions that were considered equivalent to tests run on saturated specimens. Effects of vertical effective stress on the shear behavior were investigated.

The effect of specimens height change on stress was also investigated. During shear, the sand specimen experiences contraction and dilation which are reflected in the change in axial stress, as well as the small height change allowed by the ASTM standard. The small height change allowed by the standard may cause a significant difference in the stress recorded. By using screw-nut systems with different properties, the specimens should have different height change under the same shearing conditions. Comparing the stress-strain behaviors and the height change should articulate the effect of

volumetric change.

Dynamic properties and degradation of soil strength occurring from cyclic loading were also obtained. In particular, number of cycles it took to reach failure (N_f) were plotted against the cyclic stress ratio (CSR), and the N_f vs CSR curves were compared with those obtained from cyclic tests on saturated specimens under undrained conditions.

Finally, possible methods of accounting for the stress difference from the volume change were discussed. One proposed method was to use the on-dimensional consolidation equation. This method utilizes the equation to convert the height change into stress change.

1.3   Organization of Thesis

Chapter 2 discusses the literature reviews done for this research. Topics include drained and undrained behaviors under shear of sand specimens, evaluation methods of liquefaction potential, empirical relationships for the dynamic soil properties, and the one-dimensional consolidation analysis.

Chapter 3 discusses the equipments used for this research as well the testing methods. After discussing the equipments and the modifications performed on them, test set-up steps and test details performed on the specimen are listed. Corrections to obtain the correct specimen densities are also discussed.

Chapter 4 discusses how the data obtained from the tests were analyzed.

This section discusses any necessary corrections, and how the values were converted to perform a more meaningful comparison.

Chapter 5 discusses the test results and analysis. The test results are summarized, and the findings are discussed. The findings from each tests were compared and combined to formulate an overall conclusion about the height control effect on results from a simple shear machine, which are discussed in Chapter 6. Potential scopes for future research are also proposed in this section.

Finally, the Appendix includes the summaries of the tests performed and analyzed for this research.

Chapter 2

Literature Review

2.1 Introduction

In this chapter, literatures regarding the soil behaviors under different shearing conditions are discussed. To properly compare the behavior under saturated undrained conditions and the equivalent constant volume condition, general behavioral trends of sand under shear are outlined.

Behavior of sand under monotonic loading condition were discussed in section 2.2. Under drained condition, the specimen is allowed to undergo volume change when sheared. The differences in height change under shear were compared between specimens with varying densities. Specimens under undrained condition, on the other hand, are not allowed to undergo volume change. To maintain the same volume under shearing conditions, excess pressure is developed within the specimen, altering the effective stress. The change in effective stresses were compared between specimens with different densities. For both conditions, shear stress under constant strain rate were discussed.

Section 2.3 discussed the methods of evaluating liquefaction potential. The term liquefaction was defined, and failure mechanisms behind liquefaction and the criteria that determine liquefaction triggering were discussed. Addi-

tionally, methods of analyzing liquefaction resistance were discussed. These methods include lab data analysis, which is the focus of this research, as well as correlations using in-situ test parameters.

Section 2.4 discussed the dynamic soil properties and their empirical relationships. Previous studies on the topic have found that shear modulus for cohesionless soil is strongly influenced by confining pressure, strain amplitudes, void ratio, and number of loading cycles, while the damping ratio is influenced strongly by the same factors as well as the number of cycles in a cyclic test (Seed and Idriss, 1970). This section will discuss the relationships between the factors mentioned above and the dynamic soil properties at small shear strain range ($\gamma \leq 0.001\%$), at high shear strain range ($\gamma > 0.1\%$) and at intermediate strain range.

Section 2.5 discussed the consolidation test and the one-dimensional consolidation equation. Based on Terzaghis consolidation theory, consolidation test can be used to find the soils compression and recompression indices, which are used in the consolidation equation to calculate the consolidation from change in vertical stress. Conventionally the consolidation test is used on cohesive materials, since the volume change occurs from the movement of the pore fluid. Previous studies which analyzed consolidation of cohesionless materials were discussed in this section.

2.2   Behavior of Sand in Shear

The two basic conditions soil is tested under are drained and undrained conditions. Test under drained condition allows the sample pore pressure to dissipate and the volume to change. Under undrained conditions, the volume of the specimen is held constant, and the excess pore pressure is generated. Test results from a drained test is important when analyzing the long-term conditions after the pore water pressure has been dissipated, or for sand due to its high hydraulic conductivity. Conversely, the results from an undrained test is important for short-term conditions before the pore water pressure has been dissipated, or for clay due to its low hydraulic conductivity. Undrained condition for sand is important when analyzing the effect of dynamic loading; excess pore pressure is generated within sand under transient, earthquake-like loading and the site may experience liquefaction.

To run a test under truly drained or undrained condition, the sand specimen is saturated and the pore pressure is recorded. However, with dry specimen, undrained and drained condition can be simulated by maintaining constant volume or constant vertical stress, respectively; Dyvik et al. (1987) reported the undrained tests and constant volume tests results on clay were equivalent for all practical purposes, and changes in vertical stress required to maintain the constant volume are equal to the generated pore pressure in an undrained test. The following sections will discuss the sand behavior under drained and undrained conditions.

2.2.1 Drained Condition

Behavior of sand specimen under shear in drained condition can be observed in the volumetric behavior. For a truly saturated sand specimen, the volumetric change is achieved from the intake and expulsion of water from the soil structure. The free flow of water in and out of the specimen changes the pore volume, and therefore the total volume, of the specimen; it also allows the pore pressure generated from shear to remain zero. The behavior depends heavily on the density of the specimen; loose specimen shows decrease in volume via contraction, and medium to dense specimen shows initial contractive behavior, then volume increase via dilation. These behaviors are presented in figure 2.1.

(a) Shear Stress Behavior under Drained Condition

(b) Volumetric Behavior under Drained Condition
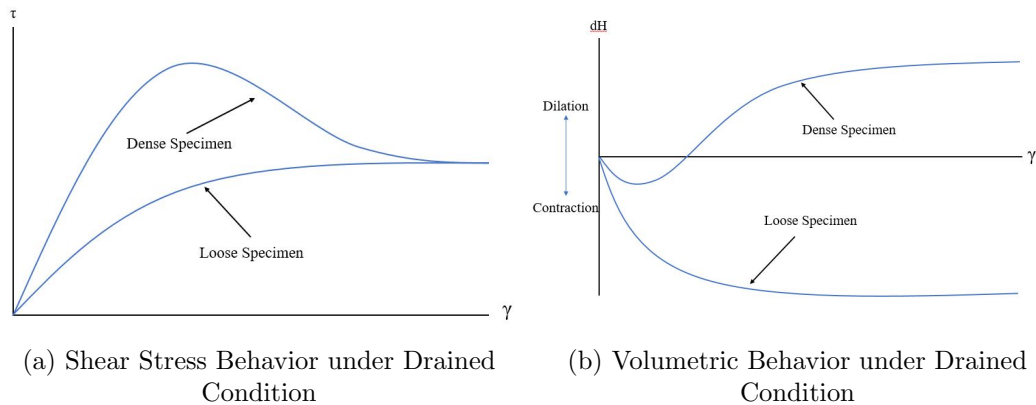
Figure 2.1: Shear Stress and Volumetric Behavior for Drained Condition

Effective confining pressure also has an effect on the volumetric behavior. Lee and Seed (1967) have shown with collection of drained triaxial test results that, for loose specimen, increase in confining pressure increased

11

the amount of compression of the specimen (figure 2.2. At very low confining pressure, the sand specimen showed a slightly dilative behavior, while the specimen showed highly compressive behavior under high confining pressure.
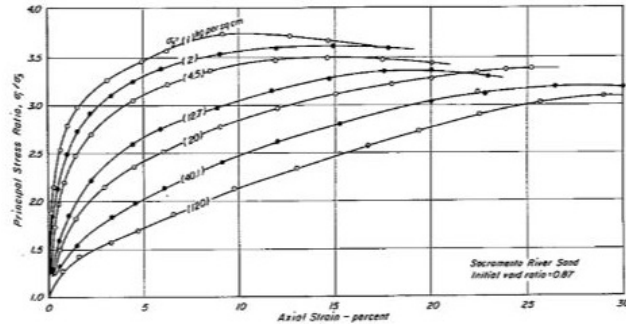
(a) Drained Shear Stress Behavior of Loose Specimens
Under Different Confining Stresses
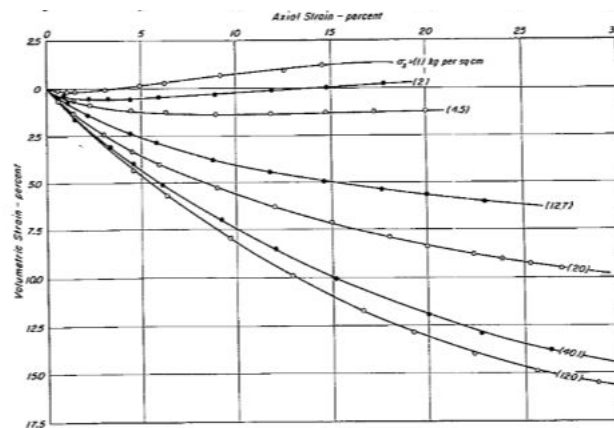
(b) Volumetric Behavior of Loose Specimens Under
Different Confining Stresses

Figure 2.2: Stress-Strain-Volume Data for Loose Sand Under Different
Confining Stresses (Lee and Seed, 1967)

The effect of confining pressure is even greater on dense specimen (figure 2.3). The drained triaxial results have shown that at low confining pressure,

the specimen showed dilative behaviors; as the confining pressure increased, specimens dilative tendencies decreased, and even showed compressive behavior after a certain compressive stress.
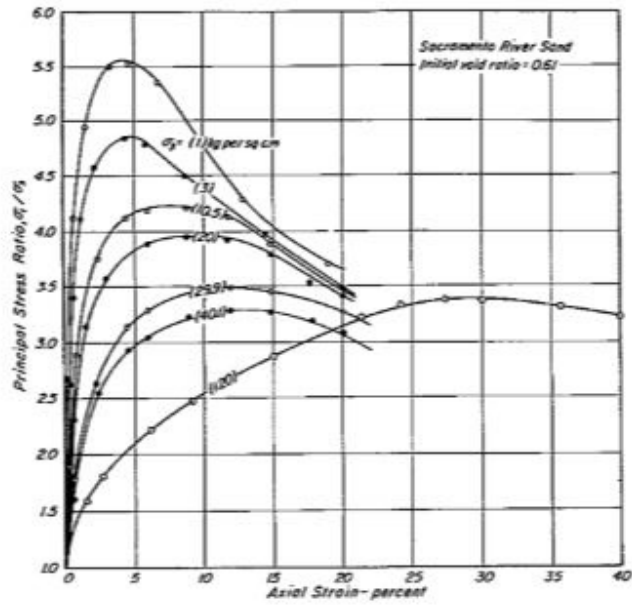
(a) Drained Shear Stress Behavior of Dense Specimen
Under Different Confining Stresses
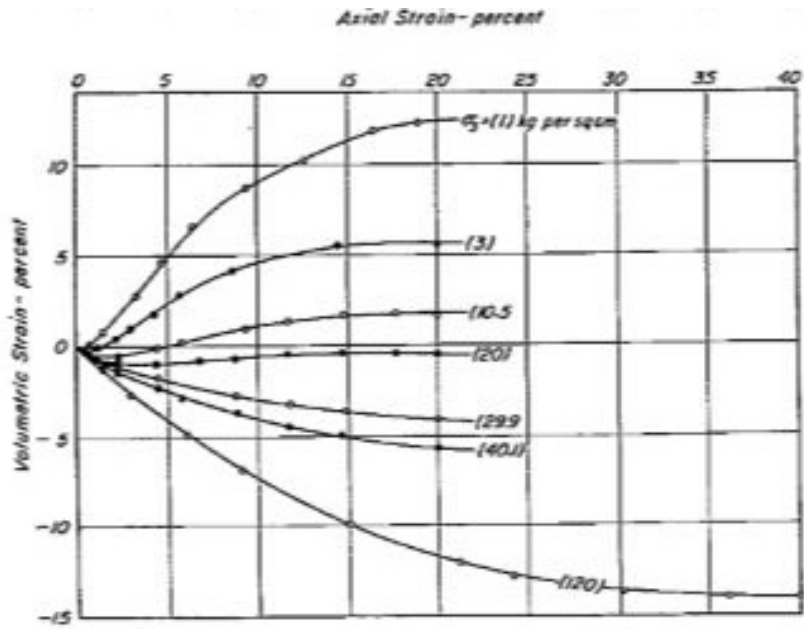
(b) Volumetric Behavior of Dense Specimen Under Different Confining
Stresses

14

Figure 2.3: Stress-Strain-Volume Data for Dense Sand Under Different
Confining Stresses (Lee and Seed, 1967)

Shear strength parameters of sand can be obtained from drained tests. Assuming granular soils are cohesionless, the drained shear strength of sand depends on the friction angle, or the resistance against the sand particles movement in the direction of shear. The strength activated from friction angle of a granular mass has 3 components: frictional resistance, resistance due to dilation, and resistance due to interference. Frictional resistance refers to the friction from the particles sliding and rolling on a flat surface, and is present for all conditions. Resistance due to dilation is caused by the volume change from the tightly packed particles rolling and climbing over each other. Resistance due to interference is from the sand particles moving around adjacent particles, which causes localized volume changes but no significant overall volume change.

Friction strength for sand specimens with low relative density is controlled by the interference resistance, while strength of specimen with high relative density is controlled by the dilation resistance; particles for low density specimen experience less interlocking so the particle can move around each other, while the particles in high density specimen has to roll over each other for movement. Friction strength for specimen under low confining pressure is controlled by dilation resistance, while strength for specimen under high confining pressure is controlled by interference resistance; low confining pressure allows the particles to dilate and total volume to change, while particles under high confining pressure are not allowed to dilate and must move around each other. Components of the friction strength depending on different densities or

confining stresses are presented in figure 2.4.

(a) Components of Strength of Sand with Relative Density(Proposed by Rowe (1962), Presented by Lee and Seed (1967))

(b) Components of Strength of Sand with Effective Confining Stress(Lee and Seed (1967))
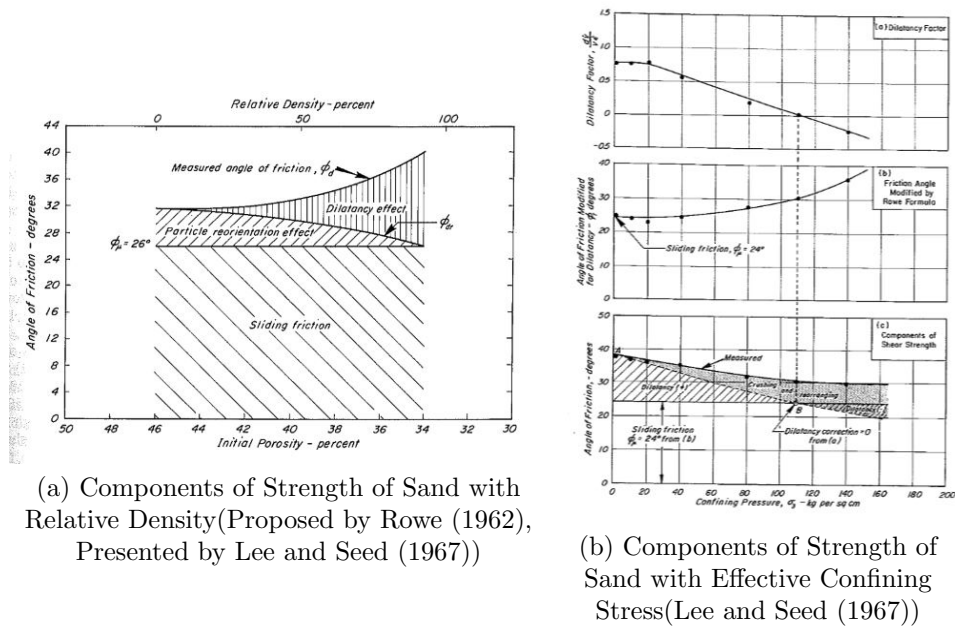
Figure 2.4: Effects of Density and Stress on Friction Angle

2.2.2 Undrained Condition

Behavior of sand specimen under shear in undrained condition can be observed in change in the pore pressure of the specimen. Undrained tests are performed with closed drainage. By not allowing movement of water in and out of the specimen, the volume in held constant throughout the test and excess pore pressure is generated.

Similar to behavior of soil under shear in drained conditions, behavior of soil under shear in undrained conditions can be described as contractive or dilative. For undrained condition, however, contractive or dilative refers to the

16

sign of the generated excess pore pressure from the shear. Contractive refers to pore pressure generated from shear being positive, thus decreasing the effective stress of the specimen. Similar to drained behavior, contractive behavior of soil under shear can be observed in loose specimens. The sand structure under shear rearrange itself into a denser packing, thus forcing the water out of its pore space. Since the drainage is closed, the forced-out water cannot leave the specimen, thus increasing the pore water pressure and decreasing the effective stress and shear resistance. Conversely, dilative behavior under shear occurs with dense specimen. Sand particles packed tightly together will move and roll over one another, and the increase in pore space within the specimen will decrease the pore pressure, thus increasing the shear resistance of the soil. Under shear, most dense specimen will exhibit small contractive behavior at the beginning before starting to dilate. These behaviors are presented in figure 2.5.
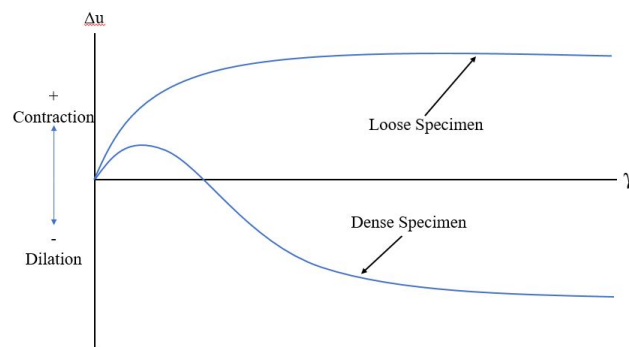
Figure 2.5: Excess Pore Pressure Behavior for Undrained Condition

Behavior of sand under shear in undrained condition is important when

17

analyzing liquefaction potential. When loose sand specimen shows contractive behavior, the generated positive pore pressure will cause the effective stress and shear resistance to decrease. When shear resistance decreases to a very low level, the specimen can experience large deformations, referred to as liquefaction. Consequences of liquefaction in real world include foundation failure, significant displacement of retaining structures, and slope failures. In lab testing, liquefaction may occur under both monotonic and cyclic loading conditions. While more prominent in loose sand specimen, liquefaction could also occur in dense sand specimen under cyclic loading. At low cyclic shear stresses, small amount of pore pressure is generated at small strains in dense specimen. As the cycling continues, generated pore pressure accumulates until it reaches zero effective stress. Liquefaction under this condition is referred to as cyclic softening or cyclic liquefaction, and does not cause large deformation, since the dilative tendencies of the specimen will generate negative pore pressure at large strains.

2.2.3 Peak and Ultimate/Critical Conditions

Few soil parameters can be found from plotting the stress-strain relationship data obtained from lab tests, as seen on figure 2.6.
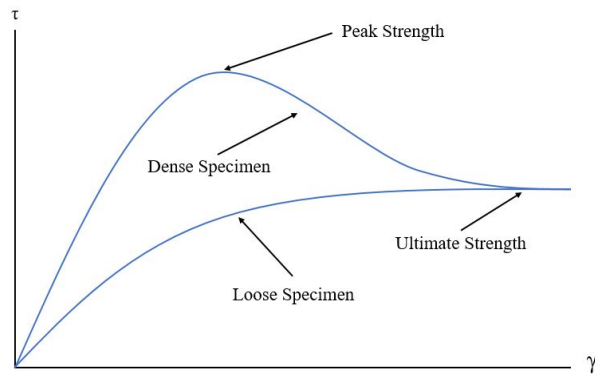
Figure 2.6: Peak and Ultimate Shear Strength for Drained Condition

As the shear strain increases, the stress-strain relationship for the dense specimen reaches a maximum stress value before decreasing and plateauing. The maximum shear stress measured in the test is considered the peak strength of the sand. As mentioned in the previous section, the peak strength is dependent on the confining stress the specimen is under. By running drained tests under different confining stresses and plotting the peak stress against the corresponding confining stress, Mohr failure envelope can be plotted, and the slope of the failure envelope is defined as the peak friction angle of the specimen (figure 2.7). Lee and Seed (1967) have found that the Mohr failure envelope is initially linear with high friction angle at low confining stresses, but becomes flatter as the confining stress increases. This effect is visible in for both loose and dense specimens, though more prominent in dense specimens. At a very high confining pressure, the friction angle for initially loose and dense specimens are practically the same. The point of peak strength is usually where the maximum rate of dilation is reached Bolton (1986).

19
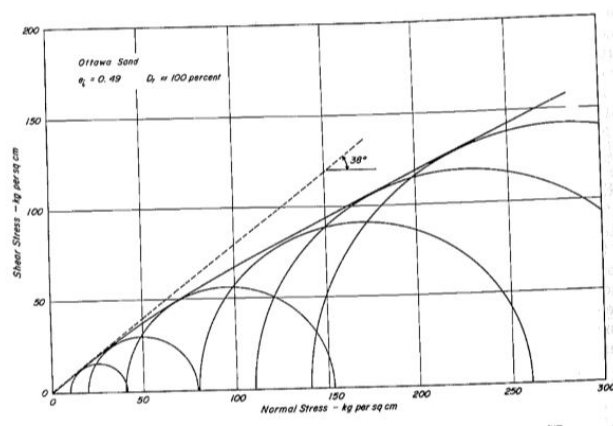
Figure 2.7: Mohr Circles and Failure Envelope for Dense Ottawa Sand (Lee and Seed, 1967)

After reaching peak strength, the shear stress decreases until it reaches a constant value. During the constant stress condition, the volume-strain plot shows that contractive/dilative behavior has subsided, and the shearing has continued at constant volume. This condition, where shearing occurred at constant effective stress and constant volume, is referred to as the critical condition, or ultimate strength. A loose specimen could reach this state without experiencing the peak strength, as could specimen under high confining stress. The critical state shear strength is related to normal stress by the following equation:

$$\tau' = \sigma'_n * tan(\phi'_c) \tag{2.1}$$

Undrained tests, by definition, are a test run under constant volume conditions. Both τ' and σ_n' changes with strain due to pore pressure gener-

ation. Critical state, in this case, is defined as the state at which the stress ratio, τ' / σ_n', is constant. Therefore, critical state friction angle of the soil, ϕ_c', can be found from finding the critical state stress ratio (figure 2.8).
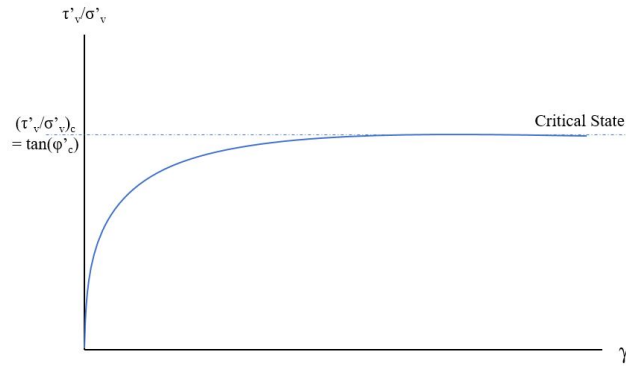
Figure 2.8: Stress Ratio and Critical State Line

Behavior of sand near the critical state can also be found by plotting the normal stress against the shear stress experienced during a shear test. By plotting the stress path of the soil under shear and comparing the point of failure, the critical state line (CSL) and the critical state strength (ϕ_c') can be found. For a drained test, the path would be purely vertical since there are no shear induced pore pressure and the normal stress remains constant throughout the test (figure 2.9a). To adopt the use of critical state line for drained condition, one could take the peak strength or the ultimate strength to be the point of failure, depending on the case. Dense sand specimen at smaller shear strains can use the peak strength since it is unlikely that it will activate the ultimate strength, while loose sand specimen or specimens expected to

21

experience high strain should use critical strength since it is unlikely for those specimens to fail at the peak strength.

For specimens experiencing shear under undrained conditions, the stress path is not a vertical line due to the shear induced pore pressure. As the shear stress increases, the effective normal stress decreases due to the positive pore pressure, and the stress path curves to the left towards the critical state line. Once the path reaches the CSL, the induced pore pressure becomes negative and the effective normal stress starts increasing, allowing the stress path to follow the CSL (figure 2.9b). The effective normal stress when the stress path reaches CSL depends on different factors such as the density and the confining stress.

(a) Drained CSL   (b) Undrained CSL
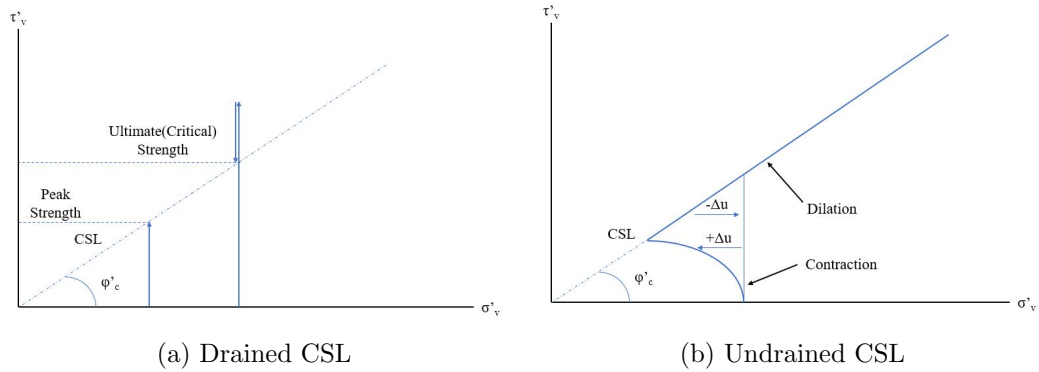
Figure 2.9: Stress Paths and Critical State Lines for Drained and Undrained Conditions

2.3   Evaluation of Liquefaction Potential

Liquefaction is the phenomena where cohesionless soil loses strength due to the increase in pore pressure caused by earthquake events or other rapid loading. Liquefaction events are usually accompanied by large deformation of the site due to the decrease in shear resistance. It occurs commonly at sites with loose, saturated cohesionless soils, but could also occur to sites with dense soils or those with gravels or fines.

There are two main types of liquefaction failures: flow-failure and cyclic mobility. Flow liquefaction failure occurs when the soil strength decreases below the stress required to maintain equilibrium. This could occur before the effective strength of the soil reaches zero, and the static load present will cause very large deformation. Flow failures are caused by monotonic and cyclic loading to saturated, loose soils. Cyclic mobility is caused when soil strength is gradually reduced by pore pressure generation during cyclic loading. The deformation, generally smaller than flow failure deformation, occurs when cyclic stress is greater than the residual strength of the soil. Cyclic mobility failure can occur in both loose and dense soil. (Kwan, 2015)

Seed and Idriss (1971) lists the factors known to influence liquefaction potential.

- Soil Type

- Relative Density, Dr

23

- Initial Confining Pressure

- Intensity and Duration of Ground Shaking

There are two ideas for determining liquefaction triggering criteria. Pore pressure based approach defines liquefaction triggering as when the ratio between excess pore pressure and initial effective stress prior to loading (ratio is commonly referred to r_u) reaches 1.0, indicating that the shear strength of the soil has reached zero. While this definition corresponds with the definition of liquefaction at rest, it is more common for flow liquefaction to occur when the shear strength reaches below the value required for equilibrium but greater than zero. Additionally, it is unlikely for a dense sand to reach the r_u value of 1.0 yet still experience liquefaction in the form of cyclic mobility. Ishihara (1993) suggests that r_u value may level out around 0.9 to 0.95. The second approach, the strain-based criterion, is more based on the seismic performance. Previous researches have tried to quantify the strain level that represented the liquefied state. However, different testing methods have provided different strains that corresponded to liquefaction. Additionally, it is difficult to measure strain in the field than in the laboratory.

Liquefaction resistance of soil can be found by plotting the liquefaction strength curve, which plots the number of cycle required to reach liquefaction (N_f) at a constant cyclic stress ratio (CSR). Generally, CSR is reported in a lab test as the ratio between the cyclic stress amplitude and the effective confining

stress. By plotting the points and creating a best-fit curve, number of constant stress cycles the specimen can undergo before failure can be estimated.

Based on Seed and Idriss (1971), CSR of earthquake loading is reported as:

$$CSR = 0.65 * \frac{PGA}{g} * \frac{\sigma_{v0}}{\sigma'_{v0}} r_d \qquad (2.2)$$

where PGA is the peak ground acceleration, g is gravitational acceleration, σ_{v0} is the total vertical overburden stress, σ'_{v0} is the effective vertical overburden stress, and r_d is the depth reduction factor.

CSR obtained for an earthquake loading can be scaled to an equivalent value for an event with a magnitude of 7.5 using the magnitude scaling factor (MSF) for better comparison. MSF increases the CSR for earthquake events with magnitude less than 7.5, and decreases the CSR for events with magnitude greater than 7.5.

Current characterization of in-situ liquefaction resistance involves finding the cyclic resistance ratio (CRR) of the site, which is the capacity of the soil to resist liquefaction. CRR is obtained using correlations with different in-situ test parameters; commonly used are SPT, CPT, and shear wave velocity data. Shear wave velocity vs CRR plot can be found on figure 2.10. Plotting the CSR or CRR of an earthquake event against in-situ parameters of the site and identifying whether liquefaction occurred or not creates a curve that separate conditions that are susceptible to liquefaction from those which

are not. The curve is created based on a compilation of case histories, and provides good prediction on whether a site will experience liquefaction for a future event.
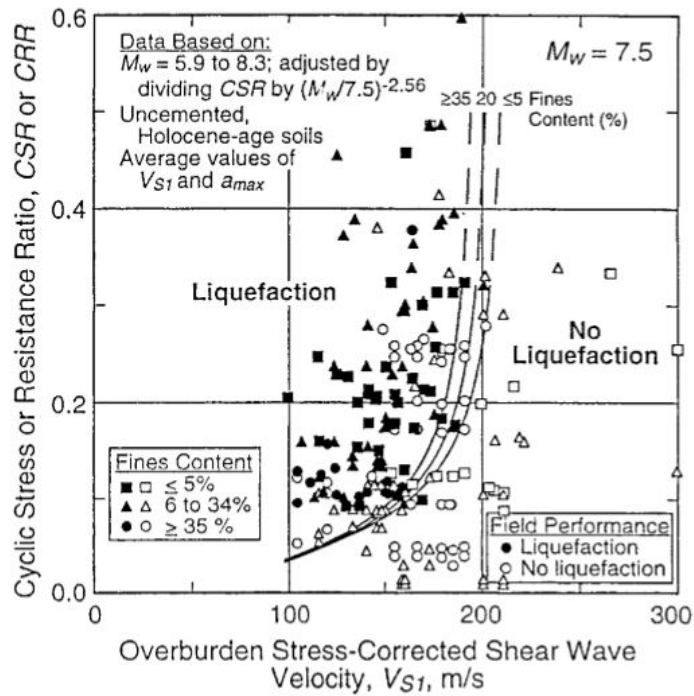
Figure 2.10: Liquefaction Relationship Recommended for Clean Uncemented Soils with Liquefaction Data from Compiled Case Histories ((Andrus and Stokoe II, 2000), Presented in Youd et al. (2001))

Using CSR, CRR, and MSF, the factor of safety against liquefaction for a given site can be can be written as follows:

$$FS = \frac{CRR_{7.5}}{CSR} * MSF \tag{2.3}$$

26

Where $CRR_{7.5}$ is the cyclic resistance ratio for a magnitude 7.5 earthquake. Figure 2.11 compares few MSF correlations for sand. It is recommended, for engineering practice, to choose from a range of MSF to choose from depending on the acceptable risk of a project, rather than using a single set of correlations. (Youd et al., 2001)
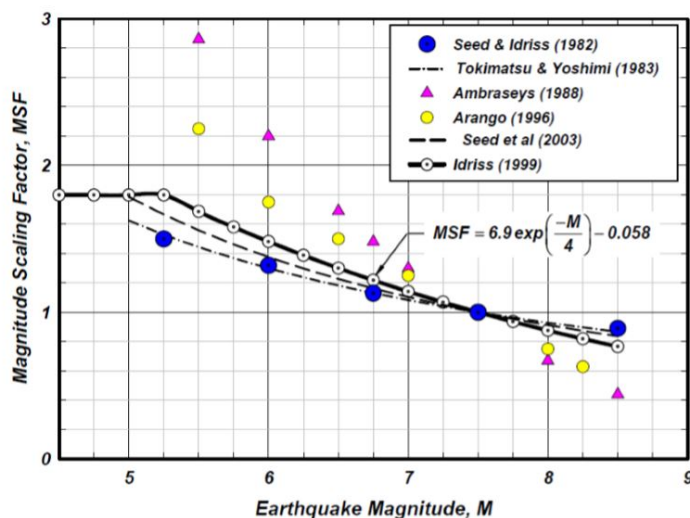
Figure 2.11: Comparison of the MSF relation for sands (Boulanger and Idriss, 2004)

2.4 Empirical Relationships for Dynamic Soil Properties

Cyclic shear stress-strain relationship is important when discussing the dynamic properties of soil. The relationship can be obtained from cyclic simple shear tests, which can characterize the horizontal movement generated from earthquakes. Generally, the test cycles between positive and negative values of

equal magnitude. When the test is cycling between equal amplitude of stress, the soil undergoes complete stress reversal, and the shear stress-strain plot forms a loop.

Shear modulus represents the shear stiffness of the soil, and obtained from the slope of the shear strain-stress plot. From cyclic test data, the shear modulus is obtained as the secant modulus of the line connecting the extreme points of the loop. Damping ratio is obtained from the hysteresis loop, and it is proportional to the area under the loop.

Dynamic behavior properties can be classified into two categories depending on the strain range. The soil is considered linearly elastic when the shear strain is less than 10^{-3} % (known as elastic threshold strain, γ_e^t), while shear strain larger than 10^{-3} % is considered to be in the nonlinear range. In the strain range close to the elastic threshold strain, 10^{-3} % $< \gamma < 10^{-2}$ %, the soil is considered to be nonlinear elastic.

There have been many studies that have developed empirical relationships between different factors of the soil to the dynamic properties. Hardin and Drnevich (1972) have found that the primary factors affecting the properties are:

- Strain amplitude, γ

- Effective mean principle stress, σ_m

- Void ratio, e

28

- Number of cycles of loading, N

- Degree of saturation (cohesive soils)

- Over-consolidation ratio, OCR (cohesive soils)

2.4.1 Shear Modulus

Hardin and Drnevich (1972) developed an empirical relationship to find the maximum shear modulus, G_{max}, in psi:

$$G_{max} = 1230 * \frac{(2.973 - e)^2}{1 + e} * (OCR)^a * (\sigma'_m)^{1/2} \qquad (2.4)$$

where σ'_m is in psi and a is a parameter depending on the plasticity index of the soil.

Hardin and Drnevich introduces the concept of reference strain, γ_r. Since soils react differently to strain under different conditions, normalizing the strain will simplify the soil behavior for comparison. By using the reference strain to normalize the strain, shear modulus at a certain strain can be obtained from the hyperbolic stress-strain relationship. The hyperbolic stress-strain relationship is defined as follows:

$$\tau = \frac{\gamma}{\frac{1}{G_{max}} + \frac{\gamma}{\tau_{max}}} \qquad (2.5)$$

where γ is the shear strain, and τ_{max} is the shear stress at failure. By defining the reference strain, the hyperbolic stress-strain relationship can be modified as follows:

$$\gamma_r = \frac{\tau_{max}}{G_{max}} \tag{2.6}$$

$$G = \frac{\tau}{\gamma} \tag{2.7}$$

$$G = \frac{G_{max}}{1 + \frac{\gamma}{\gamma_r}} \tag{2.8}$$

By defining the reference strain, the shear modulus of a soil can be evaluated at a given strain. From this relationship, normalized shear modulus reduction curve can be obtained by diving both sides of the equation by Gmax:

$$\frac{G}{G_{max}} = \frac{1}{1 + \frac{\gamma}{\gamma_r}} \tag{2.9}$$

Darendeli (2001) took this hyperbolic model, and applied a curvature coefficient, a, to better model strain amplitude beyond failure:

$$\frac{G}{G_{max}} = \frac{1}{1 + (\frac{\gamma}{\gamma_r})^a} \tag{2.10}$$

Menq (2003) reported results to find the relationships between the variables in the normalized modulus reduction curve, γ_r and a, and soil characteristics. The test results have shown that reference strain is strongly correlated to the uniformity coefficient, C_u, and mean effective stress, σ_m; γ_r decreased as C_u increased, and γ_r increased as σ_m increased. The results have also shown that the curvature coefficient was mostly independent of median grain size or uniform coefficient, but affected significantly by mean effective pressure. The empirical relationships found from the study are shown below.

30

$$\gamma_r = 0.12 C_u^{0.6} * \left(\frac{\sigma'_m}{P_a}\right)^{0.5 C_u^{-0.15}} \tag{2.11}$$

$$a = 0.86 + 0.1 log\left(\frac{\sigma'_m}{P_a}\right) \tag{2.12}$$

where P_a is the atmospheric pressure in the same unit as mean effective stress.

2.4.2   Damping Ratio

Hardin and Drnevich (1972) found a geometric relationship between damping ratio and shear modulus from the stress-strain hysteresis loops obtained from the cyclic simple shear test. Masing rule allows the viscous damping ratio to be estimated from the shape of the hysteresis loop (figure 2.12).
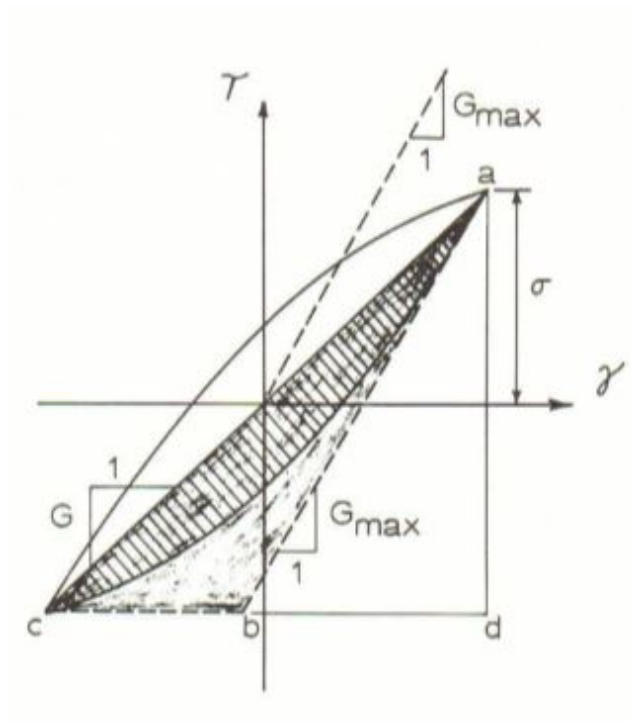
Figure 2.12: Geometric Relationship Between Shear Modulus and Damping Ratio (Hardin and Drnevich, 1972)

From this chart, the following relationship between damping ratio and shear modulus can be derived:

$$D = D_{max} * (1 - \frac{G}{G_{max}})$$
(2.13)

where D_{max} is the maximum damping ratio at high strains. Inserting this relationship in to equation 2.9, the material damping model can be found as:

$$\frac{D}{D_{max}} = \frac{\frac{\gamma}{\gamma_r}}{1 + \frac{\gamma}{\gamma_r}}$$
(2.14)

Darendeli (2001) provided a material damping model that improves upon the Masing behavior model at higher nonlinear strain level.

$$D = b * (\frac{G}{G_{max}})^{0.1} * D_{Masing} + D_{min} \tag{2.15}$$

where b is the modeling coefficient, D_{Masing} is the damping ratio predicted by the Masing behavior, and D_{min} is the minimum damping ratio at a given confining stress. The modeling coefficient is dependent on the number of loading cycle, N, and found empirically as:

$$b = 0.6329 - 0.0057 * ln(N) \tag{2.16}$$

Minimum damping ratio is the damping ratio at small strain, and can be found empirically as:

$$D_{min} = (0.8 + 0.0129 * PI * OCR^{-0.1069})$$
$$(\frac{\sigma'_m}{P_a})^{-0.2899} * [1 + 0.2919 * ln(f)] \tag{2.17}$$

where f is the loading frequency in Hz.

2.5 One-Dimensional Settlement Analysis of Granular Materials

One-dimensional consolidation equations are used to calculate the volume change of the specimen due to the vertical stress. Change in vertical stress will alter the pore volume of the specimen, causing consolidation or rebound.

Condition of consolidation can be divided into two categories. The specimen is normally-consolidated if the present stress is the largest stress the soil has ever experienced, and the specimen is over-consolidated if the specimen has experienced a larger stress than what it is currently experiencing; the maximum pressure the soil experienced in the past is called the pre-consolidation pressure, $\sigma'_{v,0}$.

One-dimensional load incremental tests are usually used when studying consolidation properties of soil. The specimen is restrained laterally with vertical drainage, and the change in height of the specimen is monitored with increased vertical stress. Each loading increment is sustained until the pore water pressure within the sample has been dissipated. The loads are unloaded to obtain the rebound curve, then reloaded to obtain the reload curve. This testing method is based on Terzaghis conventional consolidation theory, and the following assumptions are made:

- Soil is saturated and homogeneous;

- Flow of water is in the vertical direction;

- Compressibility of soil particles and pore water is negligible compared to compressibility of the soil skeleton;

- Stress-strain relationship is linear over the load increment;

- Ratio of soil permeability to soil compressibility is constant over the load increment; and

- Darcys law for flow through porous media applies.

The measured heights are converted into specimens void ratio and are plotted on the void ratio-stress plot.

$$e = e_0 - \frac{\Delta H}{H_0} \tag{2.18}$$

e is the void ratio, δH is the change in height after the stress change, and e_0 and H_0 are the initial void ratio and height of the specimen, respectively.

C_c and C_r are the compression and recompression indices, and are obtained from the graph as the slopes of the virgin loading and unload/reload curves, respectively, as shown on figure 2.13.
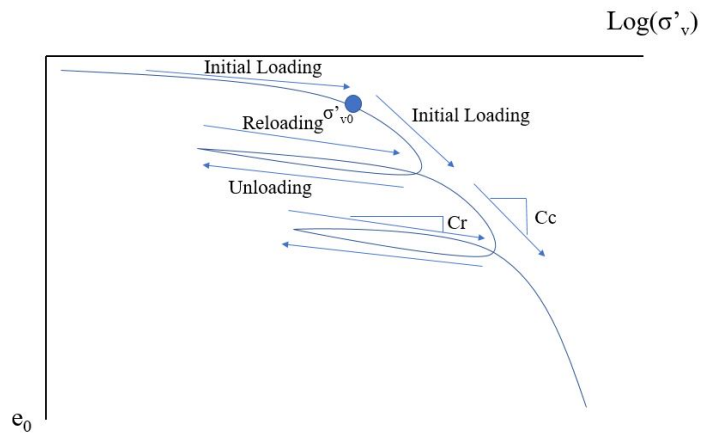

Figure 2.13: Example Loading/Unloading Curve

The consolidation of the soil specimen can be calculated using the fol-

lowing equation:

$$\Delta H = \frac{H_0}{1 + e_0} * (C_r * log(\frac{\sigma'_p}{\sigma'_{v,0}}) + C_c * log(\frac{\sigma'_{v,f}}{\sigma'_p})) \qquad (2.19)$$

$\sigma'_{v,0}$ is the initial vertical stress, and $\sigma'_{v,f}$ is the final vertical stress.

Studies of one-dimensional settlement analysis are most done on clay specimens. Pore water movement from a clay layer is a long-term effect and the predictive analysis is more crucial, whereas settlement from a sand layer is almost instantaneous. There have been some previous studies done regarding compression of granular materials. Mesri and Vardhanabhuti (2009) have studied the role particle rearrangement, rotation, and damage have on primary compression of granular materials, and presents a plot of compression indices of different sand materials (figure 2.14).
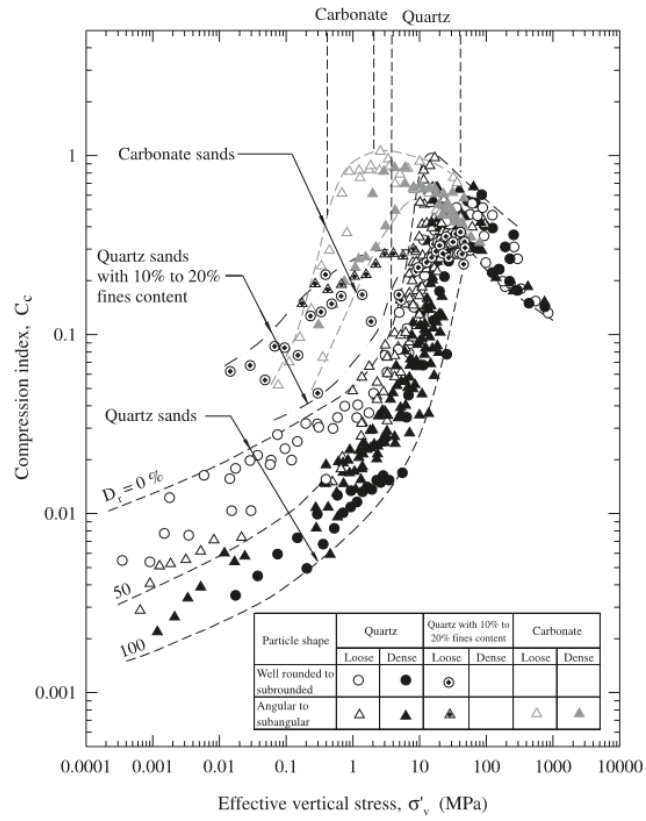
Figure 2.14: Data on C_c of Sand (Mesri and Vardhanabhuti, 2009)

Chapter 3

Testing Equipments and Testing Methods

3.1 Introduction

In this section, equipment and materials used in this research are discussed. The objective of the research involved comparing the results of tests from the new testing equipment set-up with the previous set-up. The discussion of the testing equipment will focus on the modification done on the University of Texas at Austin cyclic shear testing device. Since the same sand samples were tested, material properties were obtained from Kwan (2015)

Sample preparation and test set-up steps are also discussed in sections 3.4 and 3.5. The new cyclic shear testing set-up allows for tests on dry sand samples; dry funnel deposition method was used for the creation of the samples. To properly analyze the test results, the relative density had to be found. The calculation of the relative density, as well as the necessary corrections, were also discussed.

Finally, the details of the tests performed for this research are discussed in section 3.6. These include monotonic loading tests, cyclic loading tests, and one-dimensional consolidation test. For each test, the objective was outlined and how the data reflect the behavior of the sand under shear were discussed.

3.2   Testing Equipments

In this study, shear stress-strain behaviors and dynamic soil properties of sand were investigated using monotonic and cyclic simple shear tests. Geotechnical Consulting and Testing Service (GCTS) manufactured simple shear testing equipment at the University of Texas at Austin were used for this investigation. The soil specimen is constrained vertically by platens, and laterally by stacked rings. The top platen is held in place horizontally but able to move vertically. The load cell attached to the top platen records the axial load on the specimen when the platen is in contact with the top surface. The bottom platen is connected rigidly to the shaking table, which is connected to the shear actuator and able to move horizontally on the roller. Figure 3.1 shows a simplified diagram of the simple shear set-up.
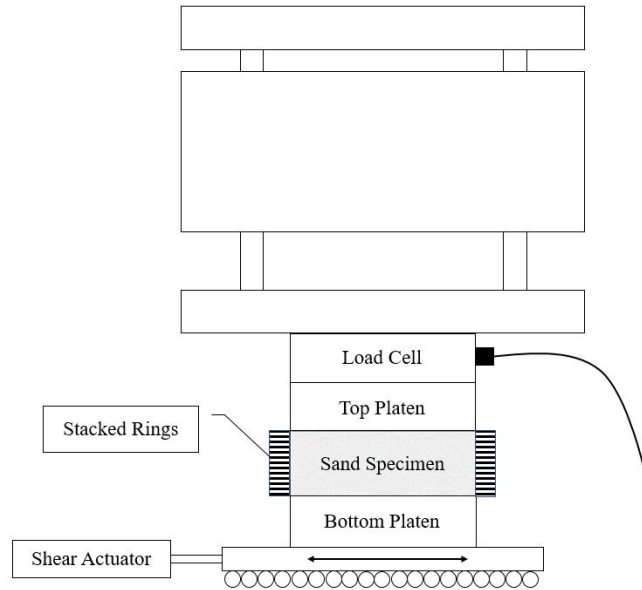

Figure 3.1: Simple Shear Test Set-Up

Kwan (2015) discusses the modification that was applied to the previous simple shear setup to improve the quality of the test. The purpose of the modification was to improve the quality of the test results by increasing the overall rigidity of the set-up. A pair of steel walls were custom-made such that they could aligned to hold the pneumatic actuator and lower the top platen on to the specimen when placed underneath (figure 3.2). The actuator was connected to the pressure panel, which provided the air pressure to control the amount of stress applied to the specimen. The walls were designed to allow the bottom platen, with the specimen and the split mold placed above, to be inserted under the actuator and be secured in place on the platform before removing the mold. The new set-up increased the resistance against lateral deformation, and attempted to minimize rocking and tilting during monotonic and cyclic loading tests (figure 3.3).
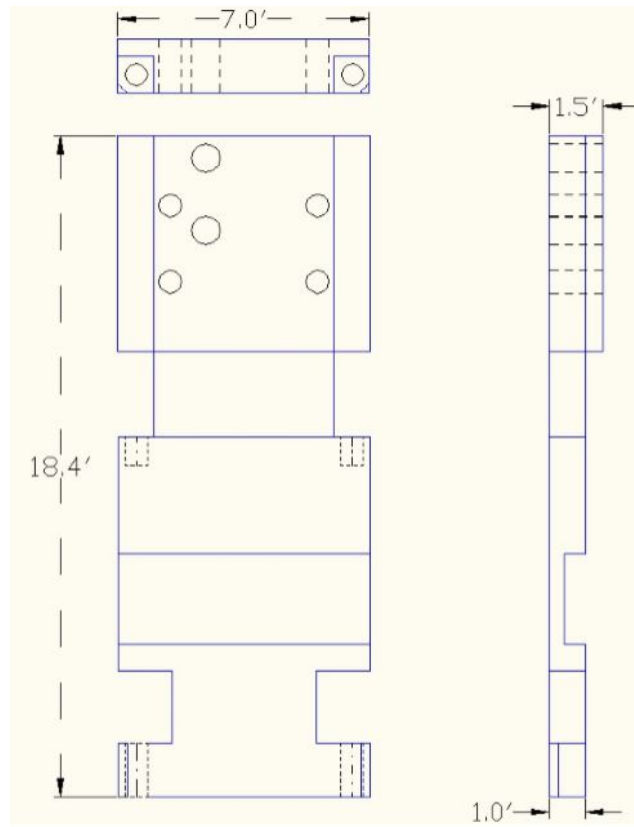
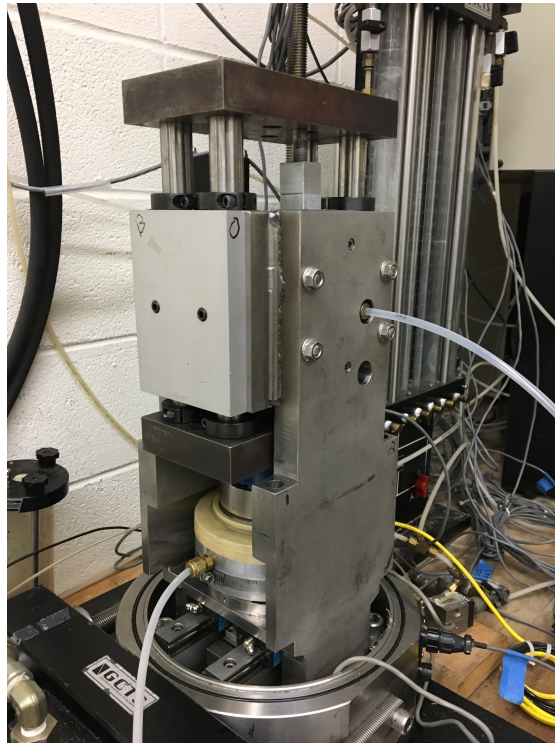Figure 3.2: Design drawing for the shear walls of the new UTCSS apparatus (Kwan, 2015)

Figure 3.3: Rigid Shear Wall

The second major modification of the system is changing the location of the hydraulic shear actuator. It was brought as close to the shaking table as possible to eliminate the misalignment at the horizontal shaft and enhance the performance of the actuator (figure 3.4). Combined with the first modification, the new configuration allowed monotonic and cyclic loading testing to high strain levels without excessive tilting occurring.

Figure 3.4: Hydraulic Shear Actuator

3.2.1 Screw-Nut Height Control System

To run a simple shear test under undrained conditions on a dry sand specimen, the volume of the specimen had to be kept constant under shear. Screw and nut height control systems were used to maintain constant volume condition. The system is made of 1 inch by 1 inch aluminum block with steel threaded bar. The restraining system prevented vertical movement of the platen; thus, keeping the specimen at constant volume during shear. Two pieces of the screw-nut systems were placed on top and bottom of the vertical actuator between the box and the plate, one on both sides of the specimen. Figure 3.5 shows a simplified diagram of the placements of the height control systems, and figure 3.6 shows the systems installed on the simple shear set-up.

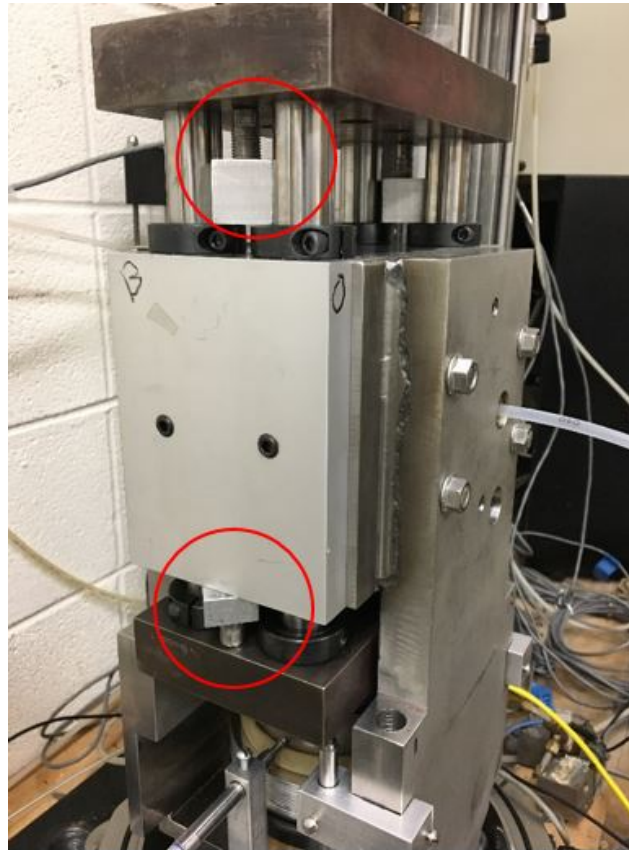Figure 3.5: Drawing of Screw-Nut Height Control System

Figure 3.6: Locations of Installed Screw-Nut Height Control Systems

Tightening the top screw decreased the vertical stress, while tightening the bottom screw increased the stress. The screws were tightened alternatively to not deviate too far from the desired vertical stress on the specimen, and repeated until all the systems were sufficiently tight. Tightening one side of the system created a bending moment in the system and had an impact on the shear stress recording. Screws on both sides were tightened evenly to minimize the moment; this was achieved by monitoring the shear load such

that it remained close to the value prior to installing the systems.

Three different diameters of steel threaded bars were used for the systems to have different Youngs Modulus: low, medium, and high stiffness. Low stiffness system uses threaded bar with diameter of 5/16 inch, medium stiffness system uses bar with diameter of 7/16 inch, and high stiffness system uses bar with diameter of 9/16 inch (figure 3.7). The system's stiffness was thought to be proportional to the cross-sectional area of the system (1 in^2 for the aluminum block and area of the threaded bar). Young's Modulus based on the dimensions of the threaded bar system is listed in table 3.1 as a ratio with the medium sized system. In addition, two 7/16 threaded bars, made with aluminum and brass, were used for comparison. Compared to steel, brass and aluminum have lower Youngs Modulus (typical Youngs Modulus for the materials are listed in table 3.2); therefore, the screw-nut system made of those materials should deform more compared to the one using the steel threaded bars.

Table 3.1: Young's Modulus Comparison of Height Control Systems with Different Diameter Threaded Bar

Diameter of Threaded Bar (inch)	Young's Modulus (Ratio with 7/16")
5/16	0.921
7/16	1
9/16	1.105

Medium sized system with steel threaded bars was used for monotonic tests with varying confining stress and for cyclic tests. Results from using

Table 3.2: Typical Young's Modulus for Materials Used for Threaded Bars

Material of Threaded Bar	Young's Modulus(GPa)
Steel	180
Brass	125
Aluminium	69

restraining system with different stiffness were compared to analyze the effect of height change on stress behavior.
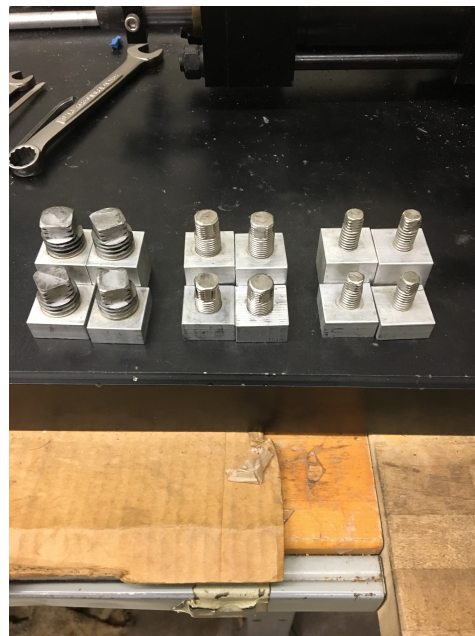

Figure 3.7: Sizes of Height Control systems
(Left:9/16", Center:7/16", Right:5/16")

3.3   Testing Materials

Cyclic simple shear tests were performed on Nevada sand, and mono-tonic simple shear tests were performed on Washed Mortar sand. Since the tests were performed on the same sand, properties were obtained from Kwan (2015).

Nevada sand used in this test is described as a uniform, fine size, angular sand with a mean size of about 0.2 mm and the tested soil ($C_c = 1.13$, $C_u = 2$) is classified as a uniform sand (SP)(Kwan, 2015). Table below shows the properties of Nevada sand from Kwan (2015), as well as from Kammerer et al. (2000) and Arulmoli et al. (1992).

Table 3.3: Properties of Nevada Sand (Kwan, 2015)

Source	G_s	$\gamma_{d,min}$ kN/m^3	$\gamma_{d,max}$ kN/m^3	e_{max}	e_{min}
Kammerer et al. (2000)	-	13.87	17.09	0.89	0.53
Arulmoli et al. (1992)	2.67	13.87	17.33	0.89	0.51
Kwan (2015)	2.67	15.14	17.09	0.76	0.56

Washed Mortar sand used is classified as a uniform sand (SP) (Kwan and El Mohtar, 2014) and relatively well grade and more angular soil (with more individual larger soil particles) (Kwan, 2015) compared to Nevada sand. Soil properties of Washed Mohtar sand are presented below.

Table 3.4: Properties of Washed Mortar Sand (Kwan and El Mohtar, 2014)

Sand	G_s	e_{max}	e_{min}	C_u	C_c
Washed Mortar	2.65	0.84	0.56	2.6	4.1

3.4 Test Set-Up

1. The membrane was placed on the bottom platen, and an O-ring was placed in the groove. The membrane had a diameter of 4 inches and thickness of 0.033 inches; using a thinner membrane caused issues with applying a tight vacuum later when preparing the specimen. The custom made brass base was firmly placed on the platen such that the openings lines up with the screw hole. A thick O-ring was placed on the top of the brass base.

2. The stacked rings were placed on top of the brass base. The rings have two holes to place the pin to prevent horizontal movements, and the pins that extended out the rings were placed in the indents on the brass base to keep them in place.

3. The split mold was placed on top of the stacked rings such that the vacuum valve lined up with the screw hole in the bottom platen for the internal shear LVDT. The special split mold made for Kwan (2015) that accommodates for the stacked rings were used for this project. The split mold was placed such that it was removable after the placement of the sample under the machine. The indents inside the split mold were

aligned with the pins extending from the stacked rings for a tight fit. An O-ring was placed on top of the split mold.

4. The vacuum line was connected to the split mold. Strong vacuum was applied and the membrane was folded over the split mold. The membrane was folded such that there were no creases in the membrane and there was a tight seal applied. Loose membrane or weak seal were caused by a leak; placements of the brass base and the O-rings were checked, and the membrane was examined for damage.

5. The specimen was created. Amount of sand needed to achieve target relative density, Dr, (30% for loose specimen, 70% for dense specimen) was calculated and placed in a bowl. The specimen was created using the dry funnel deposition method (DFD). The steps for this deposition method are discussed in section 3.5.

6. The specimen was carefully placed under the test set-up, as any excessive vibration could cause further densification of the specimen or an uneven specimen surface. The marks on the bottom platen were lined up with the marks on the bottom of the machine. Marks indicate the location the platen should be placed for the screw holes to line up.

7. The top platen was slowly lowered until it made contact with the sand face. This was done by placing a screw and nut between the vertical actuator and the platen system, and lowering the screw until the platen made contact with the specimen. Axial load was monitored while the

platen was being lowered; if the vertical load increased when the platen first entered the split mold, the specimen was not centered and it needed to be adjusted. The platen was lowered until the axial load read the weight of the actuator, at which point the screw system was removed.

8. The membrane was unfolded up around the top platen, and the O-ring placed on top of the mold was rolled up and placed in the groove on the platen.

9. The vacuum line was disconnected, and the split mold was disassembled and removed. The O-ring was placed in the groove on the top platen.

10. Internal vertical LVDTs and internal horizontal LVDT were installed. Membrane around the top platen was folded down so that the internal horizontal LVDT was making direct contact with the platen. The LVDTs were aligned such that they were normal to the surfaces they made contact with.

11. The pins were removed from the stacked rings.

12. The specimen was consolidated under K_0 condition. The vertical stress was applied by the normal actuator connected to the building air pressure system. Assuming that the top surface of the specimen is a circle with diameter of 4 inches, the vertical load was increased until the desired vertical stress was achieved.

Table 3.5: Vertical Stresses and Corresponding Axial Loads Used

Vertical Stress (kPa)	Corresponding Axial Load (N)
50	405.4
100	810.8
150	1216.2
200	1621.6

13. Screw and nut systems were installed between the normal actuator and the platen system to achieve constant volume condition. The process is discussed in section 3.2.1.

After the test was set up, final specimen density pre-test was calculated.

3.5   Sample Preparation

The material tested in this study consisted of cohesionless sand materials. The specimens were created using the dry funnel deposition (DFD) method. The tip of the funnel was placed at the bottom of the mold. The sand was placed in the funnel was released in a circular pattern to keep a constant height and the top surface even. To create a loose specimen, the funnel was raised slowly while maintaining drop height of almost zero. To create a dense specimen, the sand was deposited from a higher drop height, and was deposited in 2 layers. After the sand have reached half the target height, a custom made circular plate was placed on top of the specimen. This plate had the same diameter as the specimen with a metal rod attached to the center. A small vibratory table was flipped upside down and placed on top of the metal

rod to apply vibration to evenly compact the specimen. After satisfactory compaction, the plastic plate was removed, the second layer was deposited, and the compaction process was repeated. After the sand was deposited into the mold, the surface was leveled using a custom rod-bar apparatus (figure ??).

Figure 3.8: Custom Rod-Bar Apparatus Used to Level the Specimen Surface

3.5.1 Specimen Density Calculations

The specimen was shaped like a cylinder with a diameter of 4 inches and height of 1 inch. Small difference in height, diameter, or mass caused a significant difference in the calculated density of the specimen; therefore, it was crucial to get accurate fine measurements of the sample. The mass of the

sand was weighed using an electronic scale with the precision of 0.2 grams, and the caliper was able to measure up to one-thousandths of an inch.

Diameter of the specimen was measured as the inner diameter of one of the stacked rings minus the thickness of the membrane. The stacked ring was considered to have a constant diameter of 4.052 inches, and the thickness of the membrane was measured prior to every test to consider for wear down. The height of the specimen was measured from the top of the split mold to the platen, then subtracted the diameter of the leveling rod.

Once the specimens mass and volume was obtained, its density was calculated. In order to determine whether the specimen was in its loose or dense state, the relative density was obtained. Relative density is the ratio that compares a specimens density to the soils loosest and densest possible state. The relative density is calculated as follows:

$$n = 1 - \frac{\gamma_{specimen}}{G_s} \tag{3.1}$$

$$e = \frac{n}{1-n} \tag{3.2}$$

$$Dr = \frac{e_{max} - e}{e_{max} - e_{min}} \tag{3.3}$$

G_s is the specific gravity of the soil, n is the porosity, e is the void ratio, Dr is the relative density, and e_{max} and e_{min} are maximum and minimum void ratios for the soil, respectively. Soil properties of Washed Mortar sand and Nevada sand used for this calculations are listed below. (Kwan, 2015; Kwan and El Mohtar, 2014)

Table 3.6: Soil Properties of Washed Mortar sand and Nevada Sand (Kwan and El Mohtar (2014); Kwan (2015); Kammerer et al. (2000))

Sand Type	G_s	e_{max}	e_{min}
Washed Mortar	2.65	0.84	0.56
Nevada	2.67	0.89	0.53

After the sand specimen was placed under the test set-up and the top platen was lowered, some consolidation due to the weight of the vertical actuator occurred. To get the height of the specimen after lowering the platen, the measurement between the normal actuator and the top of the platen system was taken with the specimen in place, then compared to the same measurement with a metal block of known height placed under the platen, as shown in figure 3.9 and equation 3.4.

(a) Height Measurement With Metal Block   (b) Height Measurement With Sand Specimen
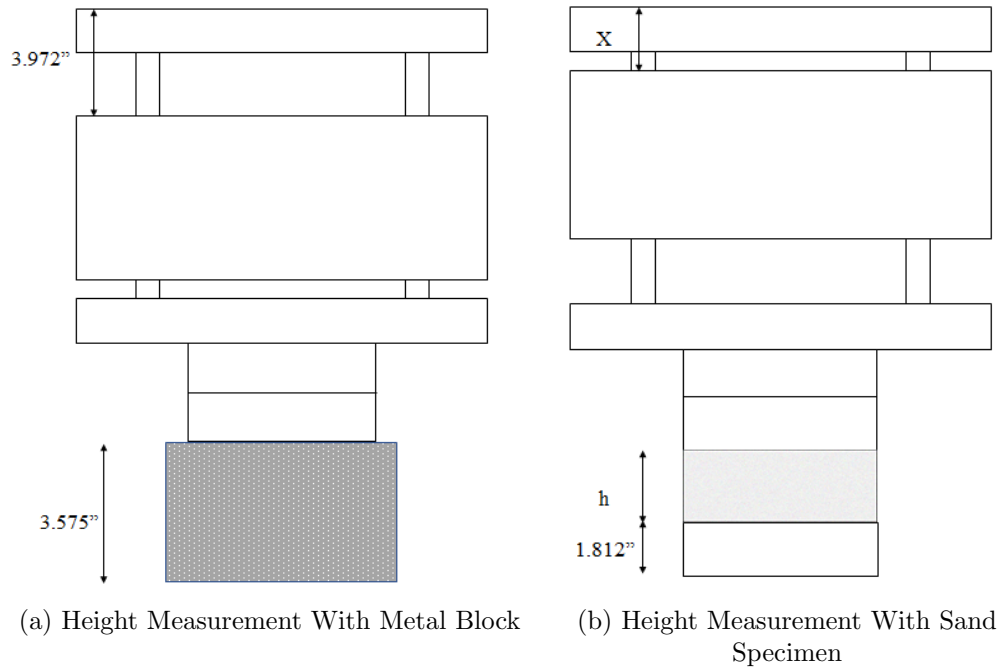
Figure 3.9: Specimen Height Calculation Method

$$h = 3.252 - (3.972 - x) - 1.812 \qquad (3.4)$$

When the metal block with the thickness of 3.252 inches was placed underneath, the distance between the top of the platen system and the normal actuator was 3.972 inches. This step was repeated after consolidation stress was applied, and this height of the specimen was used to calculate the final pre-shear density of the specimen.

3.5.2 Specimen Height Correction

The height of the specimen was measured from the top of the split mold to the platen, then subtracted the diameter of the leveling rod. The platen consisted of a pore stone with diameter of 3 inches in the center and tiny grooves surrounding it. The height of the specimen is measured to the top of the groove, so the actual volume of the specimen is larger than the calculated value. The height of the groove is measured on the outer edge of the platen where both the peak and the valley of the groove is visible. As shown in figure 3.10, the height of the groove is measured to be 0.042 inches. The distance between the peak and the pore stone was 0.035 inches. After considering the height correction of the groove, the correct volume of the specimen was calculated.
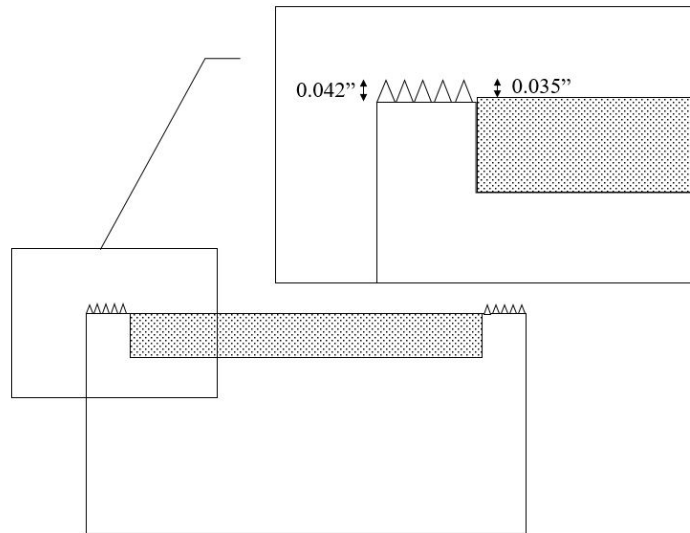
Figure 3.10: Drawing and Height Correction of the Platen

3.6 Testing Conditions Under Simple Shear

In a simple shear test set-up, the soil specimen is confined laterally, typically by a reinforced membrane or stacked rings. Previous studies (Baxter et al., 2010; Kwan and El Mohtar, 2014) have shown that test results that used reinforced membranes and stacked rings are comparable for both cohesive and cohesionless soils; for this study, stacked rings were used. Prior to applying the shear load, the specimen is consolidated to reach an at-rest condition. At-rest consolidation, or K_0 consolidation, is achieved by consolidating the specimen under normal load with a rigid lateral confinement.

Simple shear tests can simulate multiple real-world loading conditions such as slip surface of a slope failure and upward propagating seismic waves. To simulate the upward propagating wave, the specimen is sheared by the horizontal movement of the bottom platen. Shear displacement is measured as the relative movement of the bottom platen to the top platen, and from it the shear strain is calculated. Figure 3.11 shows the stress condition of the specimen under simple shear conditions.
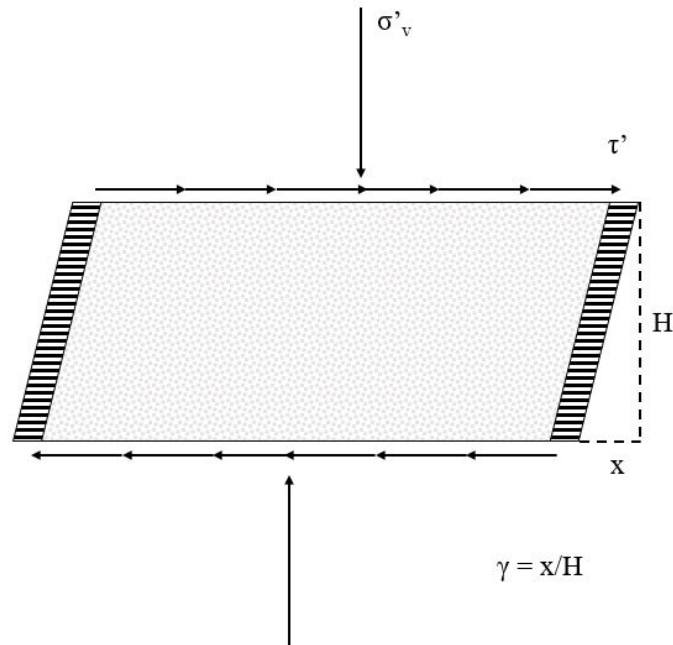
Figure 3.11: Stress Conditions Under Simple Shear

3.6.1 Monotonic Loading

Objective of monotonic simple shear test was to obtain the stress-strain behavior of the sand specimen. The specimen was subjected to monotonic loading. The specimen was consolidated to reach K_0 conditions, then sheared at a constant rate of 1% of specimen height per minute, or about 0.25mm/min, for 20 minutes. Under this test condition, the specimen was sheared enough to experience peak strength and reach critical state. Shear stress on the specimen during the constant rate of shear was recorded. Additionally, axial stress was also recorded during shearing of the specimen under constant volume conditions. Change in axial stress under constant volume condition corresponds to

the change in pore pressure under undrained condition, which is important when analyzing the liquefaction potential. Vertical movement of the platen was also monitored to make sure the testing condition remained constant volume. Vertical stress the specimen was consolidated under was altered to find the effect of confining stress.

Simple shear tests are usually loaded at a slower rate, especially for clay specimen to allow the excess pore pressure to develop or dissipate. The sand specimen for this test, since it is a dry specimen and pore pressure within sand dissipates almost immediately, was loaded at a quicker rate. Few simple shear tests loaded at a slower rate were also performed, and the results were compared with those from faster loaded tests and briefly discussed.

3.6.2 Cyclic Loading

Objective of this test was to find the number of cycles of constant stress cycles it took for the specimen to fail. The test was done under load control; specimen was consolidated under vertical stress of 100 kPa, then cyclic load of constant amplitude with a frequency of 0.2 Hz was applied to the specimen. The test continued until the displacement from the cyclic load exceeded 4.5 inches, which was the limit of the shear LVDT recording the displacement. From the data recorded, it was decided that the specimen reached liquefaction when the axial stress reached 5 kPa, or r_u value of 0.95; number of cycles it took to reach that state was recorded as number of cycles to reach failure, N_f. In addition, the shear moduli for each cycle until liquefaction were plotted

against its shear strain.

3.6.3   Consolidation

Objective of this test was to obtain the compression and recompression indices of the sand specimen. After the sample was placed under the simple shear testing equipment, changes in height of the specimen after a change in the vertical stress were monitored. Each change in the stress was done in 3 to 5 minutes to allow the specimen to fully consolidate; since it is a sand specimen, time it takes to fully consolidate was very short. Increase in vertical stress was in 50 kPa increments. After each increase, the vertical stress was decreased by more than 50 kPa to obtain a longer rebound curve, then increased back to the original value over 3 increments.

To plot the traditional consolidation curves, the void ratio of the specimen is calculated from the height and plotted against the change in vertical stress. For this research, the change in height of the specimen is directly plotted against the change in vertical stress, and the modified compression and recompression indices were obtained. The relationship between traditional and modified compression and recompression indices are presented in equations 4.1 and 4.2.

Chapter 4

Methods of Data Analysis

4.1 Introduction

This chapter will discuss the different data recorded during a simple shear test, and how they were used to analyze the result. Raw data recorded had to be altered/combined to deepen the understandings of the test results. Specifically, the loads were converted into stresses, displacements were converted into strains, and the shear modulus was calculated from shear stress and strain of each cycles of the cyclic test. Finally, the method to find the change in stress from volume change using the 1-D consolidation equation was discussed.

4.2 Data Calculation

The data from the test was recorded using the CATS software included in the SCON-2000 Universal Digital Signal Conditioning and Control Units used with GCTS testing equipment. The software was able to intake analog inputs from LVDTs, load cells, and pressure transducers, apply the appropriate corrections and calibration factors, and output engineering values that they represent. For each test, shear displacement, vertical displacement(Internal

Vertical LVDT, Normal LVDT), shear load, and axial load were recorded, then analyzed. The sensor placements can be found on figure 4.1.
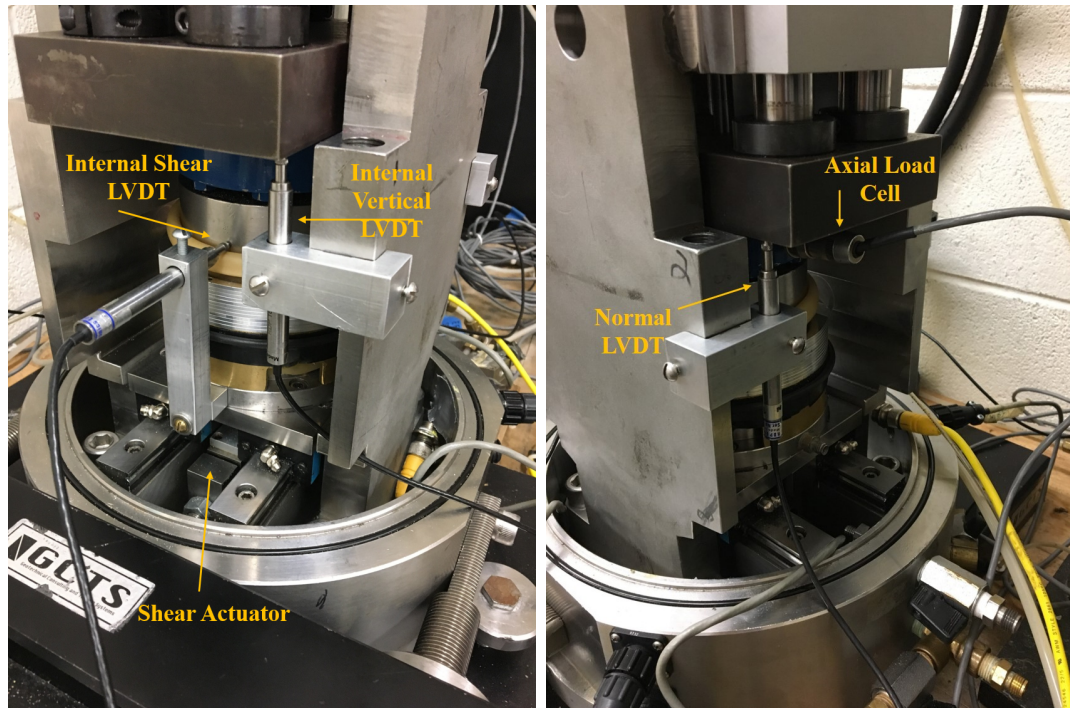
(a) Sensor Placements(Internal Vertical LVDT, Internal Shear LVDT, Shear Actuator)

(b) Sensor Placements(Normal LVDT, Axial Load Cell)

Figure 4.1: Sensor Placements

4.2.1 Axial/Shear Stress and Shear Strain

GCTS software recorded the load that the specimen experienced and the displacement it experienced under the tests. To convert the load values into stress values, the load values were normalized by the area of the top of the specimen, where the load was acting on. Shear strain, in contrast, was obtained by normalizing the shear displacement by the height of the specimen. The raw

load and displacement values were convert to stress and strain, respectively, to better understand and compare the stress state of the specimen at different points of the test.

4.2.2 Vertical Displacement and Tilting Correction

A vertical LVDT was placed on each end of the connection between the pneumatic actuator and the top platen. The LVDTs were connected from the steel walls, and they recorded the vertical movement of the top platen caused by the volume change of the specimen.

While analyzing the monotonic loading test results, tilting about the axis perpendicular to the direction of shear was observed from the vertical LVDT measurements. The LVDTs were placed on the ends of the bottom metal plates assuming that there was no tilting and both ends moved vertically the same amount. For some tests, that was not the case, as the LVDTs were showing motion in the opposite directions. Figure 4.2 shows a plot of one such case; Normal LVDT, placed in the front towards the direction of shear, was showing a dilative behavior, while the Internal Vertical LVDT, placed in the back, was showing a slightly contractive behavior. This behavior was more prominent in monotonic loading tests performed on dense specimen, which is due to its higher dilative tendency. Figure 4.3 shows the directions LVDTs were moving.
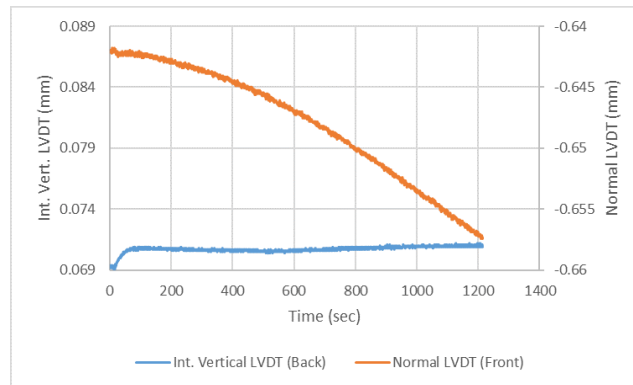
Figure 4.2: Example Plot of LVDTs Displaying Tilt(Test ID:170503)
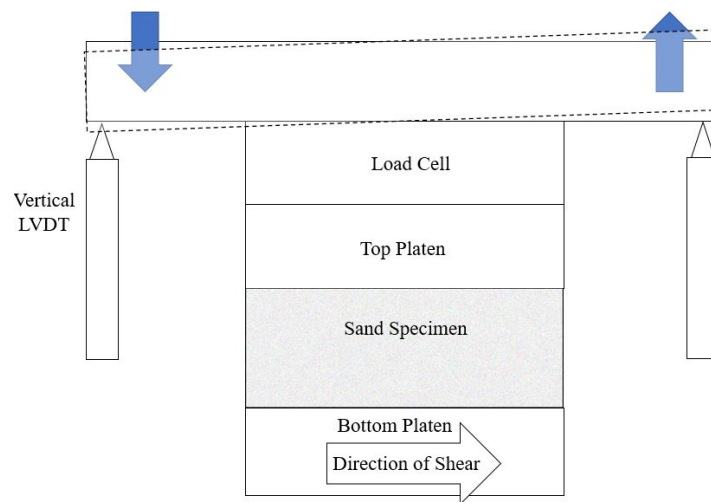
Figure 4.3: Drawing of the Tiling Behavior

To study the influence of the screw-nut height control system on tilting, a monotonic loading test was performed without the system. In this pseudo-constant stress condition, the LVDT data showed the vertical movement and tilting of the top platen purely from the equipment. Another monotonic load-

ing test was run in this pseudo-constant stress condition, this time with the vertical LVDT placed on the same end of the equipment (figure 4.4). LVDT data from this test was analyzed to check for tilting about the axis perpendicular to the direction of shear, as well as the effect from the differences in calibration factors of the LVDTs.

2 vertical LVDTs showed similar behaviors when the vertical restraints were removed (Figure 4.5a). However, the LVDT placed on the direction of the shear (Normal LVDT) showed smaller contractive behavior than the LVDT on the other end (Internal LVDT). Therefore, it was determined that the equipment was tilting in such way that Internal LVDT was compressed more than the Normal LVDT, as depicted in Figure 4.3. It was also shown that the height control systems were not the cause of the tilt, as the symptoms remained after removing the restraints.

Figure 4.5b shows the LVDT data from a test under the same conditions when they were both placed on the other side of the direction of shear. The displacements recorded by the LVDTs were practically identical. It showed that there was no tilting about the axis parallel to the shear direction, and the LVDT calibration factors were not the cause.
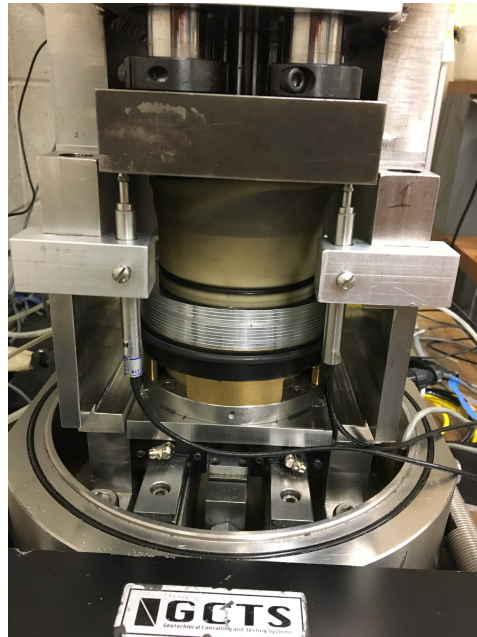
Figure 4.4: Placement of the LVDTs on the Same End
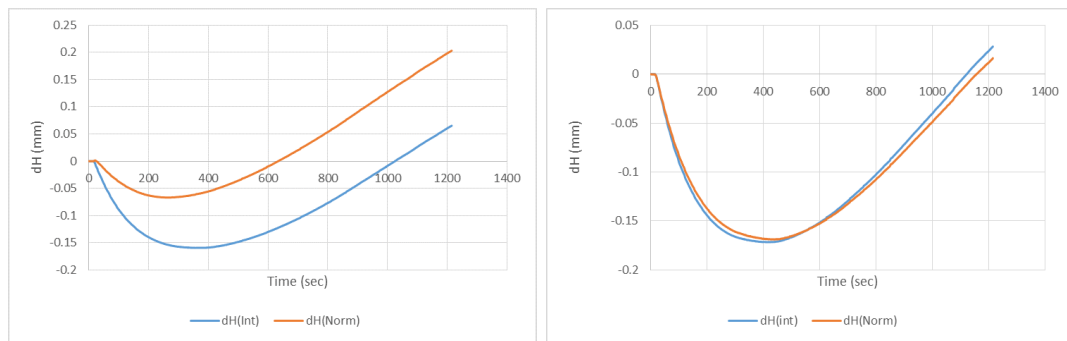
(a) LVDT Placed on Opposite Ends

(b) LVDT Placed on Same End(Figure 4.4)

Figure 4.5: LVDT Behaviors with No Vertical Restraints

After the discovery of tilting about the perpendicular axis, the vertical
LVDT data were corrected to reflect the vertical motion of the specimen. The

67

magnitudes of the vertical movement at the ends of the plate, while in the opposite direction, were small enough to be valid under the ASTM standard for a constant volume test, and the vertical movement due to the volume change of the specimen was calculated from the LVDT data using the geometry of the set-up (figure 4.6). The data from the two LVDTs were multiplied by the ratio of the diameter of the specimen to the length of the metal plate, then the average was taken of the two. The LVDT displacements were multiplied by the ratio to correct them to the displacement at the edge of the specimen, and the average of the values reflect the vertical movement caused by the volume change. Corrected vertical movement was similar to the data from the tests without tilting, as shown on figure 4.7. Maximum corrected vertical displacement was still under the 0.05% allowed by the ASTM standard, so the results from the tests were deemed valid.
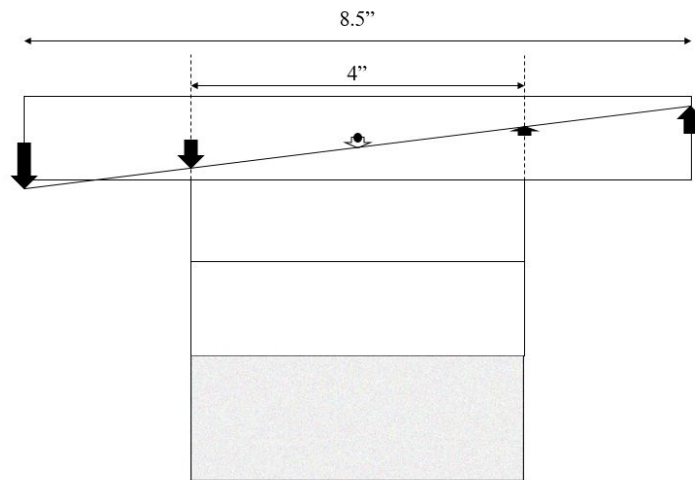
Figure 4.6: Drawing Explaining Tilt Correction
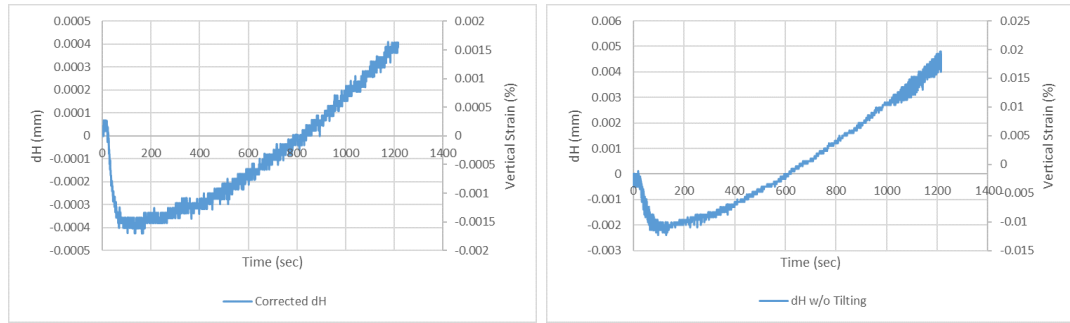
(a) Corrected LVDT Displacement (Test ID: 170621)
(b) LVDT Displacement without Tilting (Test ID: 170120)

Figure 4.7: LVDT Displacement Comparison Between Corrected and Without Tilting

4.2.3 Cyclic Stress Ratio

Cyclic stress ratio is the ratio between the cyclic stress amplitude and the effective confining stress. CSR for this report was reported as the ratio between the maximum shear stress, applied to the specimen prior to liquefaction or cyclic mobility, and the vertical effective stress prior to the application of the cyclic stress. Cyclic tests were performed under load control; therefore, the maximum shear stress should be the same for each cycle until the specimen experiences strength loss from failure, at which point the test was stopped. Under constant volume condition, the specimen experiences contractive behavior at small strains and the effective vertical stress decreases; therefore, the initial vertical stress applied for consolidation is the maximum vertical stress the specimen experiences during the test.

4.2.4 Shear Modulus

The shear modulus was calculated for each loading cycles of the cyclic test. The modulus was obtained by dividing the shear stress experienced by the specimen by the shear deformation it went through under said stress, as seen on figure 4.8. For each cycle, shear modulus was obtained by:

$$A_{stress} = 0.5(\tau_{max} - \tau min) \tag{4.1}$$

$$A_{strain} = 0.5(\epsilon_{max} - \epsilon_{min}) \tag{4.2}$$

$$G = A_{stress}/A_{strain} \tag{4.3}$$
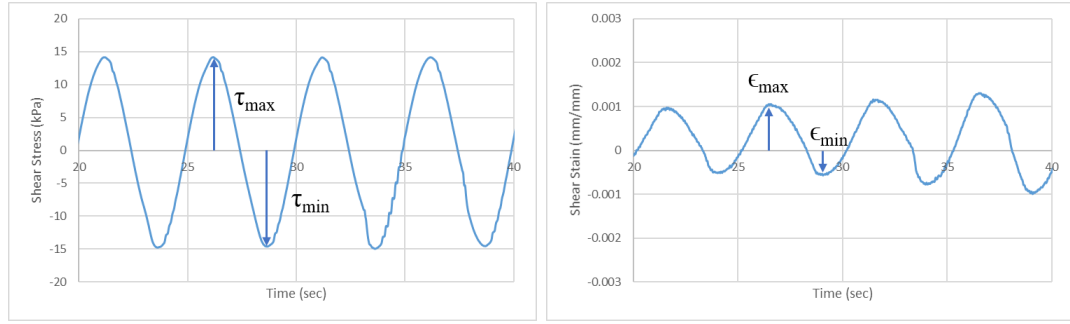
(a) Maximum and Minimum Shear Stress in One Cycle (b) Maximum and Minimum Shear Strain in One Cycle

Figure 4.8: A_{stress} and A_{strain} for Calculating Shear Modulus, G (Test ID:170217)

4.2.5 Compression Index and Vertical Stress

During the consolidation test, the change in height of the specimen with change in vertical stress was recorded. The height change was recorded by tak-

ing the difference between the vertical LVDT value after the stress change and the initial value, and was plotted against vertical stress in a semi-logarithmic scale (figure 4.9). Modified compression index and the recompression index were obtained from the stress-height plots; compression index was taken as the average of the slopes of the tangent lines before and after 100 kPa, and the recompression index was the average of the slopes of the rebound curves.
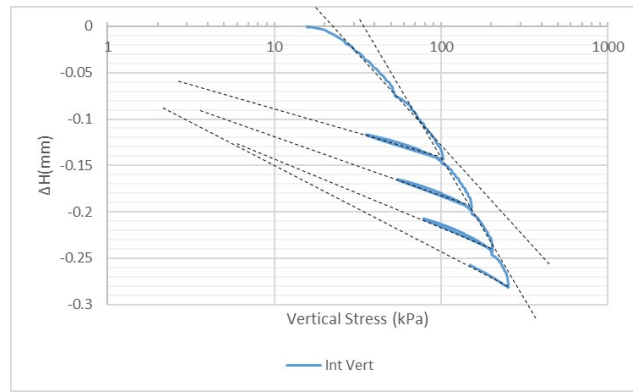
Figure 4.9: Example Modified Compression and Recompression Indices
(Test ID: 170411)

The modified indices were related to the traditional compression and recompression indices in the following way:

$$R_c = \frac{H_0}{1 + e_0} * C_c \tag{4.4}$$

$$R_r = \frac{H_0}{1 + e_0} * C_r \tag{4.5}$$

71

Chapter 5

Test Results and Analysis

5.1 Introduction

Results from monotonic and cyclic loaded simple shear tests on Nevada and Washed Mortar sand are presented in this chapter. Results from tests performed on loose and dense specimen are analyzed independently and concurrently. The test preparation steps are presented in section 3.4 and the details regarding each test are presented in section 3.6. Summaries of the tests and plots of individual tests are presented in Appendices 1

First, the one-dimensional consolidation test results are presented. The modified compression and recompression indices were obtained from these tests and used when discussing the remediation methods of the height change-stress reduction issues. The index values obtained from the tests are compared to the compression indices for granular materials presented in Mesri and Vardhanabhuti (2009).

Next, the simple shear test results from monotonic loading are presented. Results for each test, including the behaviors of axial stress, shear stress, stress ratio, and vertical displacement, are compared. Effects of consolidation stress on the shear behaviors of the specimen are analyzed. Effects of

72

vertical displacements on shear behavior are also analyzed by using different height-control devices to achieve constant volume conditions. By using devices with different dimensions or different threaded bar materials, the devices would have different Young's Modulus, thus would result in different vertical displacements under the same shearing conditions. While analyzing the monotonic test results, tilting of the equipment was discovered. This section will discuss how that was compensated for.

Finally, the simple shear test results from cyclic loading are presented. Behaviors of axial stress, shear strain, and cycles until failure (N_f) for different cyclic shear ratio (CSR) are compared for loose and dense specimens. CSR vs N_f curves are created and compared with the same curves presented in Kwan (2015), which performed the same cyclic tests under saturated, truly undrained condition. The trend of the curves with increase in CSR are analyzed.

5.2   Consolidation

One-dimensional consolidation tests were performed on sand specimens in the simple shear test equipment. Test was performed on both Nevada and Washed Mortar sand specimens at loose and dense densities. Change in specimen height with changing vertical stress was plotted, and the slopes of the curve were taken as the modified compression and recompression indices.

Figure 5.1 plots the modified consolidation curves for loose and dense Washed Mortar sand specimens. Consolidation curve for the loose WM sand specimen shows a steeper slope, therefore higher compression index, than the

73

curve for dense specimen. This agrees with the result presented in Mesri and Vardhanabhuti (2009). This also makes sense because dense tightly-packed specimens are more stiff than loose specimen, therefore the amount of height change would be less with the same change in vertical stress. Same trend is more visible for the consolidation curves for Nevada sand specimen, presented in figure 5.2.
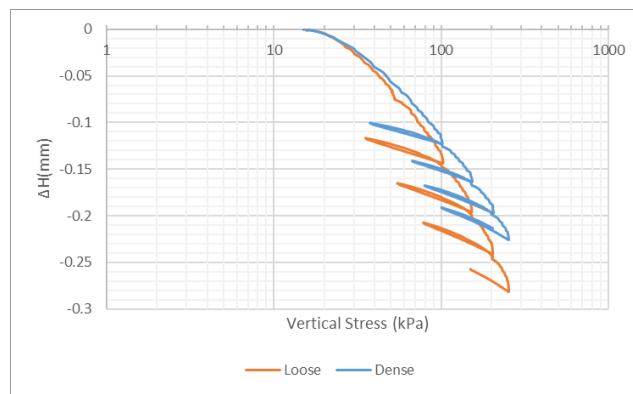
Figure 5.1: Compression Index of Loose and Dense Washed Mortar Sand
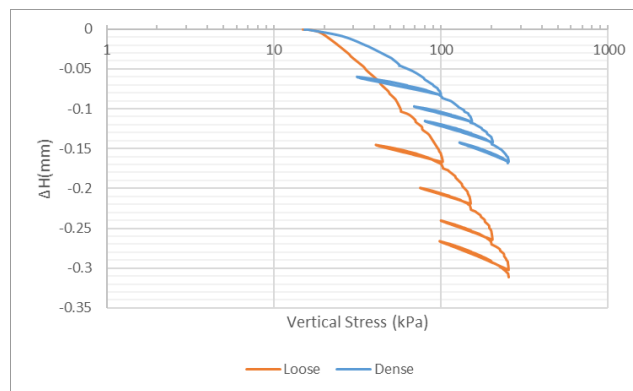
Figure 5.2: Compression Index of Loose and Dense Nevada Sand

Consolidation curve and the tangential lines for each test can be found

in Appendix 1.3. Modified compression indices are listed in table 5.1 below.

Table 5.1: Modified Compression Index for Washed Mortar sand and Nevada sand

Sand Type		R_c	R_r
Washed Mortar	Loose (Dr = 41.9%)	0.300	0.080
	Dense (Dr = 73.4%)	0.210	0.067
Navada	Loose (Dr = 32.7%)	0.278	0.072
	Dense (Dr = 80.6%)	0.168	0.058

To verify the results, modified compression indices obtained from the tests were compared with the curves presented in Mesri and Vardhanabhuti (2009) (figure 5.3). The curves present the traditional compression indices, where the values were obtained from void ratio vs vertical stress curve. For a valid comparison, values taken from the curve were converted into the modified indices using equations 4.4 and 4.5.
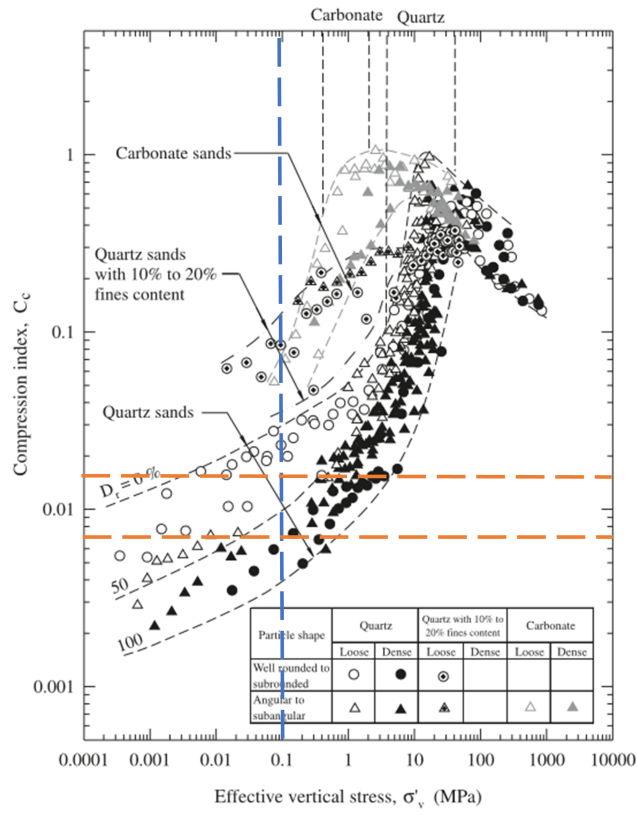
Figure 5.3: Compression Index of Loose and Dense Sand Specimens (from Mesri and Vardhanabhuti (2009))

Table 5.2: Modified Compression Index Calculated from Cc from Mesri and Vardhanabhuti (2009)

Sand Type	Density	$C_c from$ Figure 5.3	e_0	H_0 (mm)	R_c	R_c (Test)
Washed Mortar	Loose (40%)	0.017	0.71	26.2	0.306	0.300
	Dense (75%)	0.007	0.62	26.4	0.098	0.211
Nevada	Loose (40%)	0.017	0.77	27.0	0.259	0.278
	Dense (75%)	0.007	0.64	27.0	0.115	0.168

76

Compression indices for loose specimens showed good agreements with the values from figure 5.3. Compression indices for dense specimens, on the other hand, were much higher than the values calculated from figure 5.3 for both Washed Mortar and Nevada sand. This shows that the dense specimens prepared for this research were not as stiff as the dense specimens in Mesri and Vardhanabhuti (2009). Specimen stiffness could have an impact on the shear behaviors; softer specimens are more contractive and less dilative. Dense specimens that are not stiff are not able to reach high shear resistance, which will influence its liquefaction resistance.

5.3   Monotonic Loading

The sand specimens were loaded monotonically in the simple shear equipment under various conditions. Parameters that were altered to analyze their effects on the shear behavior were specimen density, vertical effective confining stress, and allowed height change. Data that were plotted against each other were axial and shear stress vs shear strain, vertical displacement vs shear strain, stress ratio vs shear strain, and axial stress vs shear stress.

The specimen was sheared at a constant strain rate of 1% of the height per minute. Specimens made of cohesionless soils are able to dissipate induced pore pressure almost immediately, therefore that loading rate was chosen. For comparison purposes, few monotonic loading tests were performed at a shear rate of 0.25% per minute. Figures 5.4 show the stress behaviors of the specimen loaded at a different rate.
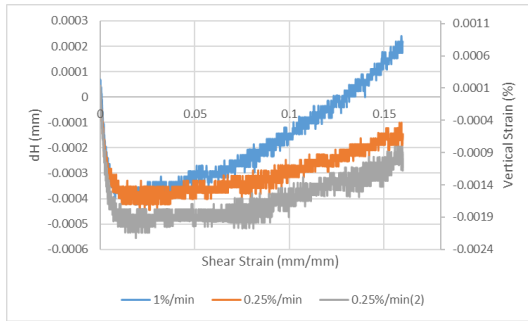
(a) dH vs Shear Strain for Loose Specimens
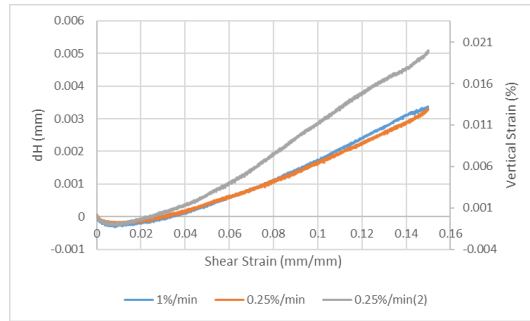
(b) dH vs Shear Strain for Dense Specimens
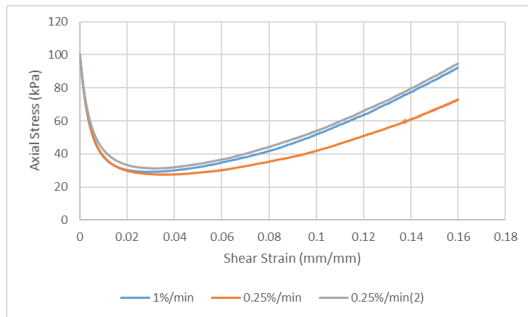
(c) Axial Stress vs Shear Strain for Loose Specimens
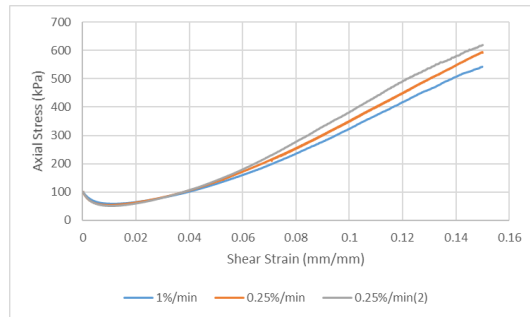
(d) Axial Stress vs Shear Strain for Dense Specimens
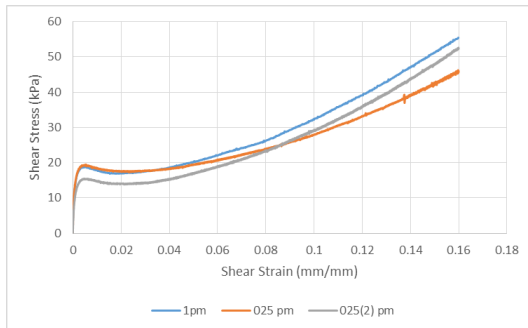
(e) Shear Stress vs Shear Strain for Loose Specimens
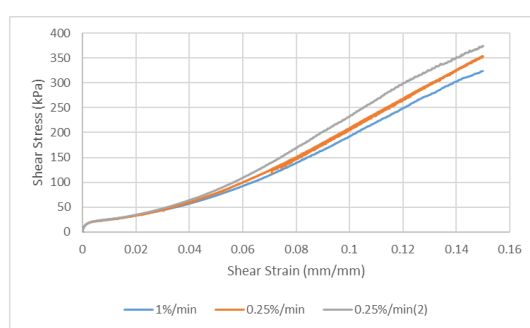
(f) Shear Stress vs Shear Strain for Loose Specimens

Figure 5.4: Monotonic Simple Shear Tests Comparing Shear Rates

Tests above show that strain rate does not have a discernible effect on

the stress behavior under shear. Based on the results, shearing rate of 1% per minute were used for the monotonic tests. Specimen height changes, on the other hand, generally agreed with the stress behavior. However, the effects of the specimen height change were different between loose and dense specimens; for loose specimens, larger dilative volumetric change led to a higher axial change, while the opposite was true for dense specimens.

5.3.1 Varying Vertical Effective Stresses

Monotonic simple shear tests were performed on Washed Mortar sand specimens at a shear rate of 1% per minute. The tests had varying vertical effective stress, meant to simulate different confining stresses the specimen is under. As discussed in Dyvik et al. (1987), for a constant volume test, the initial vertical stress the specimen is consolidated under is equivalent to the effective confining stress, and the vertical stress change the specimen experiences under shear is equivalent to the pore pressure generated in the saturated undrained condition. Undrained behavior of sand under different confining stresses were investigated by analyzing the change of axial stress, shear stress, and stress ratio with strain, as well as the relationship between axial and shear stress. General behavioral trends are discussed in this section, and the irregularity are attempted to be explained by looking at the vertical height change.

Figure 5.5 show axial and shear stress behaviors with shear strain for loose specimens. As expected, specimens initially showed contractive behav-

79

iors (decrease in effective axial stress) before starting to dilate (axial stress increase). Specimens with higher initial confining stresses maintained higher axial stresses through the entirety of the test; correspondingly, specimens with higher initial confining stresses also exhibited higher shear resistance.

(a) Axial Stress vs Shear Strain for Loose Specimen

(b) Shear Stress vs Shear Strain for Loose Specimen
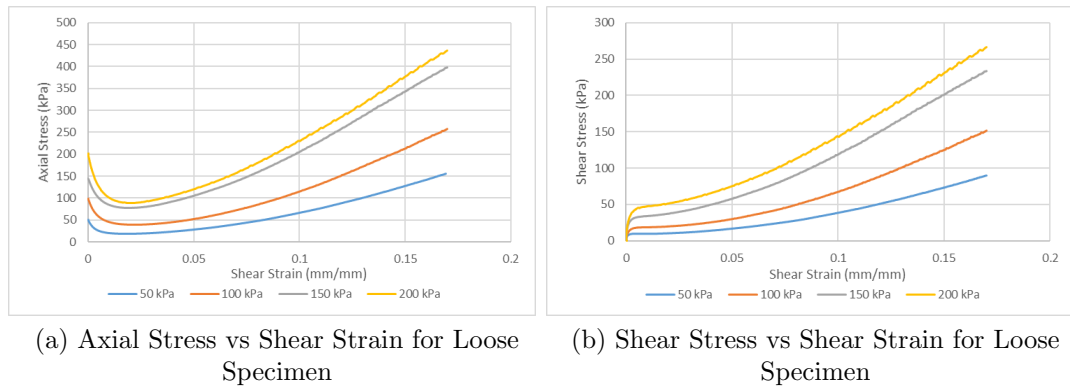
Figure 5.5: Stress-Strain Behavior of Loose Specimens Under Varying Vertical Confining Stress

To better understand the undrained behavior of the specimen under monotonic shear, change in axial stresses were plotted against strain in figure 5.6. Since the change in axial stress under constant volume condition corresponded to the pore pressure generated under undrained condition, it was plotted similar to generated pore pressure; negative change in axial stress was treated as positive generated pore pressure, and positive change as negative generated pore pressure.

$$\Delta u = \sigma_v - \sigma_v' \tag{5.1}$$

The figure showed that increase in confining stress resulted in larger magnitudes of generated excessive axial stress for both contraction and dilatancy.
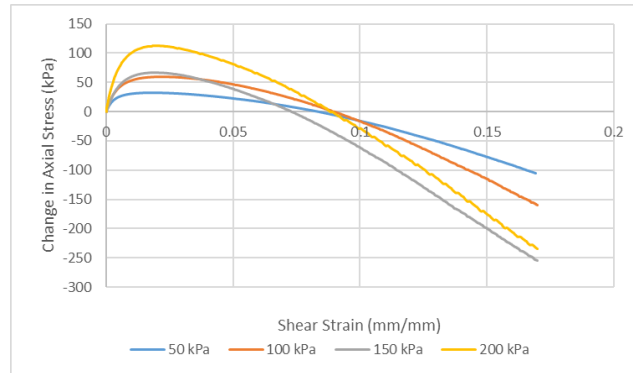
Figure 5.6: Change in Axial Stress vs Strain for Loose Specimens Under Varying Vertical Stress

The changes in heights of the specimens with shear strain were plotted in figure 5.7. Given the standard given in ASTM D6528, height change up to 0.05%, or roughly 0.013mm, was allowed to be considered a constant volume test. While all the tests were qualified as a constant volume test under the guideline, the height changed differently, which may have some effect on the stress behavior.
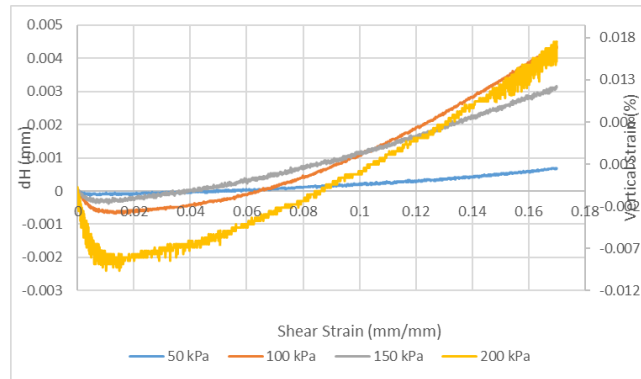
Figure 5.7: Change in Specimen Height vs Strain for Loose Specimens Under
Varying Vertical Stress

The specimen under 200 kPa vertical stress underwent larger height
change compared to the other specimens. The specimen under 50 kPa vertical
stress, on the other hand, experienced very small height change. Specimens
under 100kPa and 150 kPa, while not displaying as large contraction, dilated
as much as the 200 kPa specimen.

In figure 5.9, minimum and maximum height changes for each test
were presented along with its maximum and minimum axial stress changes,
respectively. Minimum height change and the maximum axial stress change
were found at the point where the specimen reached its peak contraction,
while the maximum height change and minimum axial stress change were
where the specimen reached its peak dilation up to a certain strain. The
contractive measurements were measured from zero to the peak, while the
dilative measurements were measured from the peak to the chosen strain, as
shown in figure 5.8. The maximum and minimum specimen height changes

82

were listed along with the axial stress change in table 5.3.
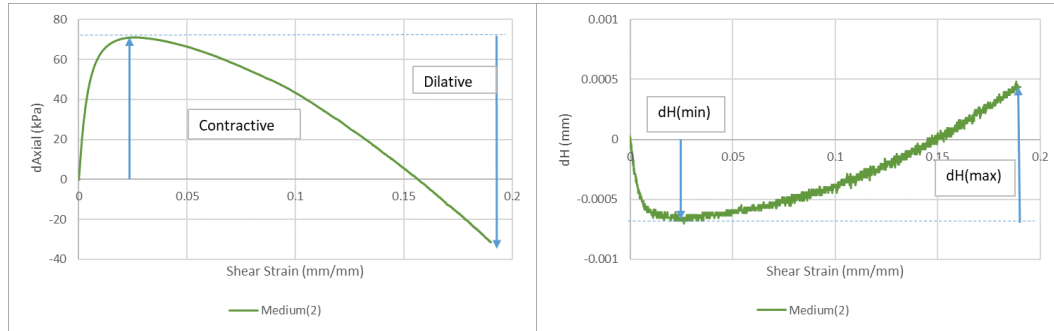
(a) Locations of Maximum Contractive and Dilative Stresses

(b) Axial Stress vs Shear Strain for Loose Specimen

Figure 5.8: Locations of Maximum Contractive and Dilative Behaviors

Table 5.3: Maximum Contraction and Dilation Values Obtained From Monotonic Simple Shear Tests on Loose Specimens Under Varying Confining Stresses(Up to 17 %)

Test ID	$\sigma_{v,i}$ (kPa)	$\Delta\sigma_{v,max}$ (kPa)	$\Delta\sigma_{v,min}$ (kPa)	ΔH_{min} (mm)	ΔH_{max} (mm)
170702	50	31.8	-137.9	-0.0001	0.00083
170416	100	59.1	-218.5	-0.0007	0.00503
170503	150	66.9	-321.6	-0.0004	0.00354
170120	200	112.6	-347.1	-0.0024	0.00690

(a) Maximum Contractive Height and Stress
Behaviors

(b) Maximum Dilative Height and Stress
Behaviors
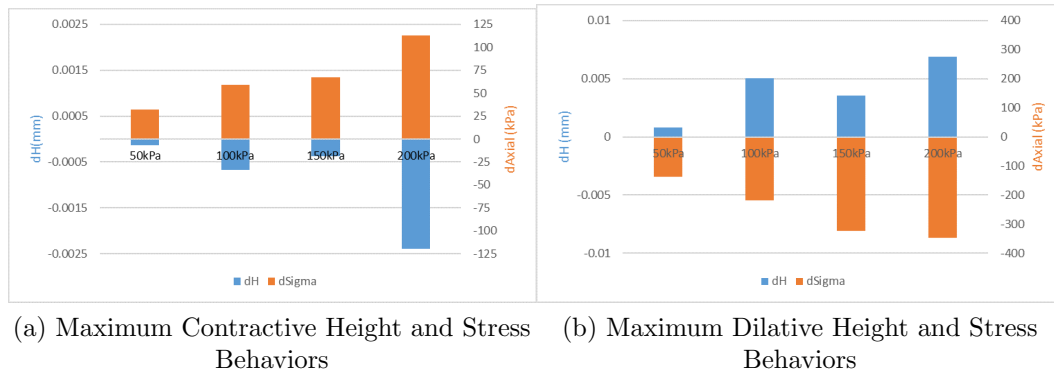
Figure 5.9: Contractive and Dilative Behaviors of Loose Specimens
(Left to Right: 50 kPa, 100 kPa, 150 kPa, 200 kPa)

As the initial vertical stress increased, magnitudes of maximum change in axial stress also increased. This agreed with the fact that the contractive tendencies of a specimen is increased as the confining stress increased. However, the increase in confining stress should also decrease the dilative tendencies of the specimen, whereas in this case the test with the highest initial vertical stress also had the highest dilative stress change. For loose specimens, increase in initial vertical stress increased both the contractive and dilative stress behaviors.

Finally, figure 5.10 plots the stress ratio of axial and shear stresses with strain, as well as axial stresses against the shear stress. From these plots, it can be concluded that the initial vertical confining stress has no bearing on the critical state of the specimen.
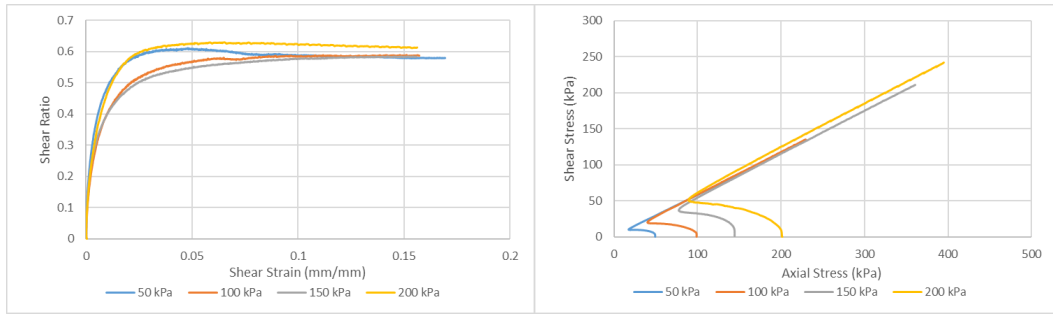
(a) Stress Ratio vs Shear Strain for Loose Specimen

(b) Axial vs Shear Stress for Loose Specimen

Figure 5.10: Stress Ratio and Critical State Line for Loose Specimen Under Varying Vertical Stress

Figures 5.11 through 5.13 plot the test results for dense specimen.

(a) Axial Stress vs Shear Strain for Dense Specimen

(b) Shear Stress vs Shear Strain for Dense Specimen

(c) Change in Axial Stress vs Strain for Dense Specimens

(d) Change in Specimen Height vs Strain for Dense Specimens
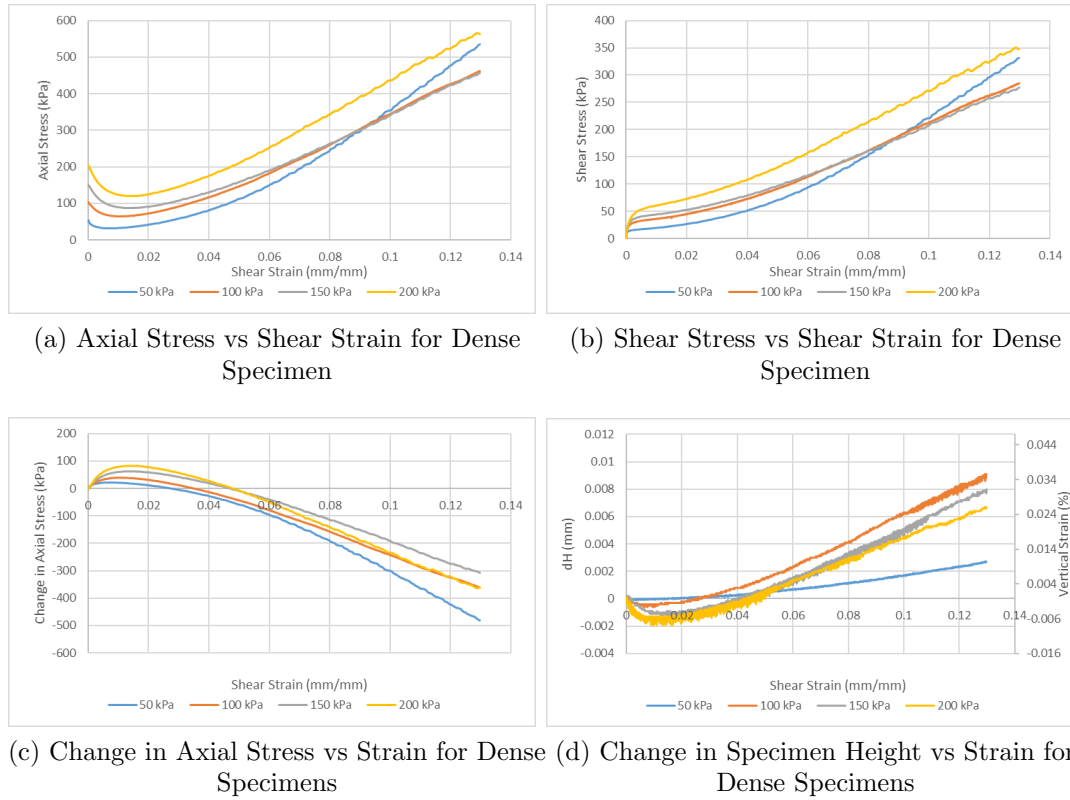
Figure 5.11: Stress-Strain Behavior of Dense Specimens Under Varying Vertical Confining Stress

Table 5.4: Maximum Contraction and Dilation Values Obtained From Monotonic Simple Shear Tests on Dense Specimens Under Varying Confining Stresses(Up to 13 %)

Test ID	$\sigma_{v,i}$ (kPa)	$\Delta\sigma_{v,max}$ (kPa)	$\Delta\sigma_{v,min}$ (kPa)	ΔH_{min} (mm)	ΔH_{max} (mm)
170505	50	21.3	-503.3	-0.0001	0.0028
170123_2	100	38.7	-398.7	-0.0006	0.0097
170124	150	62.5	-369.6	-0.0015	0.0095
170125	200	82.8	-446.1	-0.0019	0.0086

(a) Maximum Contractive Height and Stress Behaviors

(b) Maximum Dilative Height and Stress Behaviors
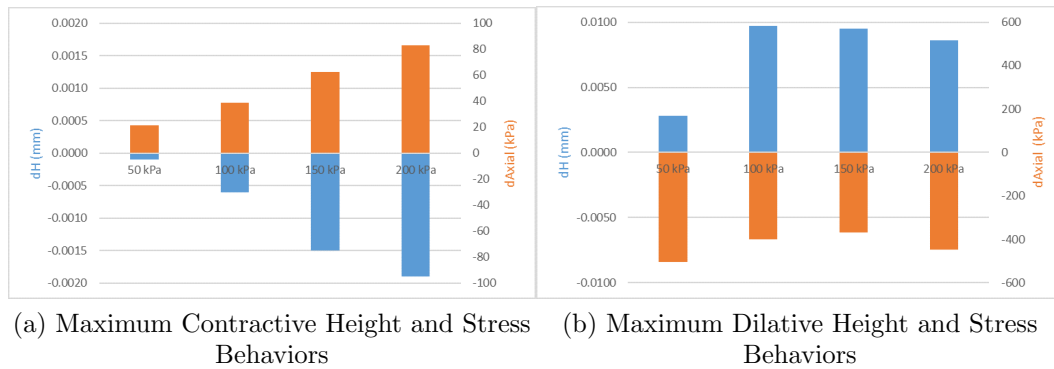
Figure 5.12: Contractive and Dilative Behaviors of Dense Specimens
(Left to Right: 50 kPa, 100 kPa, 150 kPa, 200 kPa)

(a) Stress Ratio vs Shear Strain for Loose Specimen

(b) Axial vs Shear Stress for Loose Specimen
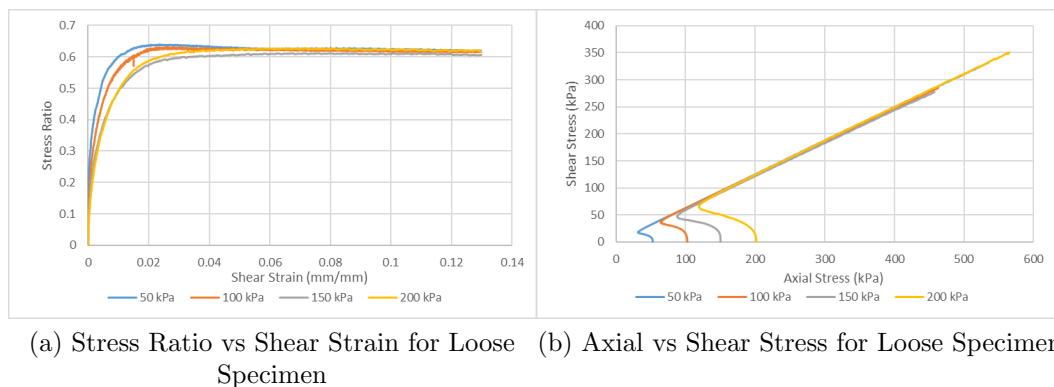
Figure 5.13: Stress Ratio and Critical State Line for Dense Specimen Under Varying Vertical Stress

Dense specimens under monotonic shearing exhibited mostly similar behaviors to their loose counterparts to a higher magnitude. As the confining stress increased, the contractive behavior of the specimen also increased. One different behavior observed in these plots was the dilative behavior of the specimen under 50kPa. At high strains, 50 kPa specimen generated greater

87

magnitude of excess axial stress compared to specimens under higher vertical stresses, resulting in higher shear resistance as well as greater range of change in stress. This could be attributed to the change in height of the specimen. Overall, dense specimens underwent larger height increase during dilation than the loose specimens. Within the dense specimens, specimens under 100 kPa, 150 kPa, and 200 kPa increased their heights 3 to 4 times the amount 50 kPa specimen increased. It was hypothesized that the magnitude of height change was a contributing factor in the difference in axial stress change.

As with the loose specimen, the initial vertical stress did not seem to have an effect on the critical state.

5.3.2   Varying Stiffnesses of Height Control Systems

To investigate the effect height change has on stress behavior under shear, screw-nut height control systems with differing properties were used. Changing the height-control systems dimensions and materials altered the Youngs Modulus, therefore allowing different height change under the same conditions. The specimens were initially consolidated to vertical stress of 100 kPa, then sheared at 1% per minute for 20 minutes.

Figures 5.14 through 5.15 compares monotonic loading tests ran using different sizes of screw-nut height control systems.
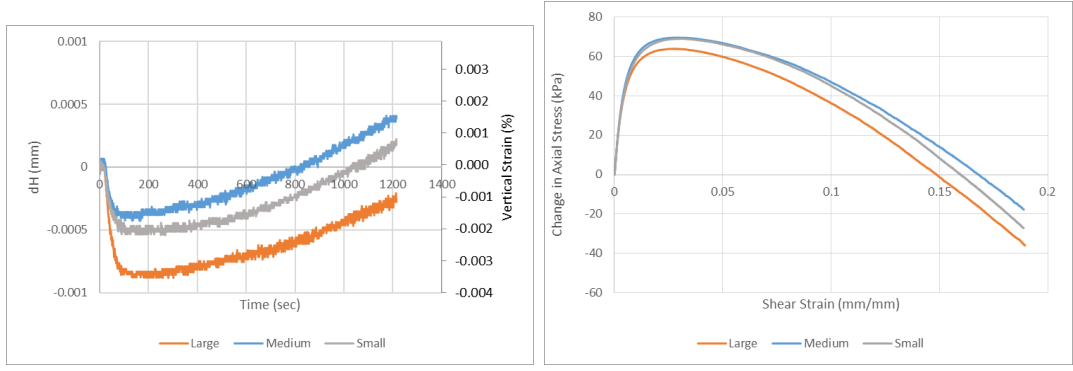
(a) Change in Specimen Height vs Strain for Loose Specimens

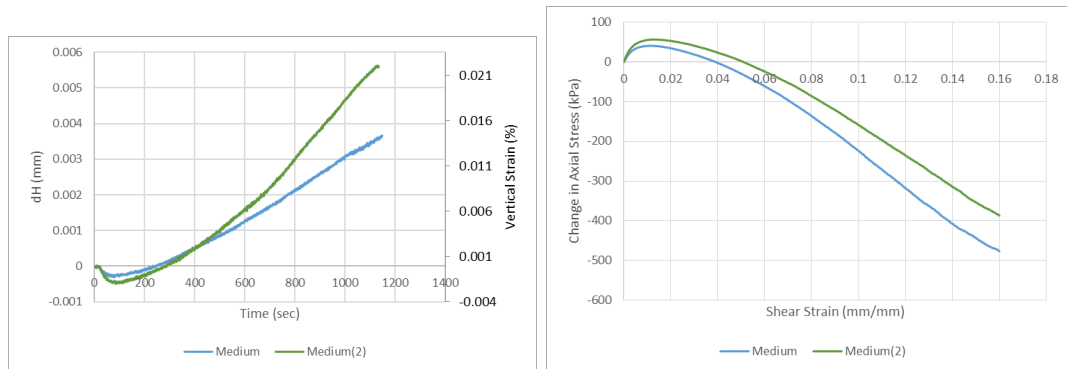(b) Change in Axial Stress vs Shear Strain for Loose Specimen
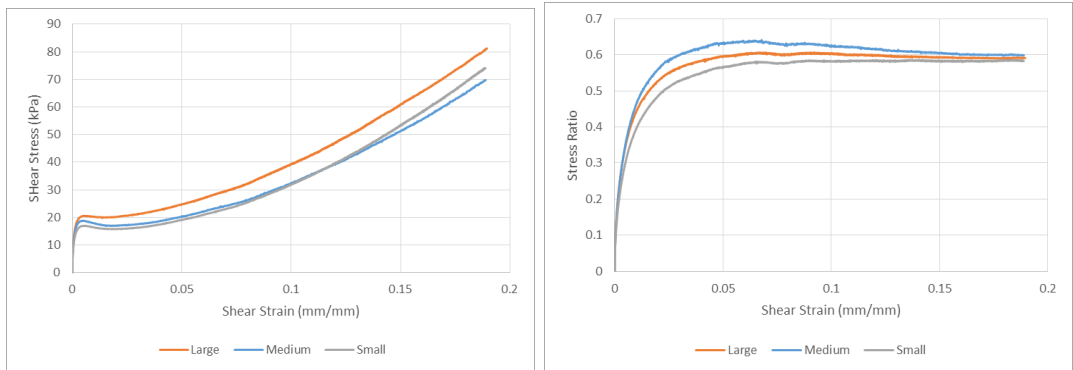
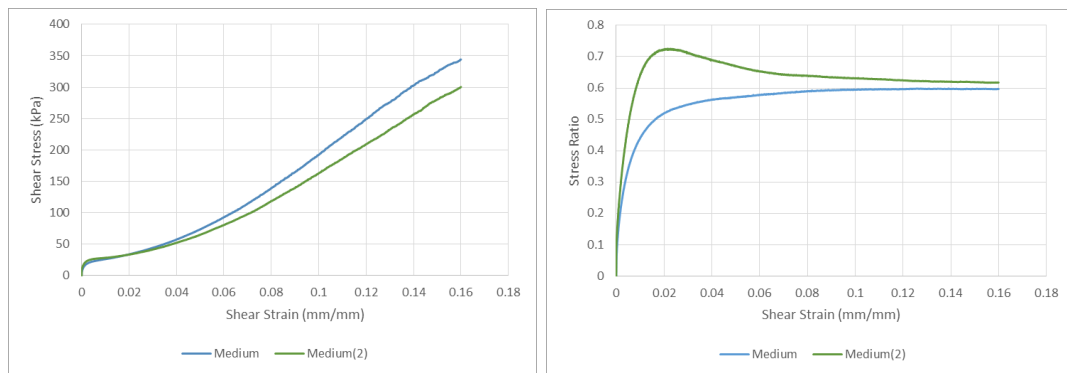(c) Shear Stress vs Shear Strain for Loose Specimen

(d) Stress Ratio vs Shear Strain for Loose Specimen

Figure 5.14: Stress-Strain Behavior of Loose Specimens Using Height Control Systems of Different Sizes
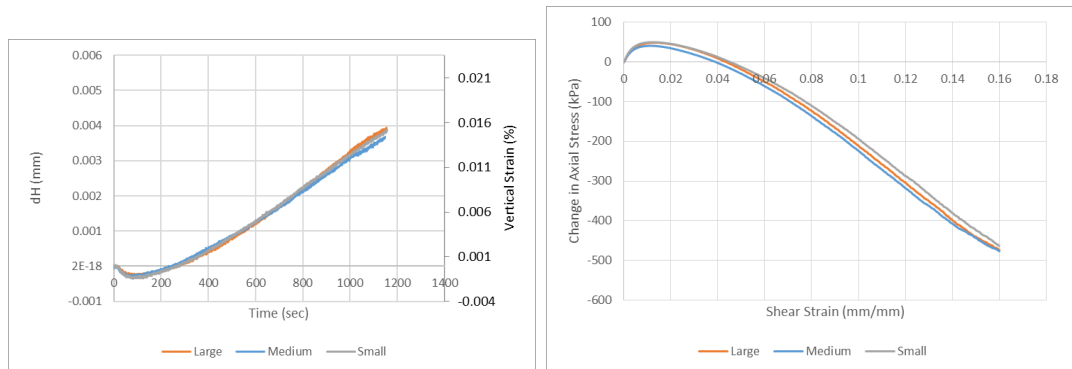
(a) Change in Specimen Height vs Strain for Dense Specimens

(b) Change in Axial Stress vs Shear Strain for Dense Specimen
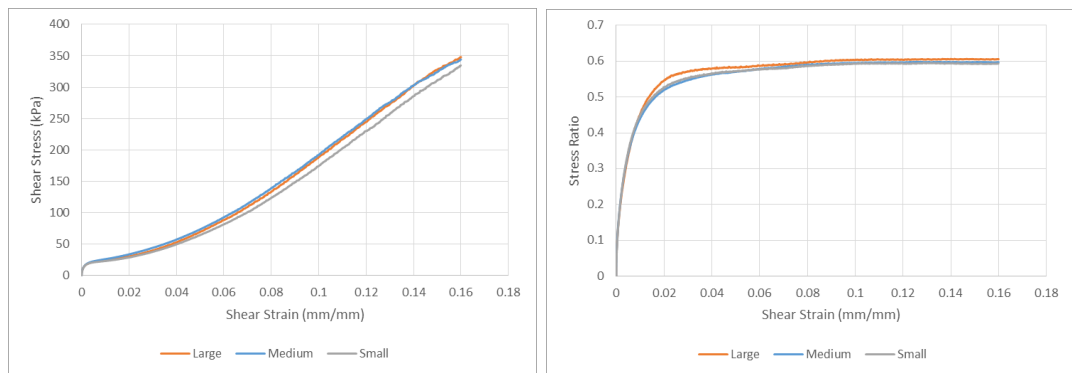
(c) Shear Stress vs Shear Strain for Dense Specimen

(d) Stress Ratio vs Shear Strain for Dense Specimen

Figure 5.15: Stress-Strain Behavior of Dense Specimens Using Height Control Systems of Different Sizes

Loose specimens showed varying magnitudes of volumetric contraction, which made it ideal to compare the effect of contraction on stress. The test using the largest screw-nut system showed the largest contractive behavior as well as the least positive pore water pressure generated and the highest shear resistance. Due to its size, this system displayed the most resistance

90

during tightening, therefore ended up the loosest of the three. Volumetric contraction decreased the amount of generated pore pressure, thus leading to an overestimation of the effective axial stress and shear strength of the specimen.

The behavior of the dense specimens were too similar to analyze the effects, but they provided the assurance that the tests were repeatable and comparable with each other. Overall, the size of the threaded bars did not have the intended effects of significantly changing the devices Youngs Modulus, but it did change the amount of specimen contraction for the loose specimens.

Figures 5.16 through 5.17 compares monotonic loading tests ran using different materials of threaded bars for the screw-nut restraining systems. As stated on Table 3.2, aluminum has the lowest Youngs Modulus and steel (used in Medium test) has the highest Youngs Modulus, with brass in the middle.
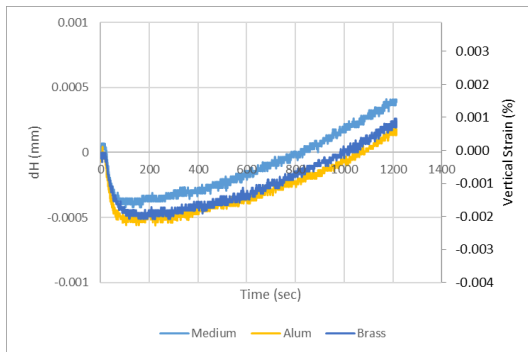
(a) Change in Specimen Height vs Strain for Loose Specimens
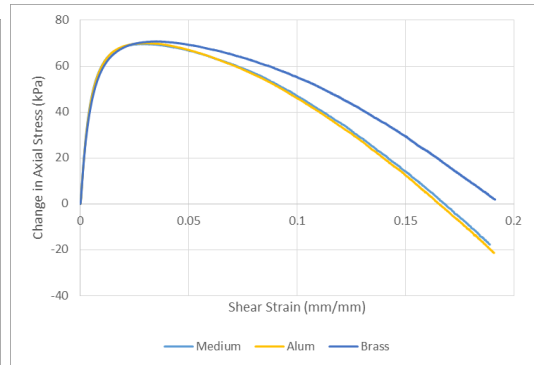
(b) Change in Axial Stress vs Shear Strain for Loose Specimen
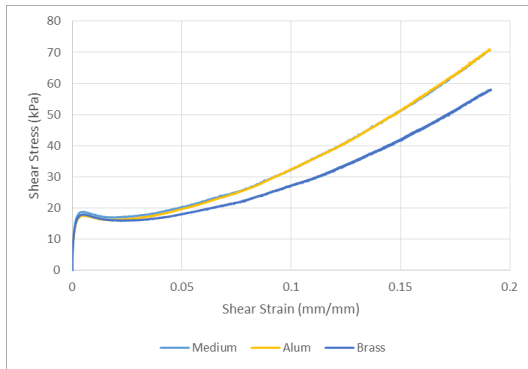
(c) Shear Stress vs Shear Strain for Loose Specimen
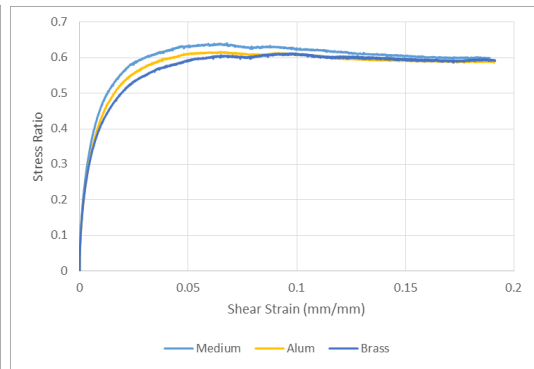
(d) Stress Ratio vs Shear Strain for Loose Specimen

Figure 5.16: Stress-Strain Behavior of Loose Specimens Using Height Control Systems of Different Threaded Bar Materials
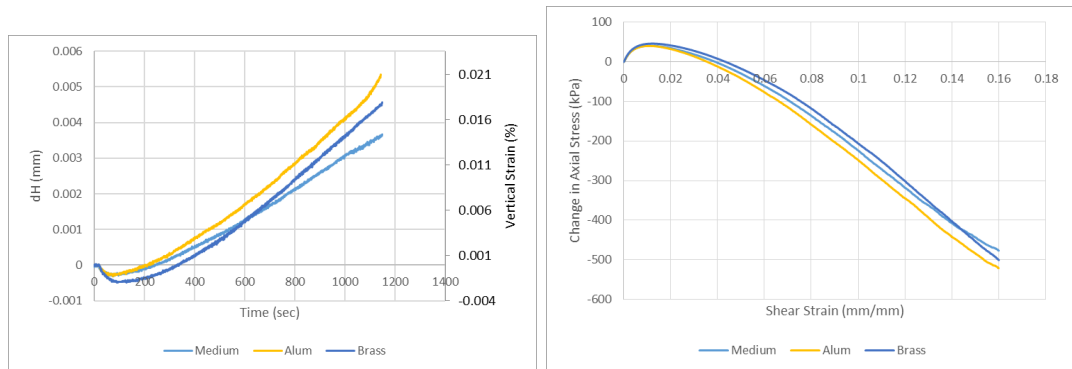
(a) Change in Specimen Height vs Strain for Dense Specimens

(b) Change in Axial Stress vs Shear Strain for Dense Specimen
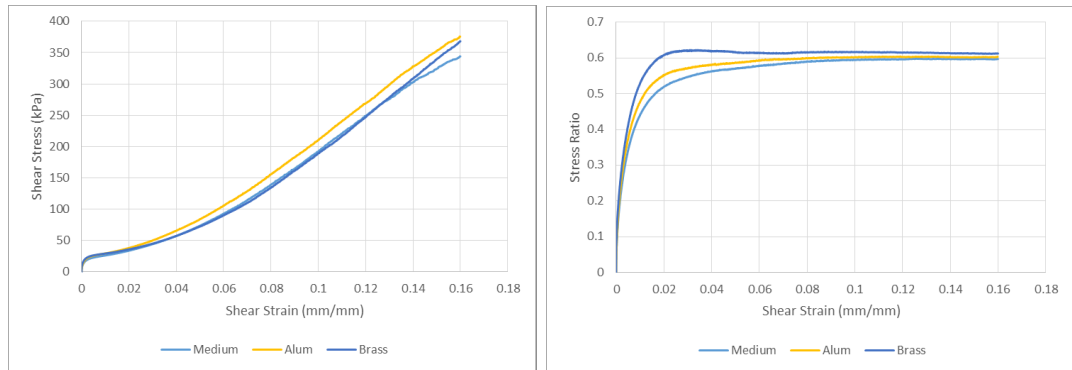
(c) Shear Stress vs Shear Strain for Dense Specimen

(d) Stress Ratio vs Shear Strain for Dense Specimen

Figure 5.17: Stress-Strain Behavior of Dense Specimens Using Height Control Systems of Different Threaded Bar Materials

The height change of the specimens corresponded to the stiffness of the threaded bar of the system. For the loose specimens, aluminum system experienced the most volumetric contraction, and steel system the least. For the dense specimens, aluminum system experienced the highest volumetric dilation at high strain, and steel system the least. Stress behaviors of dense

93

specimens agreed with the changes in specimen heights; however, the specimen which experienced the highest volumetric dilation also experienced the highest dilative stress change, and the opposite was true as well.

Finally, figures 5.18 through 5.19 compares two tests, both of which used medium size steel height-control system. The screw systems used for Medium (2) test were less tight compared to those for Medium test, allowing more height change to the specimen.
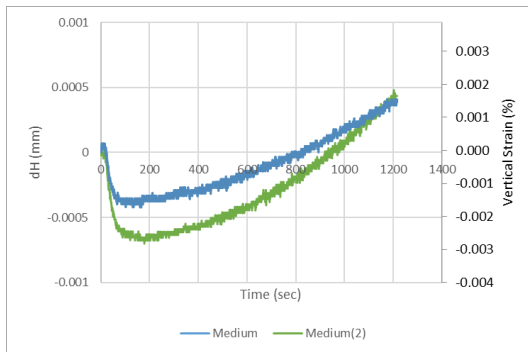
(a) Change in Specimen Height vs Strain for Loose Specimens
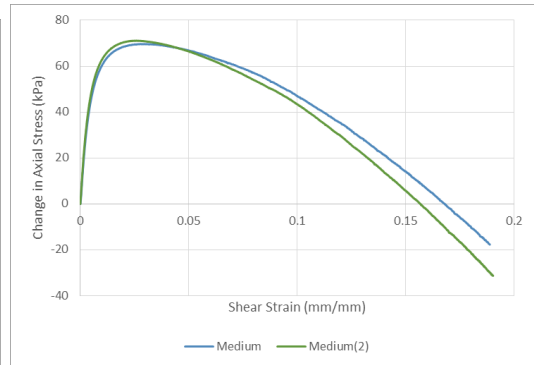
(b) Change in Axial Stress vs Shear Strain for Loose Specimen
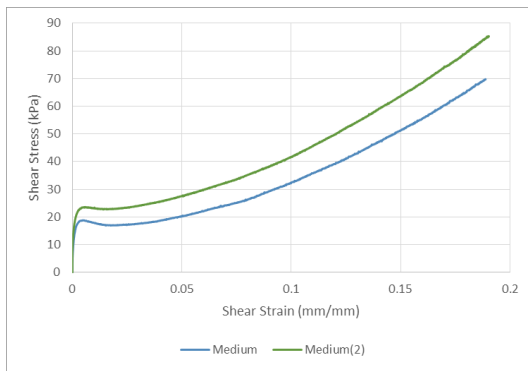
(c) Shear Stress vs Shear Strain for Loose Specimen
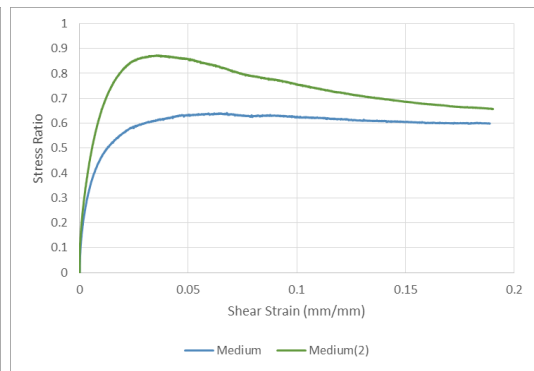
(d) Stress Ratio vs Shear Strain for Loose Specimen

Figure 5.18: Stress-Strain Behavior of Loose Specimens Using Height Control Systems Tightened Differently

(a) Change in Specimen Height vs Strain for Dense Specimens

(b) Change in Axial Stress vs Shear Strain for Dense Specimen

(c) Shear Stress vs Shear Strain for Dense Specimen

(d) Stress Ratio vs Shear Strain for Dense Specimen

Figure 5.19: Stress-Strain Behavior of Dense Specimens Using Height Control Systems Tightened Differently

By altering the amount of vertical restraints imposed by the height-control system, the stress behavior of the specimen is changed. For tests with less tight systems on both loose and dense specimens, a peak can be observed on the stress-ratio vs strain plots. The peak resembles the peak strength that might be observed in shear stress vs strain plots from drained

96

tests on loose sand specimens. It should be noted that, even at the point of maximum volumetric dilation, the height change remained under the allowed 0.05% by the ASTM guideline. Even while remaining under the guideline, stress behavior of a specimen changed drastically.

Maximum and minimum height changes and axial stress changes from each of the tests in this section (except Medium (2)) were plotted in figures 5.20 and 5.21. This was done to find a trend between the maximum and minimum height changes with the contractive and dilative behaviors.
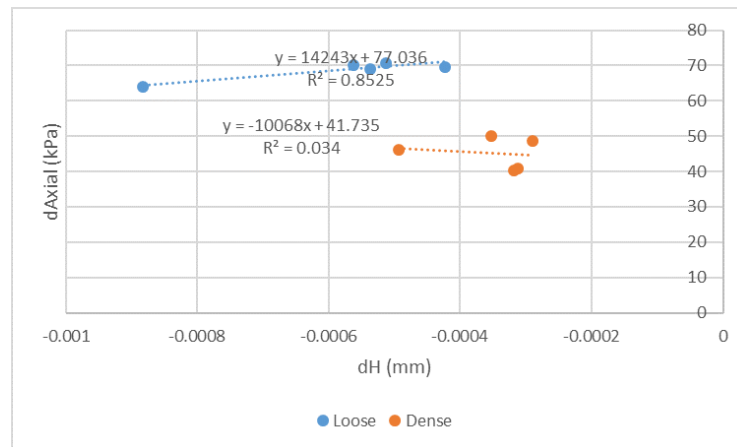
Figure 5.20: Maximum ΔH vs $\Delta\sigma_v$ for Contractive Behaviors

97
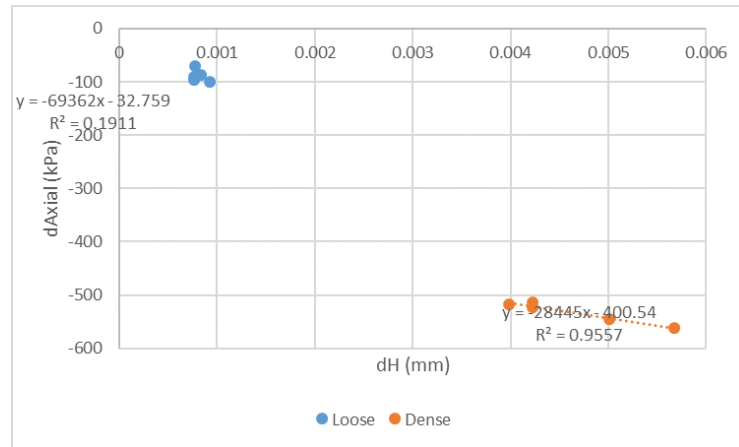
Figure 5.21: Maximum ΔH vs $\Delta\sigma_v$ for Dilative Behaviors

Contractive stress behaviors of loose specimens decreased as the magnitude of the height change increased. This result agreed with the idea that contractive volumetric behavior is decreasing the amount of positive generated pore pressure required for the specimen to maintain equilibrium. Dilative stress behaviors of dense specimens, on the other hand, increased as the magnitude of the height change increased. This result corresponds with the shear behavior trends if the stiffness of the height-control systems were treated similarly to confining stress. As the effective confining stress on dense specimens increase, the dilative behavior is reduced. In this test result, two height-control systems with the smallest Youngs Modulus, aluminum and brass, also had the largest dilative volumetric and stress behaviors. It cannot be concluded whether the larger contractive stress caused the large height change or the opposite; however, it can be said that, for dense specimens at large shear strains, tests using the least stiff vertical restraining system experienced the

largest dilative behaviors for both stress and volume.

For comparison purpose, results from section 5.3.1 were also plotted in the same manner in figures 5.22 and 5.23. The axial stress was normalized by the initial vertical stress.
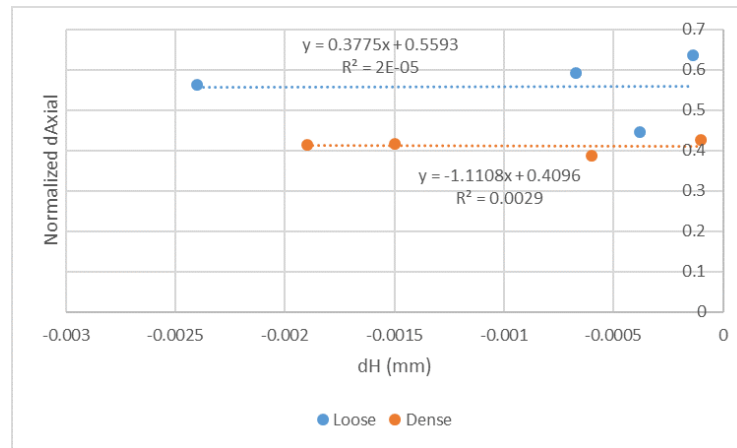
Figure 5.22: Maximum ΔH vs Normalized $\Delta\sigma_v$ for Contractive Behaviors
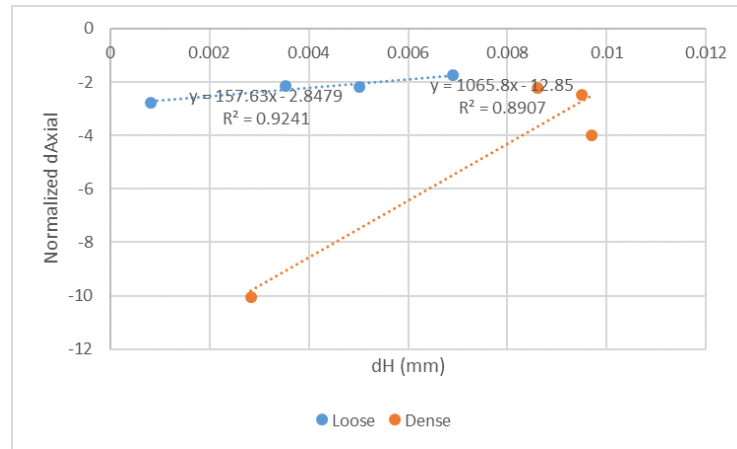
Figure 5.23: Maximum ΔH vs Normalized $\Delta\sigma_v$ for Dilative Behaviors

99

5.4   Cyclic Loading

Cyclic simple shear tests with different CSR were performed on Nevada sand specimens. The specimen was consolidated under 100 kPa, and after a 15 second waiting period, the specimen was loaded harmonically under stress control at a frequency of 0.2 Hz until the specimen experienced large shear, at which point the loading was stopped. From the data, liquefaction failure was identified as where the axial stress first decreased to below 5 kPa, indicating r_u value of 0.95. Figure 5.24 below plots the axial and shear stress, shear strain, and vertical displacement against time for an example test. Marked on the figures are the time where failure occurred and the maximum peak-to-peak vertical displacement amplitude.

(a) Axial Stress vs Time for Cyclic Loading Test

(b) Shear Stress vs Time for Cyclic Loading Test

(c) Shear Strain vs Time for Cyclic Loading Test

(d) Height Change vs Time for Cyclic Loading Test
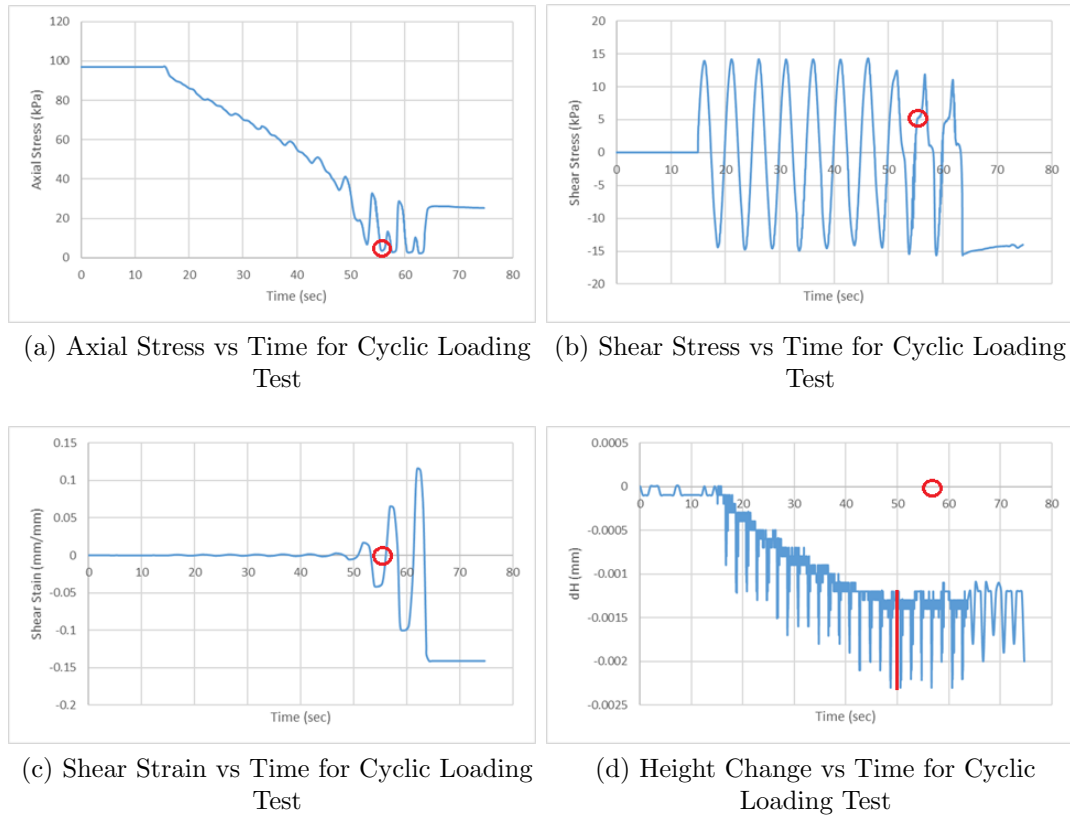
Figure 5.24: Example Stress-Strain Plots from Cyclic Loading Test (Test ID:170217)

The test data were then analyzed by a MATLAB code, which calculated and outputted the specimens CSR, N_f, and shear modulus for each cycle on to a plot.
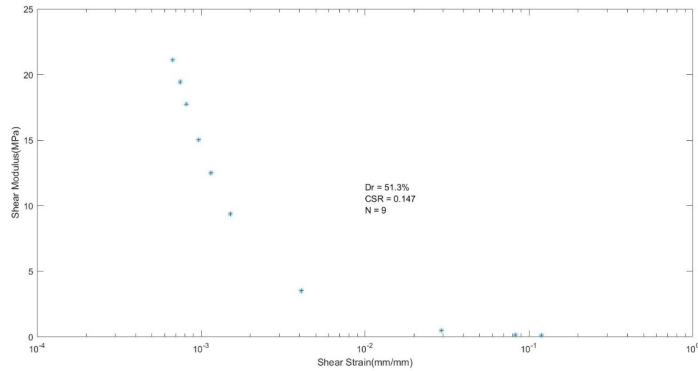
Figure 5.25: Example Plots of Shear Modulus for Each Loading Cycles
(Test ID:170217)

CSR vs N_f data points obtained from this series of tests (ran under constant volume condition), were plotted alongside the data points from Kwan (2015) (ran under truly saturated condition). Summaries of tests ran by Kwan (2015) and this research can be found in Appendix 1.4. Trendlines were fitted onto the data using the equation:

$$CSR = a * N_f^{-b} \qquad (5.2)$$

CSR vs N_f data points and the best-fit curves from both conditions are plotted on figure 5.26. The trendlines had high R^2 values, indicating good fits to the data.
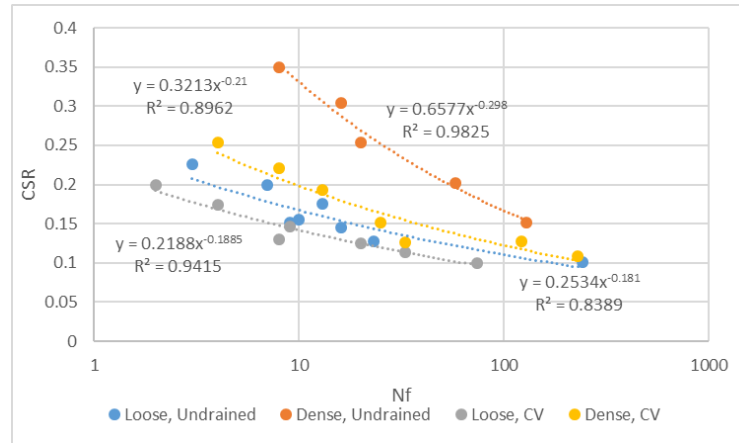
Figure 5.26: CSR vs N_f From Cyclic Loading Tests

CSR vs N_f curves for loose specimens under constant volume condition (CV) showed similar trends to the curves for loose specimens under undrained condition. CSR vs N_f curves for dense specimens under CV conditions, however, deviated from the curves for dense specimens under undrained conditions, especially towards high CSR. To better analyze this trend, ratio of CSR between undrained condition (UD) and CV condition from trendlines in figure 5.26 were plotted in figure 5.27. This ratio represents how much more stress it took for the specimen under UD condition to fail at a given number of cyclic loading compared to those under CV condition.
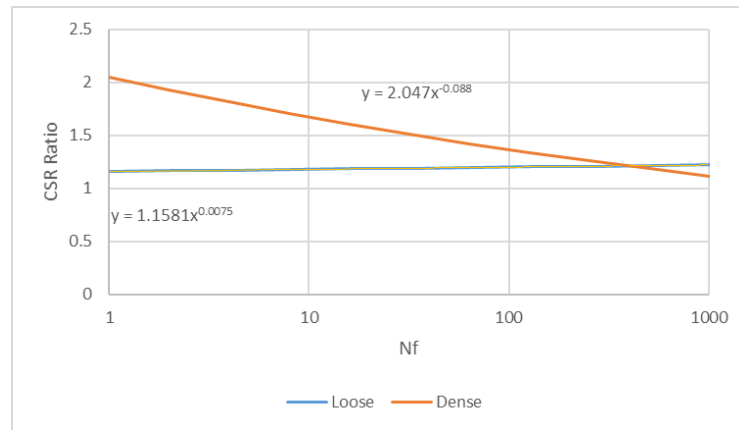
Figure 5.27: CSR Ratio vs N_f From Cyclic Loading Tests

Ratios of CSR for a given N_f increased behaved differently for each density. For loose specimen, the magnitude of ratio change was very small. For dense specimen, CSR ratio was significantly higher for lower N_f. This shows that dense specimens under CV condition exhibited lower shear resistance compared to specimen under UD condition, and it took less stress to fail given the same number of cycles of loading.

Finally, CSR ratio was calculated from N_f for each test using the trend-lines in figure 5.26, then plotted in figure 5.28 against the maximum peak-to-peak vertical displacement amplitude the specimen experienced.
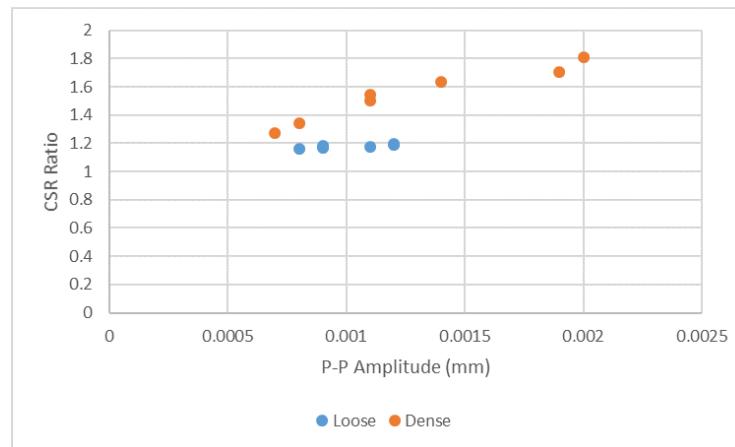
Figure 5.28: CSR Ratio vs P-P Amplitudes From Cyclic Loading Tests

From this plot, the effect of peak-to-peak vertical displacement amplitude on specimen strength can be observed; the CSR ratio doesn't change very much for loose specimen, but increases as the peak-to-peak amplitude increase for dense specimen. Volumetric dilation decreases the shear resistance of dense specimens under constant volume condition, causing the CSR ratio to increase.

It should be noted that the vertical movements for loose specimens were mostly contractive, while the vertical movements for dense specimens contained both contractive and dilative behaviors, as seen in figure 5.29. Its possible that the dense specimen experienced cyclic softening in both axial and horizontal directions, thus resulting in the specimen stiffness decreasing more rapidly.

105
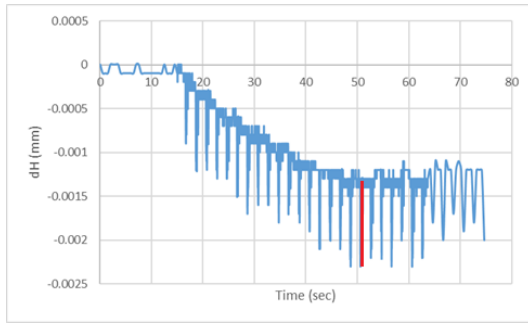
(a) dH vs Time for Cyclic Loading Test on Loose Specimen(Test ID:170217)
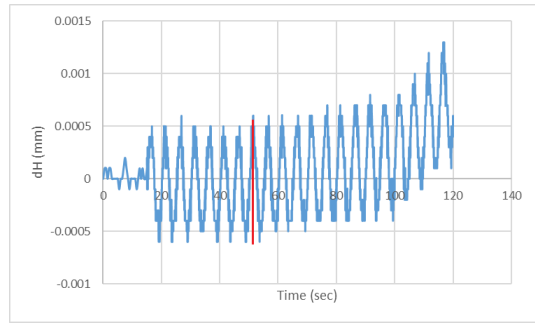
(b) dH vs Time for Cyclic Loading Test on Dense Specimen(Test ID:170301)

Figure 5.29: Difference in dH vs Time Plots Between Loose and Dense Specimens

Chapter 6

Summaries and Conclusions

6.1 Test Summaries

To investigate the effect of height control on simple shear tests under constant volume condition, the stress-strain behavior under shear was analyzed alongside the height change of the specimen. For this research, countless simple shear tests were performed on loose and dense specimens, and of those, 44 of them were analyzed: 26 monotonic loading, and 14 harmonic loading. Additionally, 4 one-dimensional consolidation tests were performed and analyzed. The summaries and the outcome of these tests can be found in Appendix 1.

First, monotonic loading tests were performed on sand specimens to investigate the general effects height control has on the shear behavior of sand specimens. The tests were performed on specimens with different vertical confining stresses, densities, and stiffness of height controlling systems. Trends between specimen height change and contractive/dilative behaviors are discussed in section 6.2. Second, cyclic simple shear test results under constant volume condition and truly undrained condition were compared. The difference in behaviors between the two conditions were discussed using trends found from comparing the monotonic loading tests. Finally, approaches to account

107

for the effects of specimen height change on stress behavior are proposed in section 6.3.

6.2 Test Conclusions

6.2.1 Effects of Specimen Height Change on Monotonic Shear Behavior

Effects to the shear behavior caused by specimen height change were mainly observed on contractive behaviors for loose sand specimens and dilative behaviors for dense sand specimens. When the specimen was allowed to contract volumetrically, it decreased the amount of positive pore pressure generated to maintain equilibrium. Even small amounts of change in height could cause a substantial difference; Figures 5.14a and 5.14b show that difference in 0.0005mm (0.0018% of the specimen height) caused a difference of 13 kPa in contractive axial stress change. The effect could be even larger, as the current standard allows change up to 0.05% of the specimen height to be considered under constant volume condition. This could lead to overestimation of the soils resistance to liquefaction under monotonic load, as the test result would indicate that the soil would have higher strength than it would in the field.

Effects of height change on dilative behaviors of dense specimen was analyzed by comparing the stresses and the height changes at the same strain. Under undrained condition, the specimen reached its critical state condition after a certain strain and both axial and shear stresses continue to increase proportionally to one another. Specimen height change and stresses were taken

from an arbitrary strain after reaching the critical state. At large strains, specimens that experienced more volumetric dilation also experienced larger stress changes, as shown in figure 5.21. It could not be determined whether the large axial stress change or the large dilative height change was causing the other to increase; however, it was found that tests using height control system with smaller Youngs Modulus experienced high dilative volumetric and stress behaviors. This trend was explained by making a connection with the effects of confining stress on dilative behaviors. Decreasing the stiffness of the height control system had a similar effect on dilative behavior as decreasing the confining stress.

6.2.2 Cyclic Shear Behavior under Constant Volume Condition vs Truly Undrained Condition

Overall, the CSS test results under constant volume condition exhibited lower stiffness and cyclic strength compared to those from specimens under truly undrained condition. For both loose and dense specimens, it took less stress for the specimen under CV condition to reach liquefaction than the one under UD condition given the same number of cyclic loading. As N_f decreased, the CSR ratio between UD and CV conditions increased for dense specimens, while it remained mostly constant for loose specimens. Increase in maximum peak-to-peak amplitude of the height change caused the CSR ratio to increase for dense specimens, indicating that volumetric dilation decreases the soil strength under constant volume condition.

The test results have shown that undrained cyclic strength for dense specimen under constant volume condition was considerably lower than the cyclic strength measured under undrained condition. This conclusion corresponds with the findings of Tatsuoka et al. (1982). After investigating the undrained stress-strain behavior of sand using torsional simple shear test, it was determined that undrained cyclic strength of dense sand specimens, compared to loose specimens, were much more susceptible to changes in factors such as sample preparation method, relative density, and stress conditions. Out of those factors, the stress conditions, affected by the height change of the specimen, would be significant in reducing the stiffness and the strength of the dense sand specimen.

6.3 Proposed Remediation Methods

6.3.1 Using One-Dimensional Consolidation Equation

One-dimensional consolidation equation calculates the height change caused by the change in vertical stress (equation 2.19). It was proposed that, by altering this equation, the change in stress caused by the specimen height change could be calculated. Ideally, there would be no height change of the specimen under constant volume condition, but the ASTM standard allows up to 0.05% of height change to be still considered valid.

During monotonic loading, the specimen will show a contractive behavior and the axial stress will decrease. When the recorded axial stress is less than the preconsolidation stress, the specimen is considered to be over-

consolidated. After the specimen reaches the minimum contracted state, it will start dilating and the axial stress will increase. When the recorded axial stress exceeds the preconsolidation pressure, the specimen is in its normally consolidated condition.
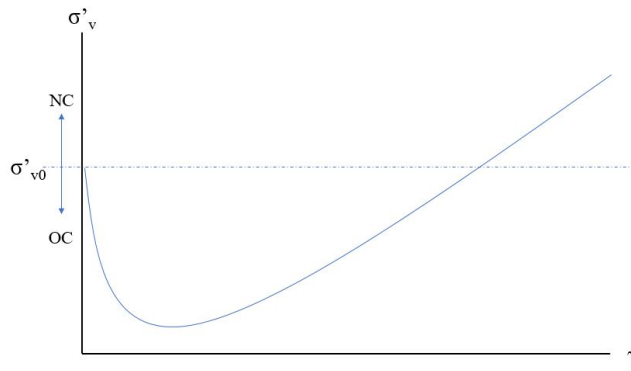
Figure 6.1: Consolidation Conditions during Monotonic Loading Test

Any height changes that occur during the contractive behavior of specimen occur in the recompression stage when the specimen is over-consolidated, and the change in stress is calculated as such:

$$\sigma'_{v,0} = \frac{\sigma'_p}{10^{(\frac{\Delta H}{R})}} \tag{6.1}$$

$$\Delta \sigma'_v = \sigma'_p - \sigma'_{v,0} \tag{6.2}$$

After the vertical stress exceeds the initial consolidation stress and the specimen is in the normally consolidated stage, the change in stress is calculated as such:

111

$$\sigma'_{v,0} = \sigma'_p * 10^{(\frac{\Delta H}{R})} \tag{6.3}$$

$$\Delta \sigma'_v = \sigma'_p - \sigma'_{v,f} \tag{6.4}$$

In a perfect constant volume test, change in height, ΔH, would be 0, and vertical stress ($\sigma_{v,0}$ or $\sigma'_{v,f}$) would be equal to the preconsolidation pressure, σ_p. Under this condition, the effect of contraction/dilation would be reflected purely in the axial stress change. When the height of the specimen changes, some of the axial stress are deviated. The difference in the axial stress due to height change can be taken as the difference in the preconsolidation stress and the calculated vertical stress from the above equation.

The signs of deviatoric stresses due to volume change has to be considered when adding it to the recorded axial stress to get the corrected value. In the contractive state, the axial stress recorded is a higher than the true axial stress since the volumetric change decrease the magnitude of negative stress; when finding the true stress, the change in stress from the volume change is subtracted from the recorded stress. Similarly, the recorded axial stress is higher than the true axial stress during dilative state at high strains, and the change in stress from volume change has to be subtracted from the recorded stress.
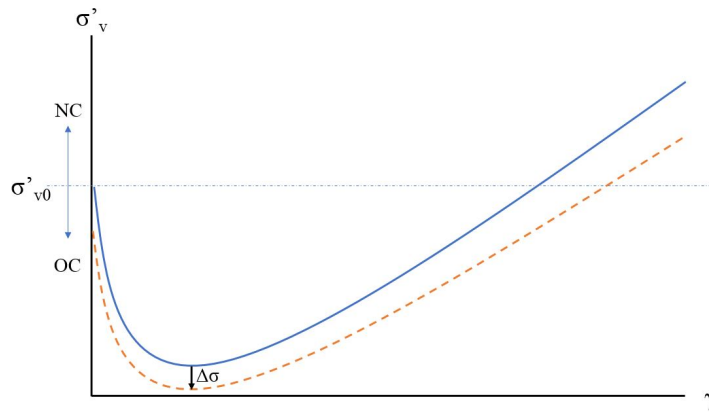
Figure 6.2: Corrected Stress vs Strain from Monotonic Loading Test Using
One-Dimensional Consolidation Test Method

Some potential issues with this method is that simple shear tests under constant volume conditions do not quite follow the assumptions Terzaghi made for his consolidation theory. Because the test is ran on dry sand specimen, it is not saturated and there is no flow of water, just air. Additionally, the stress from the height change calculated by the modified one-dimensional consolidation equation is extremely small compared to the actual difference in stress from the test results. Finally, if the calculated stress change is multiplied by a factor to better fit the data, the corrected stress-strain curve might experience a sudden slope change unrealistic for a real test result. The change would occur where the specimen enters the normally consolidated range from the over-consolidated range. However, with some modification, this method could be used to provide a better shape of the shear-strain behavior line.

113
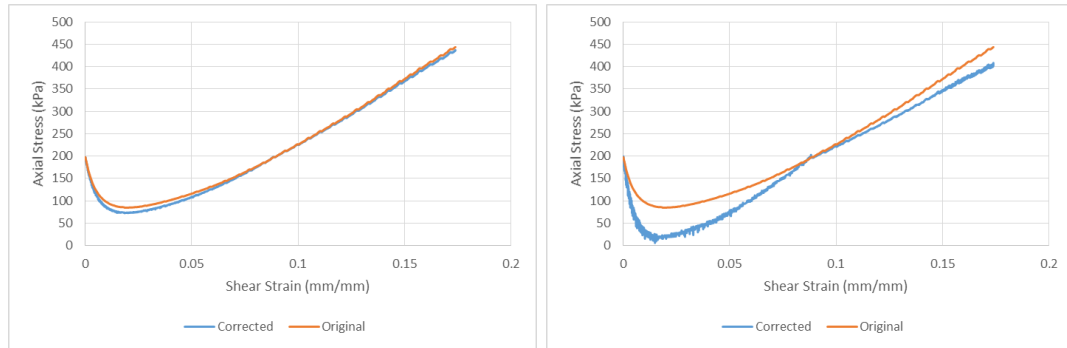
(a) Corrected Stress vs Strain Plot using
One-Dimensional Consolidation Equation

(b) Corrected Stress vs Strain Plot using
magnified One-Dimensional Consolidation
Equation

Figure 6.3: Potential Issues using One-Dimensional Consolidation Equation
Correction Method
(Test ID:170120)

6.3.2 Using ΔH and Δσ Stress Trend

The second proposed method is to create a plot similar to figures 5.20 and 5.21 plotting the relationship between the minimum/maximum height changes and maximum stress contraction/dilation. By using the trendline through the points, contractive/dilative stress change assuming there were no height change could be predicted. For example, using figure 5.20, it could be predicted that the loose specimen would have generated 77 kPa of positive pore pressure if there were no height change, and similarly for figure 5.21, the dense specimen would have generated 400 kPa of negative pore pressure at a strain of 16%. By creating a plot using the normalized vertical stress (figures 5.22 and 5.23), the correct pore pressure for no height change can be predicted for tests with different confining stress.

Some issues with this method is that it requires many test points to get a good trendline. The tests should have varying magnitudes of height changes, which is hard to control. Another issue is that soil is a non-linear material, meaning that it may not behave the same way when the height change amplitude is in the elastic range.

6.4 Future Research

The purpose of this research was to investigate the validity of using constant volume condition as an equivalent of truly undrained condition for simple shear tests on sand and the importance of height control on the stress behavior. One area of research could be to compare the monotonic loading test results from this research with the same loading tests under undrained condition and modifying the remediation methods to closer fit the undrained data. There were no undrained data for this research to compare the constant volume data with, so the remediation methods are mostly theoretical. Comparison with real data could help verify the remediation methods, or propose completely different methods for accounting for the stress difference.

It was found that specimen under constant volume condition exhibited less stiffness than specimen under truly undrained condition in a CSS test. Some topics for future research includes finding the possible causes, besides the specimen height change, for this reduced stiffness, and finding a way to modify the simple shear equipment such that it yields a closer test result as the undrained test. Effects of the height change on small strain shear modulus and

damping ratio could be analyzed by comparing the results from this research to data obtained from a torsional shear or resonant column test.

Appendix

Appendix 1

Simple Shear Test Summaries and Plots

1.1   Monotonic Loading Simple Shear Tests

Table 1.1: Summary of Monotonic Tests under Different Shear Rates

Test Type	Test ID	Dr(%)
1%/min Loose	170621	24.5
1%/min Dense	170619_2	78.2
0.25%/min Loose	170630	27.4
0.25%/min Dense	170630_2	77.3
0.25%/min(2) Loose	170713	30.2
0.25%/min(2) Dense	170628	79.6

Table 1.2: Summary of Monotonic Tests under Different Vertical Stresses

Test ID	Vert. Stress (kPa)	Dr(%)
170702	50	37.4
170416	100	43.5
170503	150	41.8
170120	200	47.9
170505	50	82.0
170123_2	100	78.7
170124	150	76.3
170125	200	82.8

Table 1.3: Summary of Monotonic Tests using Different Screw-Nut System

Test ID	Dr(%)	Properties
170620_3	25.7	Small
170621	24.5	Med
170620_2	25.4	Large
170707	28.8	Alum
170710	28.8	Brass
170711	29.6	Med(2)
170620	71.9	Small
170619_2	78.2	Med
170619	82.0	Large
170708	80.1	Alum
170710_2	83.0	Brass
170711_2	78.9	Med(2)

1.2 Cyclic Loading Simple Shear Tests

1.2.1 Summaries of Cyclic Tests

Table 1.4: Summary of Undrained CSS Tests under Harmonic Loading
(Kwan, 2015)

Test ID	Dr(%)	CSR	N_f
20130327	49	0.176	13
2013032902	39	0.200	7
2013040102	34	0.151	9
20130404	51	0.128	23
20130406	41	0.226	3
20130424	44	0.101	241
20130525	55	0.145	16
20130523	55	0.155	10
2013051502	85	0.152	129
20130516	85	0.202	58
2013051602	74	0.254	20
20130517	79	0.304	16
20130711	78	0.350	8

Table 1.5: Summary of Constant Volume CSS Tests under Harmonic Loading

Test ID	Dr(%)	CSR	N_f
170215_2	46.2	0.174	4
170216	50.0	0.125	20
170217	51.3	0.147	9
170218	46.5	0.100	74
170218_2	52.6	0.200	2
170221_2	45.2	0.130	8
170227	53.0	0.114	33
170301	85.1	0.152	25
170305	81.3	0.193	13
170306	80.4	0.221	8
170306_2	78.7	0.254	4
170307	79.4	0.126	33
170321	78.6	0.109	228
170327	86.3	0.127	121

1.2.2 Constant Volume Cyclic Simple Shear Test Plots
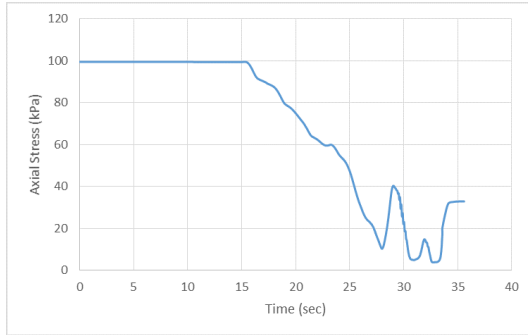
(a) Axial Stress vs Time for Cyclic Loading Test
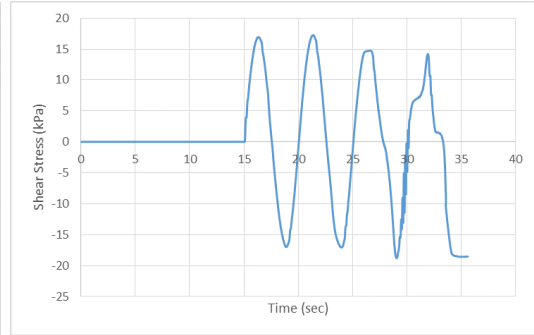
(b) Shear Stress vs Time for Cyclic Loading Test
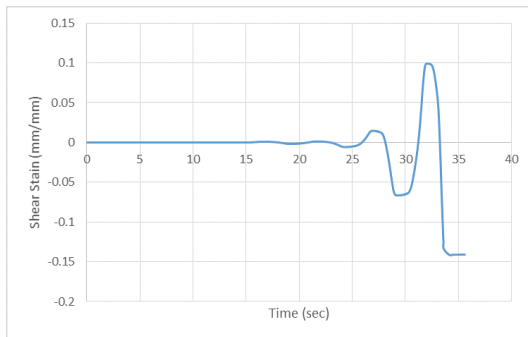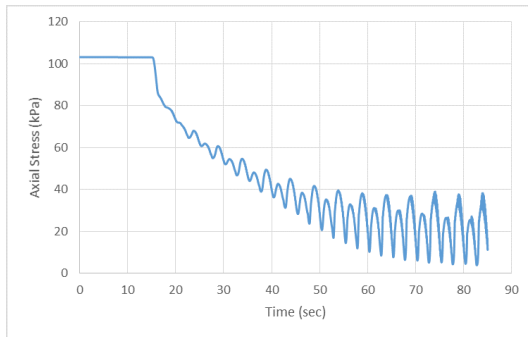

(c) Shear Strain vs Time for Cyclic Loading Test
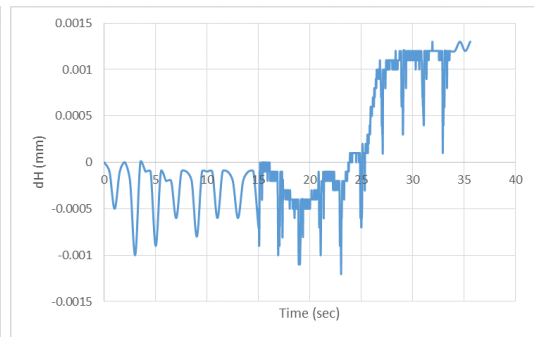
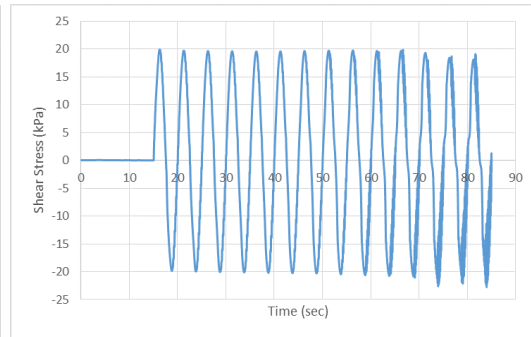(d) Height Change vs Time for Cyclic Loading Test
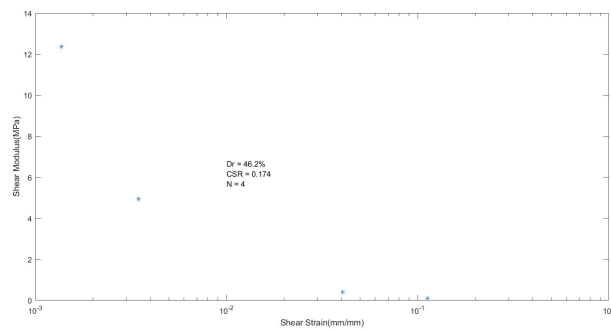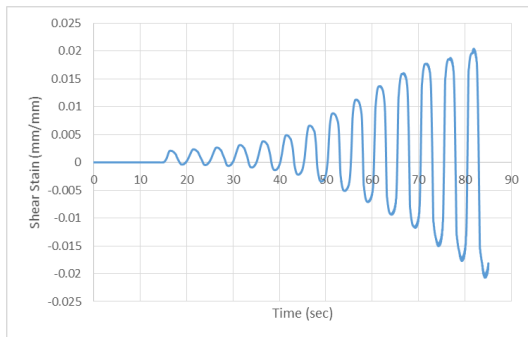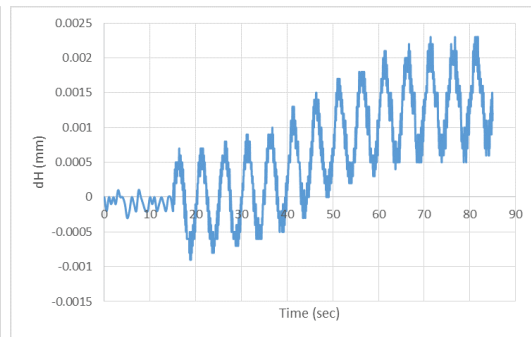

(e) Shear Modulus for Each Loading Cycles

Figure 1.1: (Test ID:170215_2)
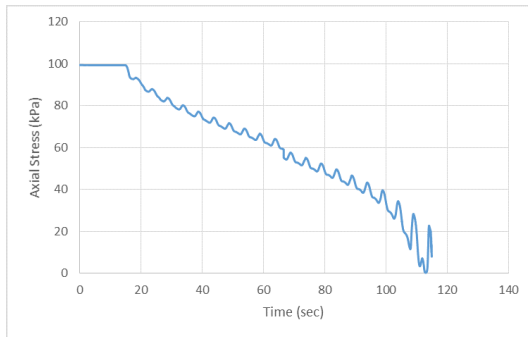
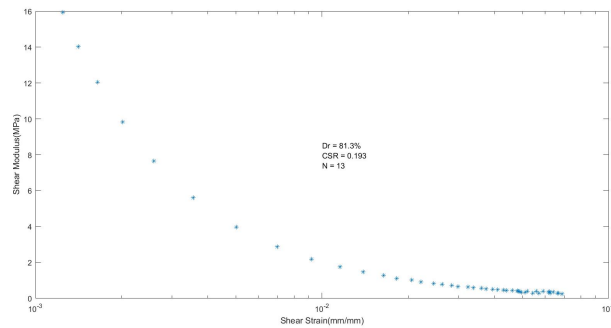(a) Axial Stress vs Time for Cyclic Loading Test
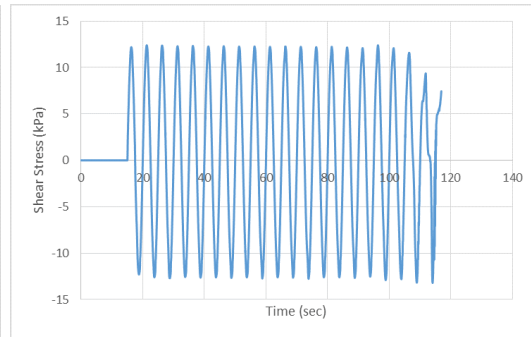
(b) Shear Stress vs Time for Cyclic Loading Test
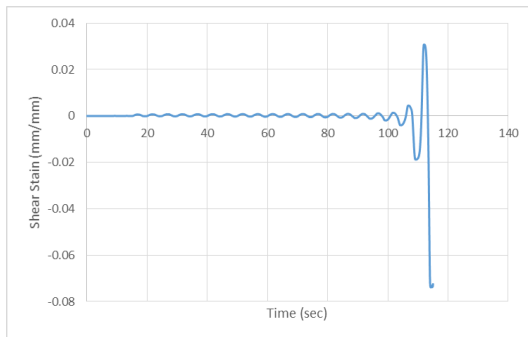
(c) Shear Strain vs Time for Cyclic Loading Test
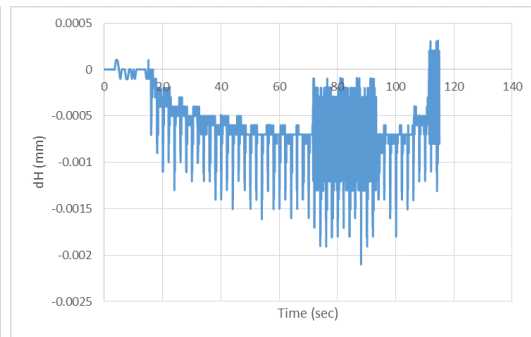
(d) Height Change vs Time for Cyclic Loading Test
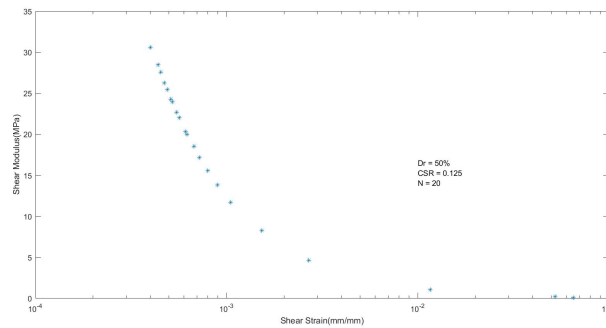
(e) Shear Modulus for Each Loading Cycles

Figure 1.2: (Test ID:170216)
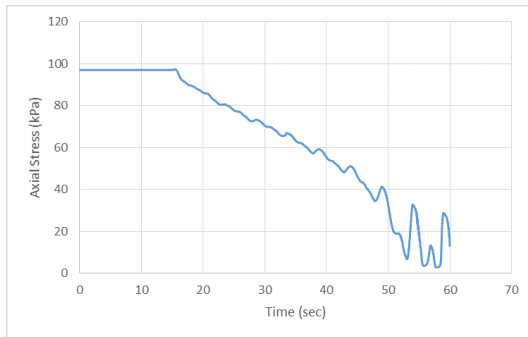
(a) Axial Stress vs Time for Cyclic Loading Test
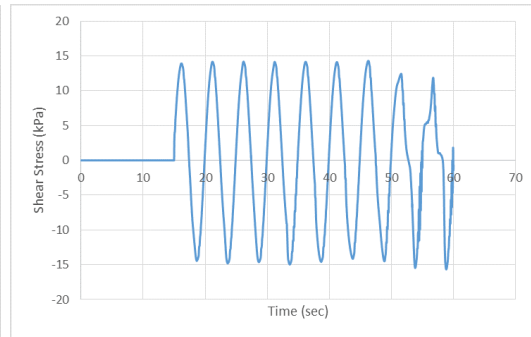
(b) Shear Stress vs Time for Cyclic Loading Test
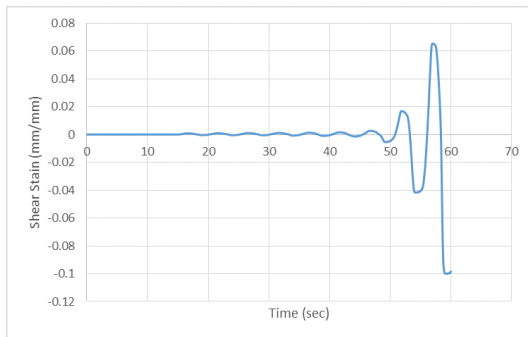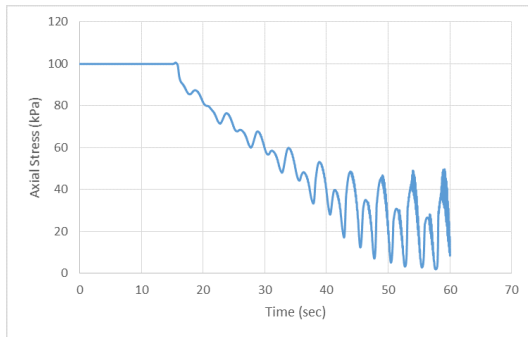

(c) Shear Strain vs Time for Cyclic Loading Test
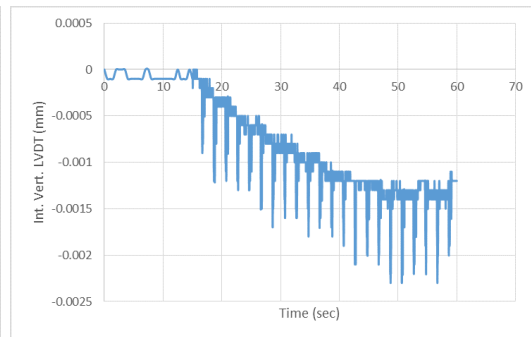
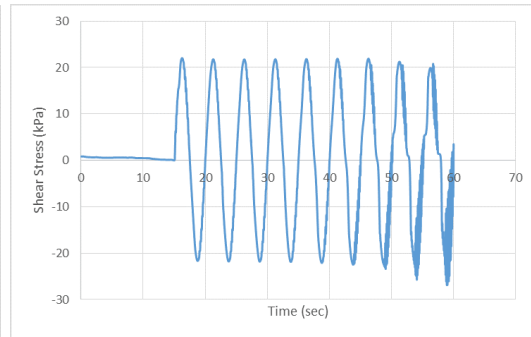(d) Height Change vs Time for Cyclic Loading Test
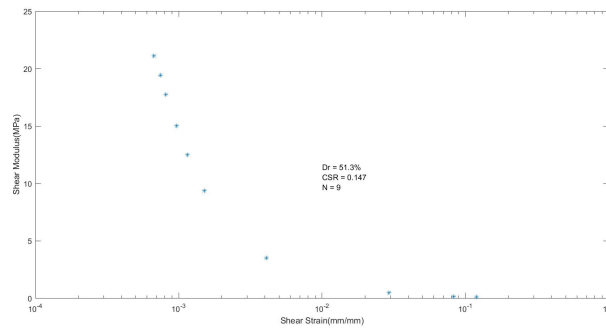
(e) Shear Modulus for Each Loading Cycles

Figure 1.3: (Test ID:170217)
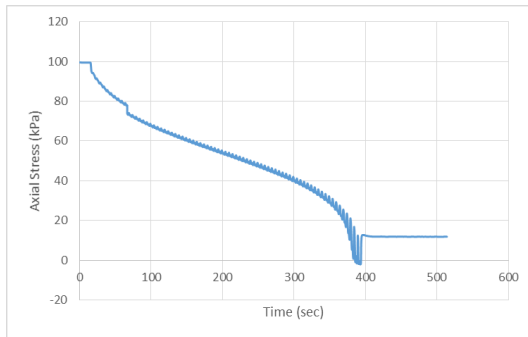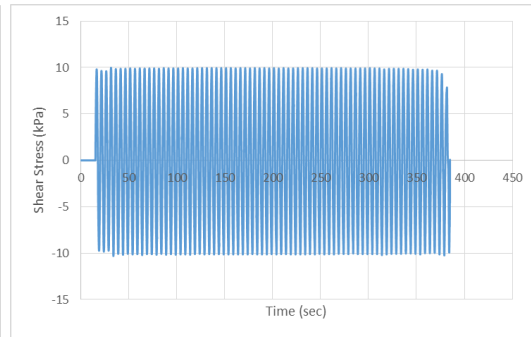
124

(a) Axial Stress vs Time for Cyclic Loading Test

(b) Shear Stress vs Time for Cyclic Loading Test
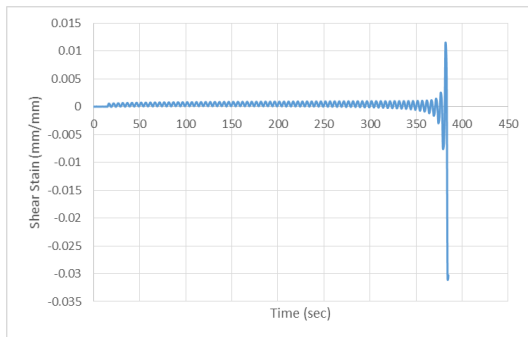
(c) Shear Strain vs Time for Cyclic Loading Test
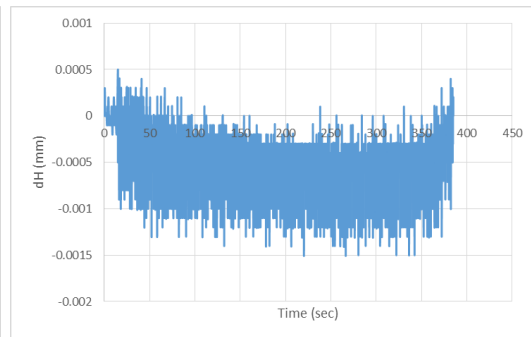
(d) Height Change vs Time for Cyclic Loading Test
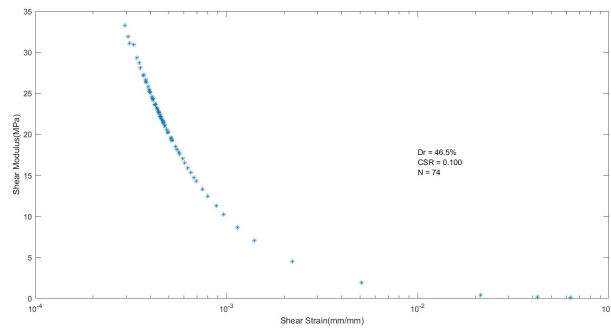
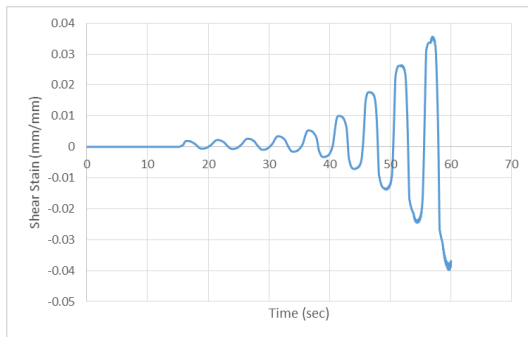(e) Shear Modulus for Each Loading Cycles

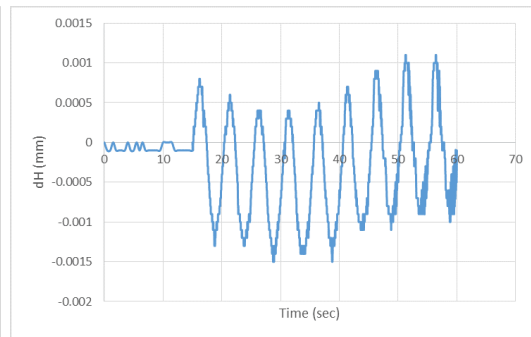Figure 1.4: (Test ID:170218)
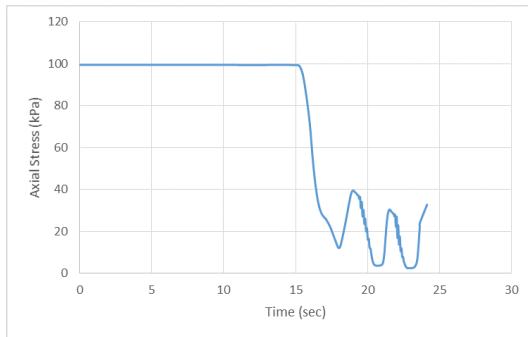
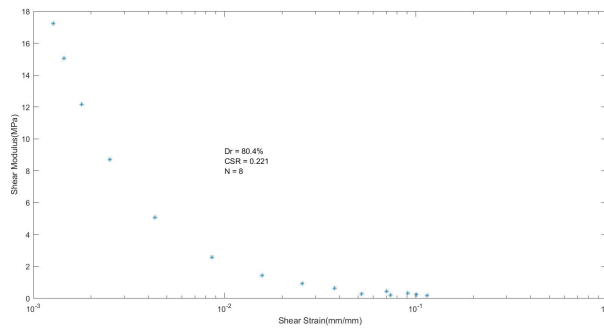(a) Axial Stress vs Time for Cyclic Loading Test
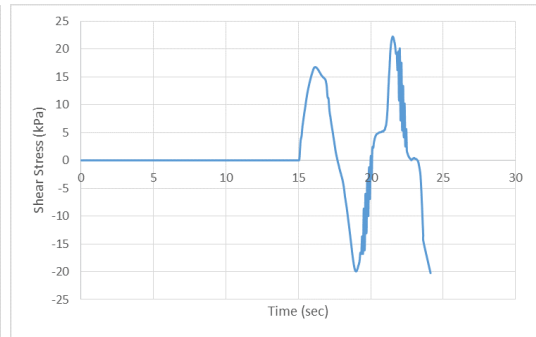
(b) Shear Stress vs Time for Cyclic Loading Test
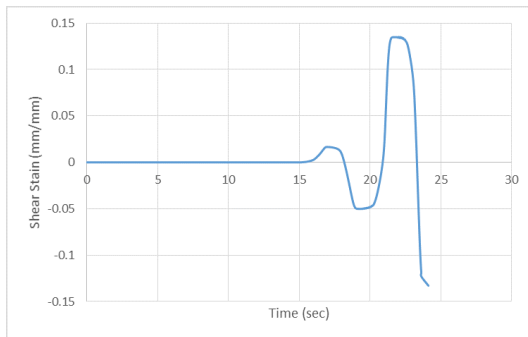
(c) Shear Strain vs Time for Cyclic Loading Test
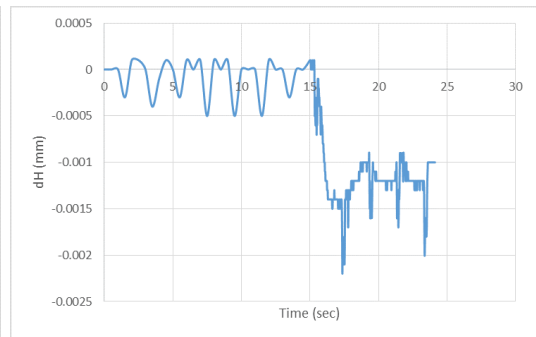
(d) Height Change vs Time for Cyclic Loading Test
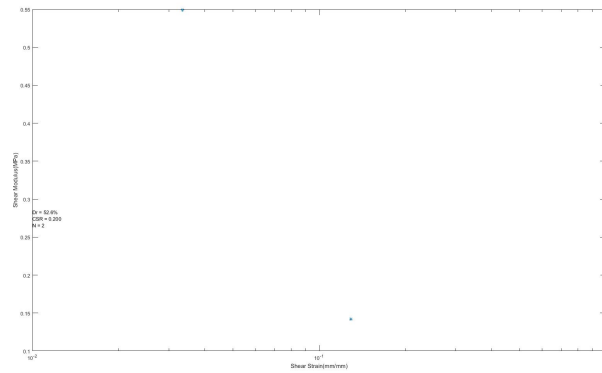
(e) Shear Modulus for Each Loading Cycles

Figure 1.5: (Test ID:170218_2)
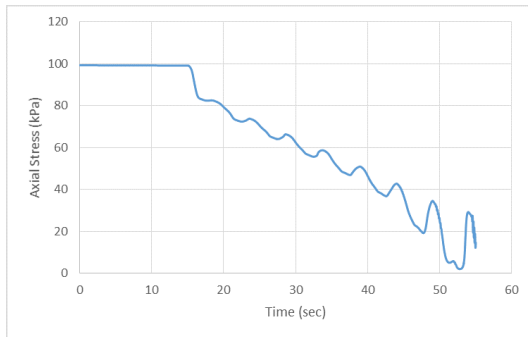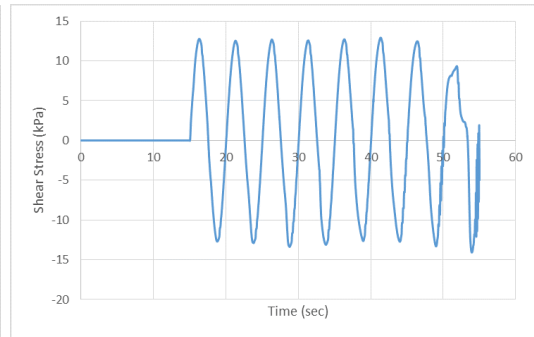
126

(a) Axial Stress vs Time for Cyclic Loading Test

(b) Shear Stress vs Time for Cyclic Loading Test
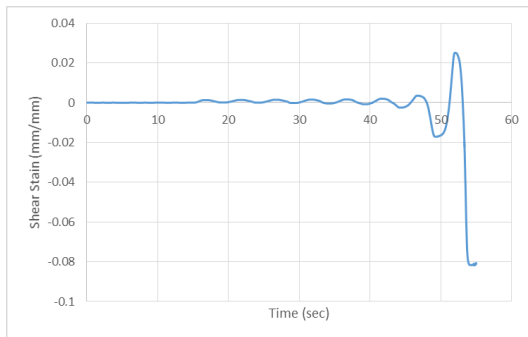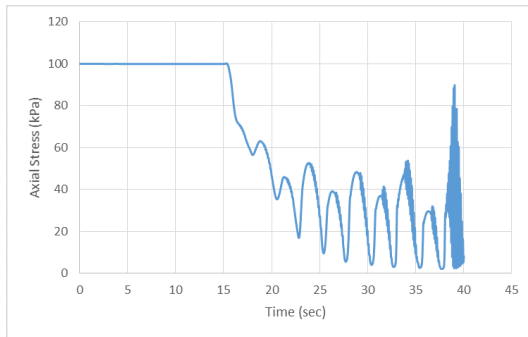

(c) Shear Strain vs Time for Cyclic Loading Test
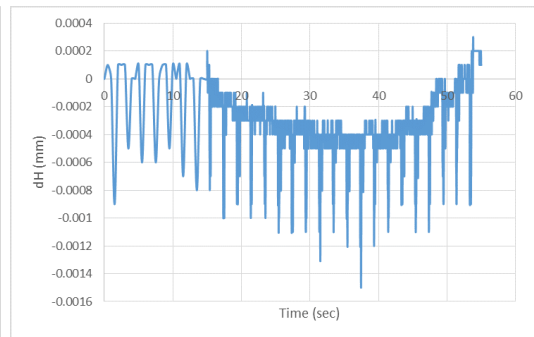
(d) Height Change vs Time for Cyclic Loading Test
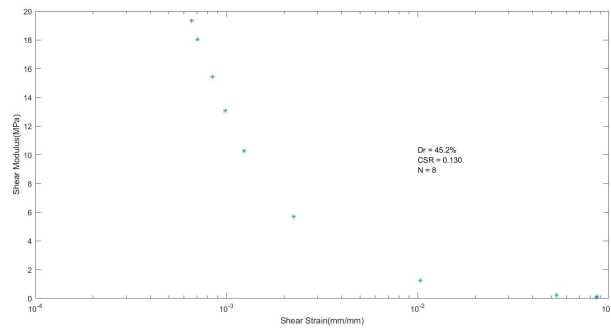
(e) Shear Modulus for Each Loading Cycles

Figure 1.6: (Test ID:170221_2)
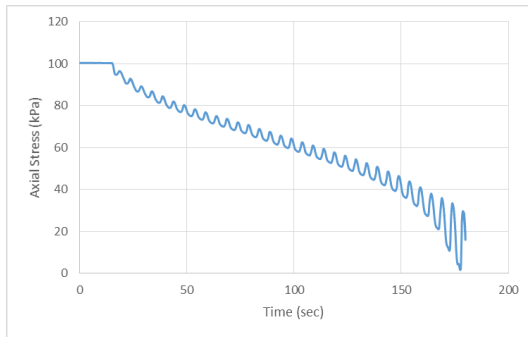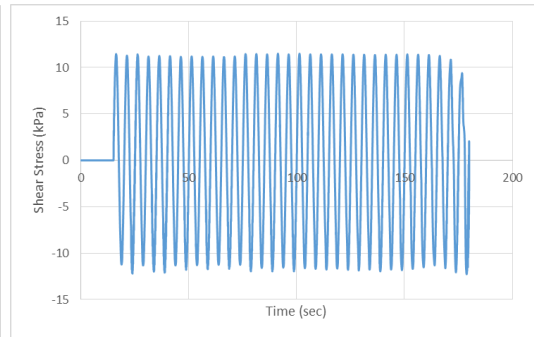
127

(a) Axial Stress vs Time for Cyclic Loading Test

(b) Shear Stress vs Time for Cyclic Loading Test
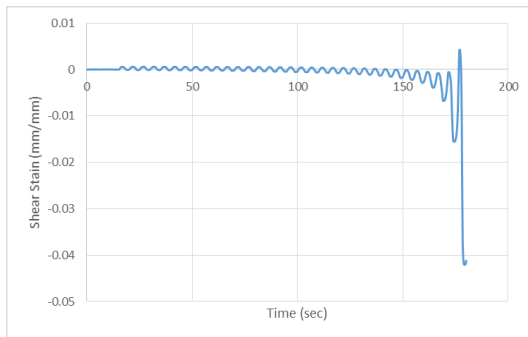
(c) Shear Strain vs Time for Cyclic Loading Test
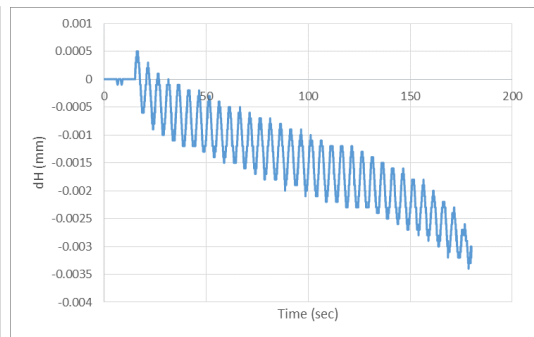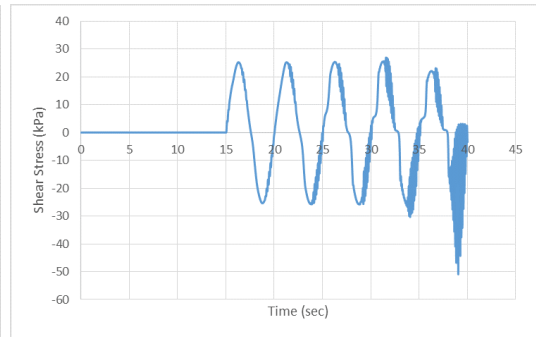

(d) Height Change vs Time for Cyclic Loading Test
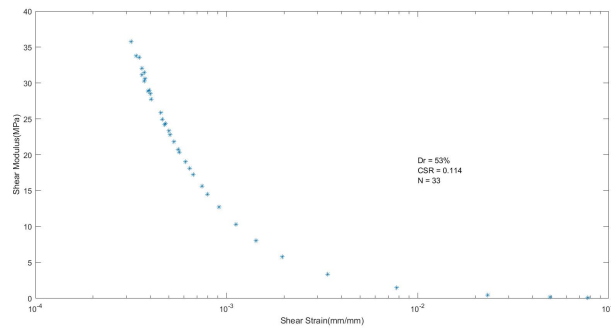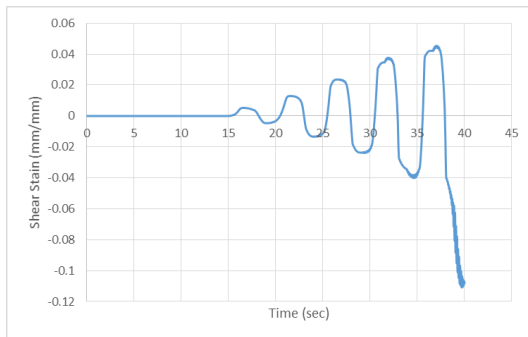

(e) Shear Modulus for Each Loading Cycles

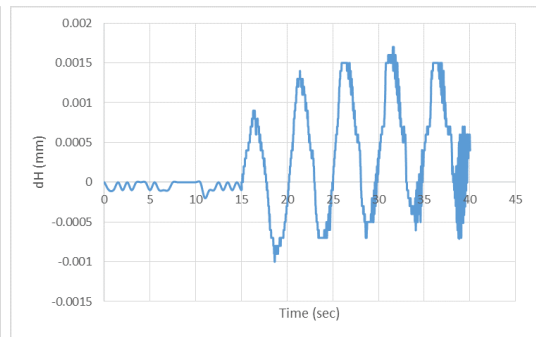Figure 1.7: (Test ID:170227)
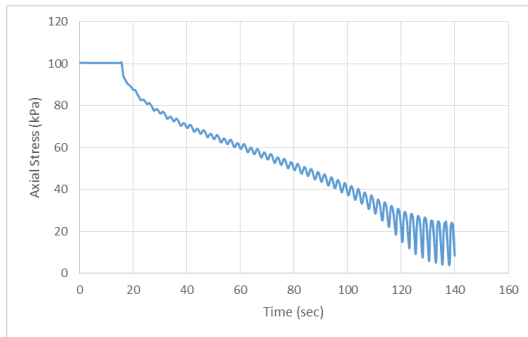
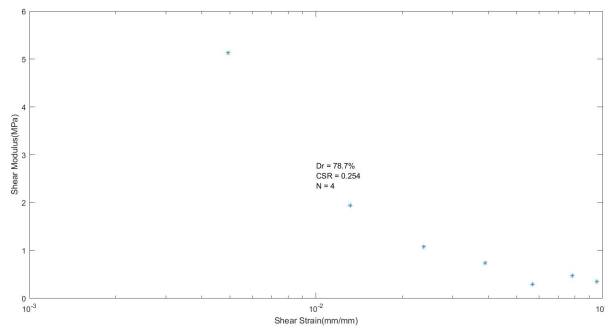(a) Axial Stress vs Time for Cyclic Loading Test
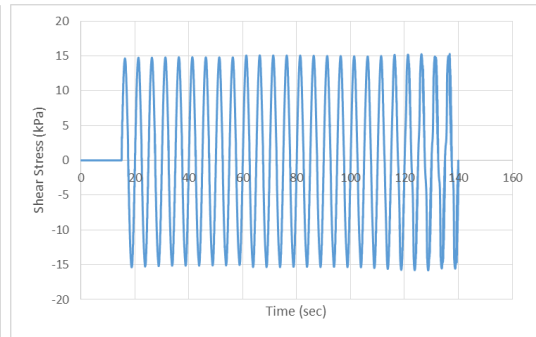
(b) Shear Stress vs Time for Cyclic Loading Test
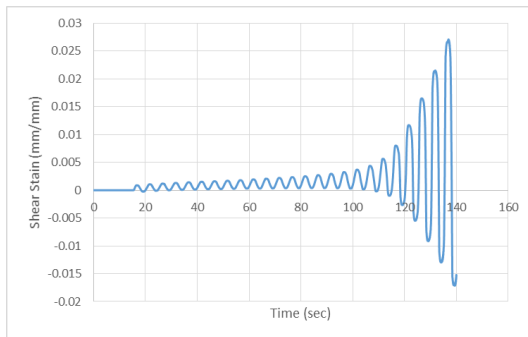
(c) Shear Strain vs Time for Cyclic Loading Test
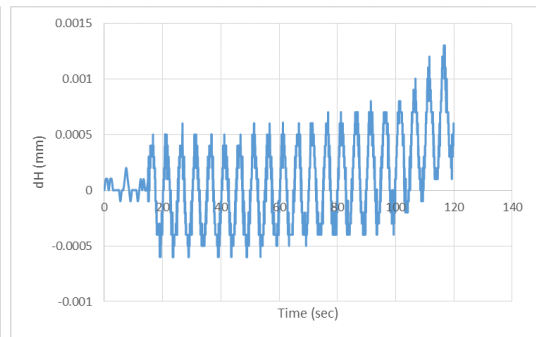
(d) Height Change vs Time for Cyclic Loading Test
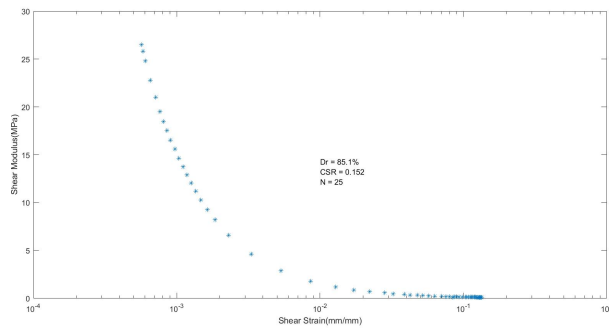
(e) Shear Modulus for Each Loading Cycles

Figure 1.8: (Test ID:170301)

(a) Axial Stress vs Time for Cyclic Loading Test

(b) Shear Stress vs Time for Cyclic Loading Test

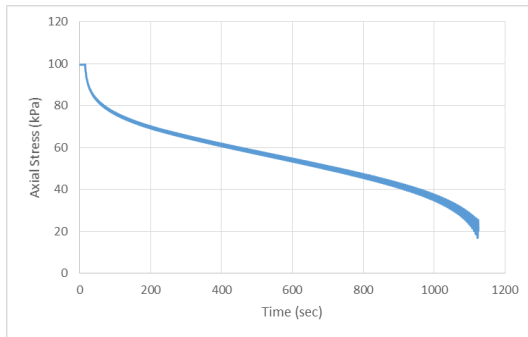(c) Shear Strain vs Time for Cyclic Loading Test

(d) Height Change vs Time for Cyclic Loading Test

(e) Shear Modulus for Each Loading Cycles

Figure 1.9: (Test ID:170305)

(a) Axial Stress vs Time for Cyclic Loading Test

(b) Shear Stress vs Time for Cyclic Loading Test

(c) Shear Strain vs Time for Cyclic Loading Test

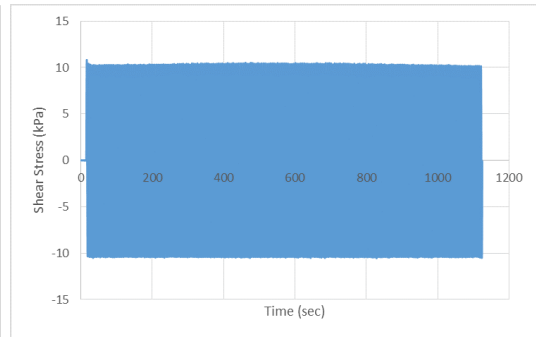(d) Height Change vs Time for Cyclic Loading Test

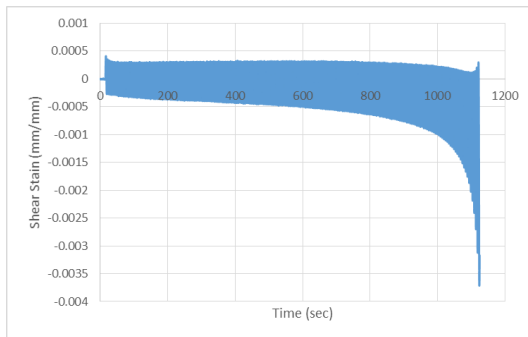(e) Shear Modulus for Each Loading Cycles
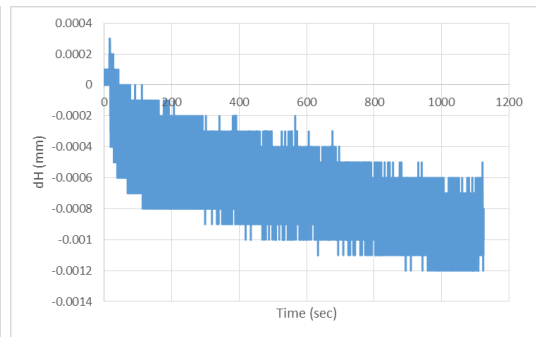
Figure 1.10: (Test ID:170306)

(a) Axial Stress vs Time for Cyclic Loading Test

(b) Shear Stress vs Time for Cyclic Loading Test

(c) Shear Strain vs Time for Cyclic Loading Test

(d) Height Change vs Time for Cyclic Loading Test

(e) Shear Modulus for Each Loading Cycles

Figure 1.11: (Test ID:170306_2)

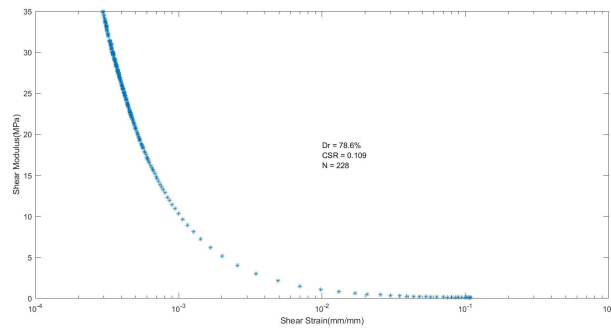(a) Axial Stress vs Time for Cyclic Loading Test

(b) Shear Stress vs Time for Cyclic Loading Test

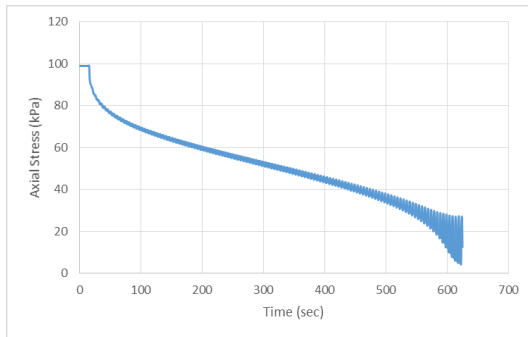(c) Shear Strain vs Time for Cyclic Loading Test

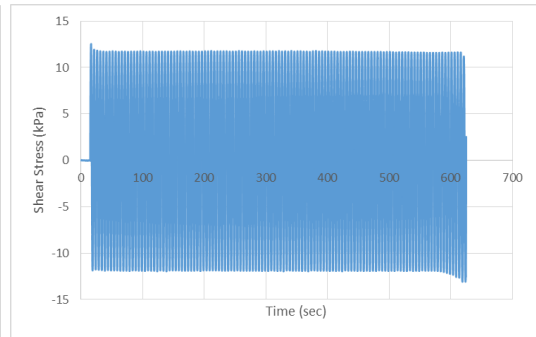

(d) Height Change vs Time for Cyclic Loading Test

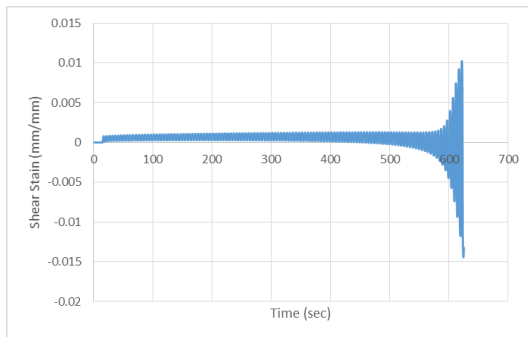(e) Shear Modulus for Each Loading Cycles

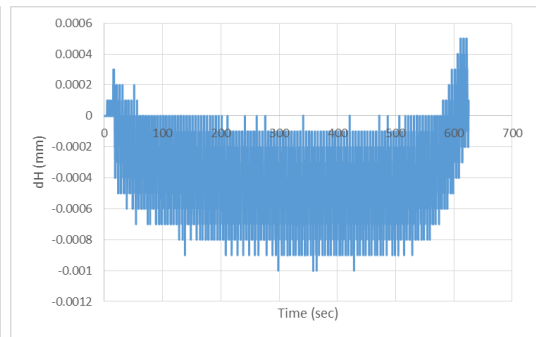Figure 1.12: (Test ID:170321)

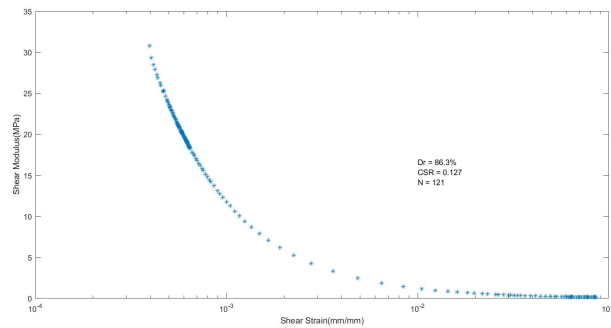(a) Axial Stress vs Time for Cyclic Loading Test

(b) Shear Stress vs Time for Cyclic Loading Test

(c) Shear Strain vs Time for Cyclic Loading Test

(d) Height Change vs Time for Cyclic Loading Test

(e) Shear Modulus for Each Loading Cycles

Figure 1.13: (Test ID:170327)

1.3 One-Dimensional Consolidation Tests

1.3.1 Consolidation Test Summary

Table 1.6: Summary of One-Dimensional Consolidation Tests

Sand Type	Test ID	Dr(%)
Washed Mortar	170411	41.9
	170424	73.4
Nevada	170512	32.7
	170515	80.6

1.3.2 Consolidation Test Plots

Figure 1.14: One-Dimensional Consolidation Test for Loose Washed Mortar
Sand and Tangential Lines
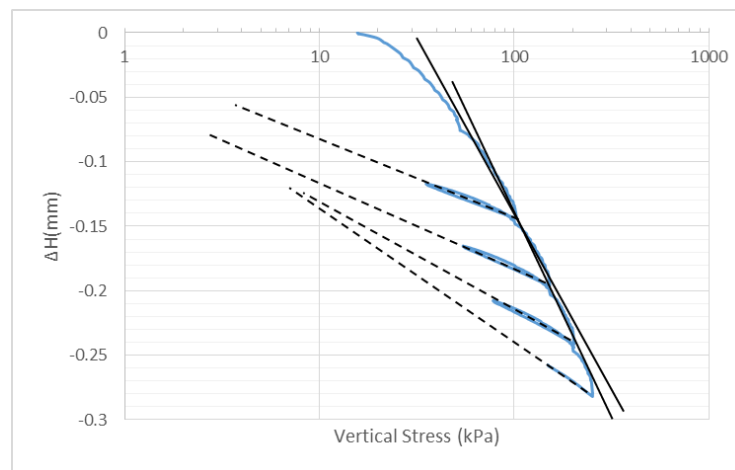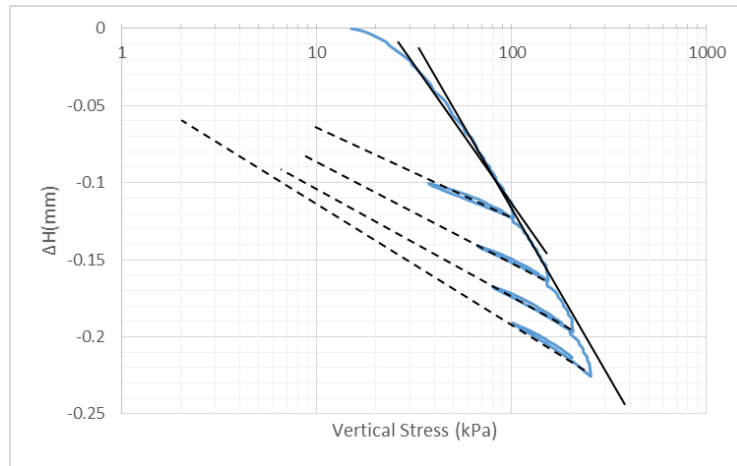(Test ID:170411)

Figure 1.15: One-Dimensional Consolidation Test for Dense Washed Mortar
Sand and Tangential Lines
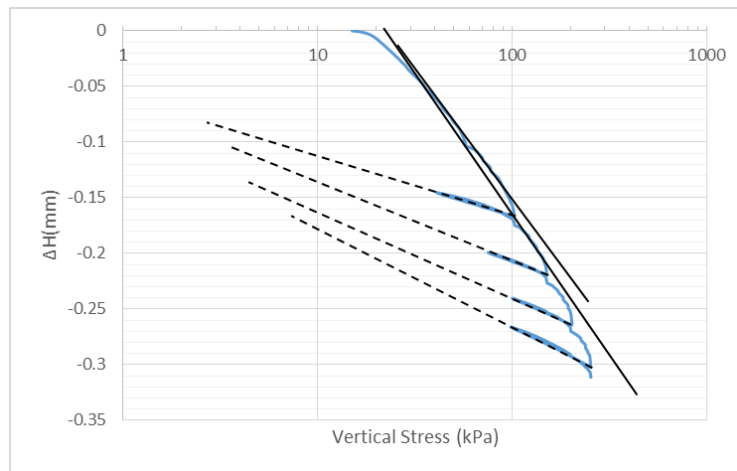(Test ID:170424)

Figure 1.16: One-Dimensional Consolidation Test for Loose Nevada Sand
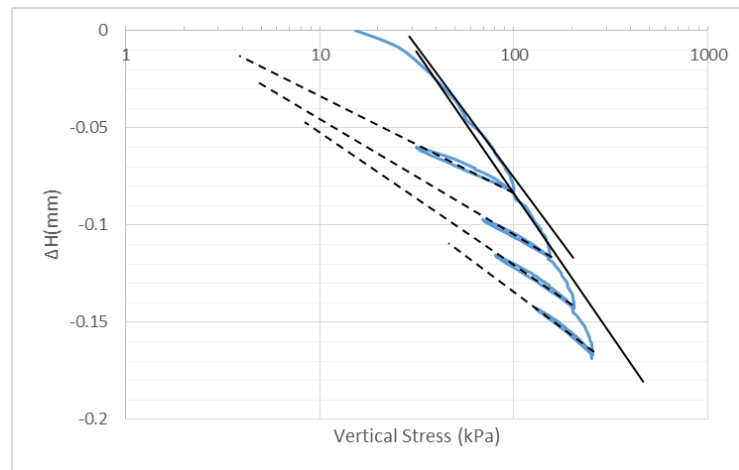and Tangential Lines
(Test ID:170512)

Figure 1.17: One-Dimensional Consolidation Test for Loose Nevada Sand
and Tangential Lines
(Test ID:170512_2)

Bibliography

Andrus, R. D. and Stokoe II, K. H. (2000). "Liquefaction resistance of soils from shear-wave velocity." *Journal of geotechnical and geoenvironmental engineering*, 126(11), 1015–1025.

Arulmoli, K., Muraleetharan, K., Hossain, M., and Fruth, L. (1992). "Velacs: Verification of liquefaction analyses by centrifuge studies, laboratory testing program, soil data report." *Earth Technology Corporation*, 51–58.

ASTM (1996). "D2435-96: Standard test method for one-dimensional consolidation properties of soils." *American Society for Testing Materials.*

ASTM (2007). "D6528-07: Standard test method for consolidated undrained direct simple shear testing of cohesive soils." *American Society for Testing Materials.*

Baxter, C., Bradshaw, A., Ochoa-Lavergne, M., and Hankour, R. (2010). "Dss test results using wire-reinforced membranes and stacked rings." *GeoFlorida 2010: Advances in Analysis, Modeling & Design*, 600–607.

Bolton, M. (1986). "The strength and dilatancy of sands." *Geotechnique*, 36(1), 65–78.

Boulanger, R. W. and Idriss, I. M. (2004). *Evaluating the potential for liquefaction or cyclic failure of silts and clays.* Center for Geotechnical Modeling.

Darendeli, M. B. (2001). "Development of a new family of normalized modulus reduction and material damping curves." PhD dissertation, The University of Texas at Austin, The University of Texas at Austin.

Dyvik, R., Berre, T., Lacasse, S., and Raadim, B. (1987). "Comparison of truly undrained and constant volume direct simple shear tests." *Geotechnique*, 37(1), 3–10.

El Mohtar, C. (2015). "Lecture notes in ce387l.1: Consolidation and shearing properties of soil: Behavior of cohesionless soils.

Hardin, B. O. and Drnevich, V. P. (1972). "Shear modulus and damping in soils: design equations and curves." *Journal of Soil Mechanics & Foundations Div*, 98(sm7).

Ishihara, K. (1993). "Liquefaction and flow failure during earthquakes." *Geotechnique*, 43(3), 351–451.

Kammerer, A., Wu, J., Pestana, J., Riemer, M., and Seed, R. (2000). "Cyclic simple shear testing of nevada sand for peer center project 2051999." *Geotechnical Engineering Research Report UCB/GT/00-01, University of California, Berkeley, Calif.*

Kwan, W. S. (2015). "Laboratory investigation into evaluation of sand liquefaction under transient loadings." PhD dissertation, The University of Texas at Austin, The University of Texas at Austin.

Kwan, W. S. and El Mohtar, C. (2014). "Comparison between shear strength of dry sand measured in css device using wire-reinforced membranes and stacked rings." *Geo-Congress 2014: Geo-characterization and Modeling for Sustainability*, 1111–1119.

Lee, K. L. and Seed, H. B. (1967). "Drained strength characteristics of sands." *Journal of Soil Mechanics & Foundations Div.*

Menq, F.-y. (2003). "Dynamic properties of sandy and gravelly soils." Ph.D. thesis, Ph.D. thesis.

Mesri, G. and Vardhanabhuti, B. (2009). "Compression of granular materials." *Canadian Geotechnical Journal*, 46(4), 369–392.

Rowe, P. W. (1962). "The stress-dilatancy relation for static equilibrium of an assembly of particles in contact." *Proceedings of the royal society of London a: mathematical, physical and engineering sciences*, Vol. 269, The Royal Society, 500–527.

Seed, H. B. and Idriss, I. M. (1970). "Soil moduli and damping factors for dynamic response analyses." *Report no.*

Seed, H. B. and Idriss, I. M. (1971). "Simplified procedure for evaluating soil liquefaction potential." *Journal of Soil Mechanics & Foundations Div.*

Tatsuoka, F., Muramatsu, M., and Sasaki, T. (1982). "Cyclic undrained stress-strain behavior of dense sands by torsional simple shear test." *Soils and Foundations*, 22(2), 55–70.

Youd, T., Idriss, I., Andrus, R. D., Arango, I., Castro, G., Christian, J. T., Dobry, R., Finn, W. L., Harder Jr, L. F., Hynes, M. E., et al. (2001). "Liquefaction resistance of soils: summary report from the 1996 nceer and 1998 nceer/nsf workshops on evaluation of liquefaction resistance of soils." *Journal of geotechnical and geoenvironmental engineering*, 127(10), 817–833.

Vita

Yuta Nakamura was born in Tokyo, Japan on 4 February 1993. He is the first son of Hideyo and Noriko Nakamura, and has one sister, Erisa Nakamura. He moved to Champaign, Illinois in 2002. After graduating from Champaign Centennial High School, he attended University of Illinois at Urbana-Champaign. He graduated from UIUC in 2015 with a Bachelor of Science degree in Engineering Physics with a concentration in Geology/Earth Science. He then attended the University of Texas at Austin in 2015 studying Geotechnical Engineering in the department of Civil and Environmental Engineering.

Permanent address: ynakamu2@utexas.edu
ynakamu2@gmail.com

This thesis was typeset with LaTeX† by the author.

---

†LaTeX is a document preparation system developed by Leslie Lamport as a special version of Donald Knuth's TeX Program.